Development of a self-amplifying RNA vaccine against Rift Valley fever

Paul Kato Kitandwe

Thesis submitted in accordance with the requirements for the degree of Doctor of Philosophy of the University of London

London School of Hygiene and Tropical Medicine
Faculty of Infectious and Tropical Diseases
Department of Infection Biology

Funded by: Engineering and Physical Sciences Research Council

Research group affiliation(s): MRC/UVRI & LSHTM Uganda Research Unit
Uganda Virus Research Institute

July 2025

DECLARATION

I, Paul Kato Kitandwe, confirm that the work presented in this thesis is my own. Where information has been derived from other sources, I confirm that this has been indicated in the thesis.

ABSTRACT

Background: Rift Valley fever (RVF) is a mosquito-borne zoonosis caused by the Rift Valley fever virus (RVFV), which leads to high mortality in livestock and severe or fatal complications in humans. Despite its severity, no licensed RVF vaccine exists for humans, and licensed livestock vaccines have suboptimal safety and immunogenicity. This thesis aimed to design and preclinically evaluate self-amplifying RNA (saRNA) vaccines against RVF and transfer saRNA vaccine development capacity to a resource-limited setting (Uganda).

Methods: Mutations enhancing plasma membrane expression and glycoprotein stability were introduced into a consensus RVFV medium (M) segment sequence (WT consensus) and evaluated for *in vitro* expression of glycoprotein n (Gn) and c (Gc) after cloning into the pcDNA3.1(+) vector. The WT consensus and the mutated construct with the highest plasma membrane Gn expression (Furin-T2A) were individually cloned into a Venezuelan equine encephalitis virus (VEEV) pDNA replicon, transcribed *in vitro* into saRNA and capped. The saRNA constructs were then assessed for immunogenicity in BALB/c mice after formulation in lipid nanoparticles (LNPs) in the UK and cationic lipids in Uganda.

Results: LNP-formulated saRNA WT consensus and Furin-T2A candidate vaccines induced high levels of anti-Gn IgG after two vaccinations (mean = 522,000 ng/mL, SD = 424,736 ng/mL, $p < 0.01$) and (mean = 522,848, SD = 366,604, $p < 0.01$), respectively. However, only the WT consensus induced significant RVFV pseudovirus-neutralising activity (median IC50 = 5089, IQR = 5500, $p < 0.01$) compared to the unvaccinated control group. In contrast, saRNA RVF vaccines formulated in cationic lipids induced variable and weak humoral and T-cell immune responses.

Conclusion: This thesis demonstrated that an LNP-formulated saRNA RVF vaccine can induce robust humoral immune responses in mice and merits further development. It also

demonstrated the transfer of saRNA vaccine development technology to Uganda, advancing local vaccine research and development capacity.

Acknowledgements

First and foremost, I would like to express my deepest gratitude to my supervisors, Prof. Pontiano Kaleebu and Prof. Robin Shattock, for their support and guidance as I embarked on this challenging PhD journey. Their expertise and advice have been instrumental in helping me achieve this significant academic milestone.

I am also very grateful to the members of Prof. Robin Shattock's laboratory at Imperial College London, who provided me with invaluable technical support and a friendly and supportive working environment. In particular, I thank Dr. Anna K. Blakney for performing vaccine formulation and immunisations in the mouse studies conducted at Imperial College London. I also thank Dr. Hu Kai for running the initial RVFV pseudovirus neutralisation assays performed at Imperial College London and training me in this assay. Special thanks also go to Dr. Paul McKay for his technical assistance and to Paul Rogers, my primary trainer.

I would also like to acknowledge and appreciate the technical support from the Uganda Virus Research Institute (UVRI) staff, particularly the Laboratory Technologists Owen Nayebare and Laban Kato and fellow PhD students Dennis Omara and Dr. Zacchaeus Anywaine.

Additionally, I thank the staff of Makerere University School of Veterinary Medicine and Animal Resources (MAK-SVAR), who conducted mouse immunisations and collected samples for the immunogenicity studies in Uganda.

I would also like to acknowledge my funders, the Engineering and Physical Sciences Research Council (EPSRC), MRC/UVRI and LSHTM Uganda Research Unit, the International AIDS Vaccine Initiative (IAVI), and the Government of Uganda. Their financial support made this work possible. Additionally, I am thankful to the administrative staff at Imperial College London, particularly Dr. Benjamin Pierce, and to the training support team of MRC/UVRI and LSHTM Uganda Research Unit, led by Achilles Kiwanuka, for their assistance in ensuring smooth day-to-day operations.

On a personal note, I owe immense gratitude to my wife, Rose, for her unconditional love, prayers, encouragement, patience, and understanding throughout this journey. I also thank my children, Albert, Marcel, Angela, and Joel, for their patience and understanding while I was in the UK for nearly two years at the start of this PhD. I am also immensely grateful to my mother and siblings for their prayers, encouragement, and support. To my elder brother Joseph, thank you for checking on me and taking good care of me when I was in the UK. To Ms Cathy Kalemera and Auntie Sale, I sincerely thank you for hosting and caring for me for nearly two years during my stay in London.

This thesis is dedicated to my late father, Dr. Amans Musisi Kitumba, who, together with my mother, supported and inspired me to achieve my full potential.

Table of Contents

DECLARATION **2**

ABSTRACT **3**

1.0 CHAPTER ONE: INTRODUCTION ..... **- 15 -**

1.1 Background ..... **- 15 -**

1.2 Statement of the research problem ..... **- 18 -**

1.3 Objectives ..... **- 19 -**

1.4 Study hypothesis ..... **- 20 -**

2.0 CHAPTER TWO: LITERATURE REVIEW ..... **- 21 -**

2.1 Rift Valley fever epidemiology ..... **- 21 -**

2.2 Pathogenesis of Rift Valley fever ..... **- 24 -**

2.2.1 Animal infections with RVFV ..... - 24 -

2.2.2 Human infections with RVFV ..... - 24 -

2.3 Rift Valley fever diagnosis ..... **- 26 -**

2.4 The Rift Valley fever virus replication cycle ..... **- 27 -**

2.5 Rift Valley fever virus genome organisation and viral structure ..... **- 29 -**

2.6 Immunity against Rift Valley fever virus infection ..... **- 31 -**

2.6.1 RVFV immune evasion mechanisms ..... - 31 -

2.6.2 Innate immune responses to RVFV infection ..... - 32 -

2.6.3 Adaptive immune responses to RVFV infection ..... - 33 -

2.7 Rift Valley fever vaccines ..... **- 34 -**

2.8 Self-amplifying RNA vaccines ..... **- 36 -**

2.8.1 Structure of self-amplifying RNA vaccines ..... - 36 -

2.8.2 Synthesis of saRNA ..... - 38 -

2.8.3 Functions of the different components of saRNA ..... - 38 -

2.8.4 Optimisation of the saRNA sequence ..... - 40 -

2.8.5 Purification of saRNA ..... - 42 -

2.8.6 Self-amplifying RNA vaccine delivery methods ..... - 44 -

2.9 Immune responses to self-amplifying RNA vaccination ..... **- 47 -**

2.9.1. Innate immune responses to self-amplifying RNA vaccines ..... - 47 -

2.9.2. Modulation of innate immune responses induced by saRNA ..... - 48 -

2.9.3. Adaptive immune responses to saRNA vaccination ..... - 50 -

3.0 CHAPTER THREE: METHODOLOGY ..... **- 53 -**

3.1 Generation of the consensus RVFV M segment sequence ..... **- 53 -**

3.1.2 Retrieval of RVFV M segment sequences from ViPR ..... - 53 -

3.1.3 Alignment to obtain the RVFV wild-type consensus sequence ..... - 54 -

3.1.4 Phylogenetic analysis of the RVFV wild-type consensus sequence ..... - 54 -

3.2 Cloning the RVFV M segment consensus sequence into pcDNA3.1 ..... **- 55 -**

3.2.1 Preparation of glycerol stocks ..... - 55 -

3.3 Introduction of the desired mutations into the RVFV M segment consensus sequence ..... **- 56 -**

3.3.1 Diagnostic restriction digestion ..... - 57 -

3.4 Transfection of HEK 293 F cells with RVFV pDNA vectors ..... **- 62 -**

3.5 Assessment of *in vitro* expression of RVFV pDNA using western blot ..... - 62 -

3.6 Assessment of plasma membrane expression of RVFV pDNA using flow cytometry ..... - 64 -

3.7 Generation of RVFV saRNA constructs ..... - 65 -

3.7.1 Selection of constructs for *in vitro* transcription into saRNA ..... - 65 -

3.7.2 Cloning of the RVFV Gn/Gc sequences into the VEEV vector ..... - 65 -

3.7.3 Generation of saRNA constructs by *in vitro* transcription ..... - 66 -

3.8 Assessment of saRNA quality using a denaturing agarose gel ..... - 67 -

3.9 Transfection of HEK293T/17 cells with saRNA encoding RVFV Gn and Gc ..... - 67 -

3.10 Assessment of *in vitro* expression of RVFV saRNA using western blot ..... - 68 -

3.11 Assessment of plasma membrane expression of saRNA using flow cytometry ..... - 68 -

3.12 Formulation of RVFV saRNA ..... - 69 -

3.12.1 Formulation of saRNA using LNPs ..... - 69 -

3.12.2 Formulation of saRNA using *in vivo*-jetRNA and *in vivo*-jetRNA+ ..... - 70 -

3.13.1 Immunisation of mice with LNP-formulated saRNA RVF vaccines ..... - 72 -

3.13.2 Mice immunisation with *in vivo*-jetRNA and *in vivo*-jetRNA+ saRNA RVF vaccines ..... - 72 -

3.14 Study ethics approvals ..... - 73 -

3.15 RVFV Gn and Gc IgG ELISA ..... - 74 -

3.16 RVFV pseudovirus neutralisation assay ..... - 75 -

3.16.2 RVFV pseudovirus titration ..... - 76 -

3.16.3 RVFV pseudovirus neutralisation ..... - 77 -

3.17 Enumeration of interferon-gamma production using ELISpot assay ..... - 77 -

3.18 Cytokine quantification using the LEGENDplex™ mouse Th cytokine panel ..... - 79 -

3.18.1 Principle of the LEGENDplex assay ..... - 79 -

3.18.2 Procedure for running the LEGENDplex assay ..... - 79 -

CHAPTER FOUR RESULTS: GENERATION AND OPTIMISATION OF RVFV M SEGMENT CONSTRUCTS ..... - 81 -

4.1 Introduction ..... - 81 -

4.2 Generation of the RVFV M segment consensus sequence ..... - 82 -

4.3 Mutation of the RVFV M segment consensus ..... - 86 -

4.4 Expression of Gn and Gc using SDS-PAGE and western blot ..... - 87 -

4.5 Cell surface expression of Gn and Gc by flow cytometry ..... - 90 -

CHAPTER FIVE RESULTS: SYNTHESIS AND CHARACTERISATION OF SaRNA ENCODING A CONSENSUS AND A MUTATED RVFV M SEGMENT SEQUENCE ..... - 94 -

5.1 Introduction ..... - 94 -

5.2 Cloning of the RVFV M segment sequences into the VEEV plasmid DNA vector ..... - 95 -

5.3 Self-amplifying RNA transcription and quality control ..... - 97 -

5.4 *In vitro* expression of RVFV Gn from saRNA ..... - 99 -

5.5 Measurement of encapsulation efficiency ..... - 100 -

CHAPTER SIX RESULTS: IMMUNE RESPONSES IN MICE IMMUNISED WITH CANDIDATE saRNA RVF VACCINES ..... - 104 -

6.1 Introduction ..... - 104 -

6.2 Induction of anti-Gn IgG by RVFV pDNA vaccines ..... - 104 -

6.3 Anti-Gn IgG responses in mice immunised with LNP-saRNA RVF vaccines..... - 105 -

6.4 Pseudovirus neutralising activity in LNP-saRNA RVF vaccine immunised mice ..... - 107 -

6.5 Anti-Gn IgG responses in mice immunised with *in vivo*-jetRNA formulated vaccines ..... - 108 -

6.6 Anti-Gn IgG levels in mice immunised with *in vivo*-jetRNA+ saRNA RVF vaccines..... - 110 -

6.7 Pseudovirus neutralising activity in serum of mice immunised with *in vivo*-jetRNA+ candidate saRNA RVF vaccines..... - 113 -

6.8 Assessment of IFN-γ production by ELISpot..... - 114 -

6.9. Multiple cytokine analysis..... - 115 -

CHAPTER SEVEN: DISCUSSION..... - 118 -

7.1 Introduction..... - 118 -

7.2 RVFV M segment consensus sequence characteristics..... - 118 -

7.3 *In vitro* expression of Gn and Gc by SDS-PAGE and western blot ..... - 120 -

7.4 Cell surface expression of Gn and Gc by flow cytometry..... - 120 -

7.5 Encapsulation efficiency of *in vivo*-jetRNA and *in vivo*-jetRNA+..... - 122 -

7.6 Immunogenicity of LNP-Formulated saRNA RVFV Candidate Vaccines..... - 123 -

7.7 Immunogenicity of cationic lipid-formulated candidate saRNA RVFV vaccines ..... - 125 -

CHAPTER EIGHT: CONCLUSION..... - 127 -

References..... - 134 -

Table of Abbreviations

Abbreviation	Definition
AEC	3-amino-9-ethylcarbazole
APC	Antigen-presenting cell
ATP	Adenosine triphosphate
CMV	Cytomegalovirus
CNE	Cationic nanoemulsion
CoVAB	College of Veterinary Medicine, Animal Resources and Biosecurity
CTP	Cytidine triphosphate
DCs	Dendritic cells
DIVA	Differentiating infected from vaccinated animals
DMEM	Dulbecco's Modified Eagle's Medium
DMF	Dimethyl Formamide
DOTAP	1,2-Dioleoyl-3-trimethylammoniumpropane chloride
EDTA	Ethylenediaminetetraacetic acid
ELISA	Enzyme-linked immunosorbent assay
ER	Endoplasmic reticulum
Gc	Glycoprotein n
Gn	Glycoprotein c
GTP	Guanosine triphosphate
HEK	Human embryonic kidney
HPLC	High-performance liquid chromatography
HRP	Horseradish peroxidase
IC50	Half-maximal inhibitory concentration
IgG	Immunoglobulin G
IL	Interleukin
LNP	Lipid nanoparticles
MAK-SVAR	Makerere University School of Veterinary Medicine and Animal Resources
MEGA	Molecular Evolutionary Genetics Analysis
MFI	Median florescence intensity
MHC	Major histocompatibility complex
mRNA	Messenger RNA
MUSCLE	Multiple sequence comparison by log expectation
MUST	Mbarara University of Science and Technology
NK	Natural killer
NLRs	NOD-like receptors
NSm	Non-structural protein m
NSs	Non-structural protein s
OAS	2′-5′-oligoadenylate synthetase
pABoL	Poly(CBA-co-4-amino-1-butanol)
PAMPS	Pathogen associated molecular patterns
pDNA	Plasmid DNA

PEI	Polyethyleneimine
PKR	Protein kinase R
PRRs	Pattern recognition receptors
RdRp	RNA-dependent RNA polymerase
RIG-I	Retinoic acid-inducible gene I
RNA	Ribonucleic acid
RVF	Rift Valley fever
RVFV	Rift Valley fever virus
saRNA	Self-amplifying RNA
SDS-PAGE	Sodium dodecyl sulphate–polyacrylamide gel electrophoresis
SFV	Semliki Forest Virus
SINV	Sindbis virus
TAE	Tris-acetate-EDTA
$TCID_{50}$	Tissue culture infectious dose 50
TLR	Toll-like receptor
TNF	Tumour necrosis factor
UTR	Untranslated Region
VEEV	Venezuelan equine encephalitis virus
ViPR	Virus Pathogen Database and Analysis Resource
VNT	Virus neutralisation assay
VRPs	Virus replicon particles
WT	Wild type

Glossary of Terms

Term	Definition
Adaptive Immune Response	A specific and memory-driven immune response involving activation of B lymphocytes (antibody production) and T lymphocytes (cytokine release and cytotoxic activity) against antigens.
Alphavirus Replicon System	A self-replicating RNA system derived from alphaviruses, containing nonstructural proteins for replication and a subgenomic promoter driving antigen expression, used in saRNA vaccine platforms.
Cap 1 Structure	A 5′ cap structure added to RNA molecules that includes an N7-methylguanosine and 2′-O-methylation of the first nucleotide, mimicking eukaryotic mRNA to enhance stability, translational efficiency, and immune evasion.
Cytoplasmic Translation	Cytoplasmic translation is the process of protein synthesis that occurs in the cytoplasm of a cell, where ribosomes translate messenger RNA (mRNA) into functional protein.
DIVA Property	An acronym for "Differentiating Infected from Vaccinated Animals," referring to a vaccine's ability to allow serological distinction between infection-induced and vaccine-induced immune responses, essential for disease eradication programs.
Encapsulation Efficiency	The percentage of RNA successfully encapsulated within a lipid-based nanoparticle delivery system critical for protecting RNA from degradation and ensuring cellular uptake.
Endosomal Escape	A critical step in RNA delivery where lipid nanoparticles destabilise the endosomal membrane, releasing encapsulated RNA into the cytoplasm for translation.
Furin-T2A	A genetic engineering strategy introducing a furin cleavage site and a T2A self-cleaving peptide sequence to enhance the expression and trafficking of the RVFV glycoproteins Gn and Gc to the cell surface.
Gn and Gc Glycoproteins	Structural proteins encoded by the RVFV medium segment, essential for virion assembly, host receptor binding, and entry into target cells. They are key antigens in vaccine development.
Golgi Targeting Signal	A sequence motif within the RVFV glycoproteins that directs their localization to the Golgi apparatus for proper assembly, processing, and secretion during virion maturation.
Immunogenicity	The capacity of an antigen or vaccine to elicit an immune response, including the production of antigen-specific antibodies and activation of T-cell responses.
In vitro Transcription (IVT)	A method for synthesizing RNA using a DNA template and a phage-derived RNA polymerase (e.g., T7), often followed by capping and purification for therapeutic or vaccine applications.
Innate Immune Response	The immediate, non-specific defence mechanism against pathogens, mediated by pattern recognition receptors (PRRs) such as Toll-like receptors (TLRs) and retinoic acid-inducible gene I (RIG-I)-like receptors.
Lipid Nanoparticles (LNPs)	Nanocarriers composed of ionizable lipids, cholesterol, phospholipids, and polyethylene glycol-lipids, used to encapsulate RNA and facilitate endosomal escape for intracellular delivery.

Neutralising Antibodies (nAbs)	Antibodies that bind to viral surface epitopes and prevent virion attachment or fusion with host cells, playing a critical role in immunity against RVFV.
Pathogen-Associated Molecular Patterns (PAMPs)	Conserved molecular motifs present on pathogens (e.g., dsRNA, LPS) recognized by the innate immune system through pattern recognition receptors, initiating immune signalling cascades.
RiboGreen Assay	A fluorescence-based assay that quantifies RNA by selectively binding to nucleic acids, commonly used to measure encapsulation efficiency in nanoparticle formulations.
Rift Valley Fever (RVF)	An arboviral disease characterized by fever, hepatic necrosis, and haemorrhagic syndrome in animals, with zoonotic potential leading to encephalitis and retinitis in humans.
RVFV (Rift Valley Fever Virus)	A negative-sense RNA virus belonging to the genus *Phlebovirus* in the family *Phenuiviridae*. It causes Rift Valley Fever (RVF), a zoonotic disease transmitted primarily by mosquitoes, affecting humans and ruminants.
Self-amplifying RNA (saRNA)	A next-generation RNA vaccine platform derived from alphavirus genomes, capable of intracellular replication via a viral replicase, enabling prolonged antigen expression and reduced RNA dosage.
T2A Peptide	A self-cleaving peptide sequence that facilitates the co-expression of multiple proteins from a single open reading frame by ribosomal skipping during translation.
Venezuelan Equine Encephalitis Virus (VEEV)	An alphavirus used as a backbone for saRNA systems, leveraging its subgenomic promoter for robust antigen expression.

List of Figures

Figure 1: Rift Valley fever virus global distribution. ..... - 22 -
Figure 2: The RVFV transmission cycle ..... - 23 -
Figure 3: Rift Valley fever virus replication cycle ..... - 29 -
Figure 4: Rift Valley fever virus genome organisation ..... - 30 -
Figure 5: Adaptation of the alphavirus genome to make self-amplifying RNA..... - 37 -
Figure 6: Mutations made to the RVFV medium (M) segment consensus sequence..... - 61 -
Figure 7: RVFV M segment consensus sequence..... - 83 -
Figure 8: Phylogenetic analysis of the RVFV M segment consensus sequence..... - 85 -
Figure 9: Verification of cloning of RVFV M segment sequences into pcDNA3.1(+)..... - 87 -
Figure 10: Gn and Gc expression from whole-cell lysates using SDS-PAGE and western blot- 88 -
Figure 11: Cell surface expression of Gn and Gc by flow cytometry ..... - 91 -
Figure 12: Sequencing of WT consensus and Furin-T2A plasmid DNA replicons ..... - 96 -
Figure 13: Verification of pDNA linearisation and saRNA quality ..... - 97 -
Figure 14: In vitro expression of Gn from saRNA-transfected HEK293 cells..... - 100 -
Figure 15: Encapsulation efficiency of saRNA measured by the RiboGreen assay..... - 101 -
Figure 16: Anti-Gn IgG responses in BALB/c mice vaccinated with RVFV pDNA..... - 105 -
Figure 17: Anti-Gn IgG in mice immunised with candidate LNP-saRNA RVF vaccines- 106 -
Figure 18: Pseudovirus neutralising activity in the serum of mice immunised with candidate LNP-saRNA RVFV vaccines ..... - 108 -
Figure 19: Anti-Gn IgG in mice immunised with in vivo-jetRNA saRNA RVFV vaccines .... - 109 -
Figure 20: Baseline RVFV glycoprotein n (Gn) IgG ELISA responses in study mice .... - 111 -
Figure 21: Anti-Gn and anti-Gc IgG in mice immunised with in vivo-jetRNA+ saRNA RVFV candidate vaccines..... - 112 -
Figure 22: RVFV pseudovirus neutralising activity in serum from mice immunised with in vivo-jetRNA+ candidate saRNA RVFV vaccines..... - 114 -
Figure 23: IFN-γ production by ELISpot in splenocytes from mice vaccinated with candidate saRNA RVFV vaccines ..... - 115 -
Figure 24: T-helper cytokine production in mice immunised with in vivo-jetRNA+ saRNA RVFV vaccines..... - 116 -

1.0 CHAPTER ONE: INTRODUCTION

1.1 Background

Rift Valley fever (RVF) is a serious zoonosis caused by the Rift Valley fever virus (RVFV), an arthropod-borne pathogen primarily transmitted through mosquito bites [1]. It derives its name from the Rift Valley region of Kenya, where RVFV was first described in 1931 during a disease outbreak that was characterised by high rates of abortion in pregnant ewes and acute deaths of newborn lambs [2]. RVFV can infect humans and various domestic and wild animals. In domestic ruminants, RVFV infection leads to high rates of foetal and neonatal mortality, while in humans, it can cause severe symptoms such as ocular complications, meningoencephalitis, and a frequently fatal haemorrhagic fever [3, 4]. There is no specific antiviral treatment for RVF for humans or animals, but supportive care can be provided to manage symptoms [5].

Rift Valley fever is a disease of significant global public health importance. Although currently confined to Africa and parts of the Middle East, RVF poses a risk of spreading to new territories due to several contributing factors including the presence of competent mosquito vectors, a variety of susceptible domestic and wild animals, and the effects of climate change [6]. Due to its ability to cause severe consequences during an outbreak, RVF is considered a potential bioterror threat [7]. It is also listed as a notifiable disease by the World Organisation for Animal Health (OIE) [8] and a select overlap agent by the United States Department of Agriculture (USDA) and the Centers for Disease Control and Prevention (CDC) [9]. Additionally, RVF is included in the World Health Organisation (WHO) Research and Development Blueprint as a severe emerging disease requiring urgent and accelerated R&D to develop efficacious drugs or vaccines [10].

Several strategies can be used to control and prevent RVF, including surveillance and early detection, mosquito vector control, animal vaccination, culling of infected animals, restricting animal movement, implementing slaughter bans, and enforcing sanitary measures. However, these measures are difficult and often costly to implement, hindering their effectiveness. For example, animal importation and quarantine regulations are often poorly adhered to, while restrictions on animal exports can result in substantial economic loss [11, 12]. Slaughter bans are difficult to implement in pastoralist communities, which believe that sick animals should be slaughtered before they die so that their meat can be salvaged [13]. Although vector control through spraying and managing mosquito breeding grounds can effectively curb the spread of RVF, particularly during periods of heavy flooding, this strategy is often hampered by its high cost and the vast geographical extent of the endemic areas [14]. Culling may require the slaughter of numerous animals, making it a costly strategy to control RVF spread [15]. Surveillance and early detection as a method for preventing RVF have encountered difficulties because of the extended time between issuing an alert and confirming the initial RVF infection case [16]. Finally, sanitary measures to control RVF spread are often complicated by inadequate resources, lack of public awareness about RVF transmission, and cultural practices among pastoralist communities like consuming raw milk or blood from livestock [13].

Given the lack of RVF-specific treatment and the limitations of existing RVF control and prevention strategies, developing a safe and effective RVF vaccine is critically needed. Vaccination is considered the most effective way to prevent RVF outbreaks in animals in areas where the disease is endemic [14, 17]. There is currently no licensed RVF vaccine for human use, although two inactivated vaccines and a live attenuated vaccine have been tested and have had limited use in humans [18]. In contrast, a handful of live attenuated and inactivated RVF vaccines have been licensed for veterinary use, but they are generally characterised by suboptimal safety and potency, respectively [19]. Live attenuated RVF vaccines are associated

with risks of teratogenicity and residual virulence, while inactivated RVF vaccines require multiple doses to induce and maintain protective immunity. Additionally, nearly all livestock RVF vaccines lack the DIVA property (differentiating infected from vaccinated animals), making them unsuitable for use in RVF-nonendemic countries [20]. The shortcomings of current RVF vaccines highlight the urgent need for the development of new vaccines that are both safe and effective.

Recent advancements in vaccine technology have led to the development of self-amplifying RNA (saRNA) vaccines. This messenger RNA (mRNA)-based vaccine platform uses the genome of positive-sense single-stranded RNA viruses to replicate the mRNA encoding the antigen of interest within host cells. Self-amplifying RNA vaccines contain the essential regulatory elements of mRNA such as a 5′ cap, a 5′ untranslated region (UTR), a coding sequence (CDS), a 3′ UTR, and a poly (A) tail. In addition, saRNA encodes four non-structural proteins (nsP1–4) and a subgenomic promoter [21]. The non-structural proteins serve as the functional components of RNA-dependent RNA polymerase (RdRp), which is responsible for the extensive replication of the subgenomic mRNA that encodes the vaccine antigen. These additional elements of saRNA result in high and sustained levels of antigen expression, enabling the administration of a lower vaccine dose compared to conventional mRNA vaccines [22]. Self-amplifying RNA, like conventional mRNA, is also versatile and can be rapidly manufactured, making it suitable for developing vaccines against emerging infectious diseases like RVF [23].

Self-amplifying RNA vaccines against various infectious diseases have been evaluated in several studies including clinical trials for COVID-19 and rabies and preclinical studies for influenza, HIV, cytomegalovirus (CMV), respiratory syncytial virus (RSV), Zika, Ebola and other pathogens [24]. These studies have demonstrated the ability of this platform to induce humoral and cellular immune responses that are protective against the targeted pathogens. In

2022, the COVID-19 vaccine ARCT-154 became the first saRNA vaccine to receive emergency use authorisation for humans, approved for use in Vietnam [25].

1.2 Statement of the research problem

Rift Valley fever poses a serious threat to public health and the livestock industry globally. In humans, RVF infection may cause severe symptoms such as ocular complications, meningoencephalitis, or an often fatal haemorrhagic fever. Communities experiencing RVF outbreaks can face significant economic losses due to the high mortality rates among infected livestock and the effects of the control measures implemented, such as culling and restrictions on animal export and sale. RVF can be controlled and prevented using several strategies; however, vaccination remains the most effective way to prevent RVF outbreaks in animals in areas where the disease is endemic. A significant limitation of RVF vaccination is the lack of a licensed human vaccine and the suboptimal safety and immunogenicity of the licensed livestock vaccines. Self-amplifying RNA offers a promising platform for developing safe and effective RVF vaccines. This platform shares the desirable characteristics of conventional mRNA vaccines such as a good safety profile, the ability to induce a strong humoral and cellular immune response, suitability for rapid production, versatility, and scalability. Furthermore, the self-replicating nature of saRNA allows for more robust and prolonged antigen expression, which enables the use of lower doses than those of conventional mRNA vaccines.

Several candidate RVF vaccines have been developed using various vaccine platforms, including virally delivered RNA replicons and conventional mRNA [26-28]. However, no studies have yet reported on the development of a non-virally delivered saRNA RVF vaccine. Developing an effective vaccine requires a thorough understanding of the immune correlates of protection against the pathogen. The correlates of protection for RVF are not yet fully

understood, although neutralising antibodies targeting the virus's surface glycoproteins n (Gn) and c (Gc) have been shown to prevent infection, with their titres correlating with protection against virulent RVFV challenge [29-31]. These glycoproteins, which are encoded by the virus's medium (M) segment, are not efficiently delivered to the cell surface due to a Golgi apparatus-localising signal and endoplasmic reticulum (ER)-retention motif located in the cytoplasmic tails of these glycoproteins [32]. The removal or mutation of the M segment sequences encoding these cytoplasmic tails has been shown to increase the expression of these glycoproteins on the plasma membrane [33, 34]. However, it remains to be demonstrated whether increasing the cell surface expression of Gn and Gc by mutation enhances immunogenicity.

1.3 Objectives

Primary Objective

To design a saRNA RVF vaccine and evaluate its immunogenicity in mice

Specific objectives

1. To design and evaluate the *in vitro* expression of Gn and Gc from a consensus and mutated RVFV M segment sequences optimised to enhance cell surface expression.
2. To synthesise and characterise saRNA constructs encoding a consensus and a mutated RVFV M segment sequence optimised to enhance cell surface expression.
3. To assess the humoral and cellular immune responses elicited in mice immunised with candidate saRNA RVF vaccines.

1.4 Study hypothesis

Directing Gn and Gc expression to the plasma membrane by mutation enhances the immunogenicity of the RVFV envelope glycoproteins.

2.0 CHAPTER TWO: LITERATURE REVIEW

2.1 Rift Valley fever epidemiology

Rift Valley fever has been identified in most countries on the African continent, and in Madagascar, the Comoros Islands, Saudi Arabia, and Yemen (Figure 1) [35-42]. Some notable RVF outbreaks include the one in Kenya in 1931, which was the first documented [43, 44], the 1950–1951 outbreak in Kenya [39], and the 1974–76 outbreak in South Africa, where the first human fatality from RVFV was recorded [45]. One of the largest RVF outbreaks occurred in Egypt between 1977 and 1979, when RVF spread outside sub-Saharan Africa for the first time, causing an estimated 20,000-200,000 human infections and 598 deaths [46]. Other major RVF outbreaks include those in Kenya, Somalia, and Tanzania in 1997-98 and 2007 [47], Saudi Arabia and Yemen in 2000 when the first cases of RVF were recorded outside Africa [48], and those in South Africa in 2008 and 2010, Sudan in 2008, and Mauritania in 2010 [42]. Generally, major RVF outbreaks have been associated with heavy rainfall and flooding, which create ideal conditions for mosquito breeding, the primary vectors of RVFV [49].

A systematic literature review of RVFV seroprevalence in livestock, wildlife, and humans in Africa from 1968 to 2016 reported variations in the prevalence of this infection among these groups. The median RVFV seroprevalence in sheep, cattle, wildlife, goats, camels, and humans was 12.9% (range 0–100%), 12.6% (range 0–100%), 11.3% (range 0–87.5%), 10.1% (range 0–69.6%), 8.8% (range 0–57.1%), and 5.9% (range 0–81.0%) respectively. Notably, RVFV seroprevalence was significantly higher during outbreaks compared to interepidemic periods in goats and sheep but not in cattle, camels, or humans [50].

Figure 1: Rift Valley fever virus global distribution.

This figure shows a map of countries where RVF has been reported. Adapted from Centers for Disease Control and Prevention (May 2024). *Rift Valley Fever: About*. Retrieved August 1, 2024, from https://www.cdc.gov/rift-valley-fever/about/index.html [51].

Transmission of RVFV in animals occurs through mosquito bites. In humans, RVFV may be transmitted via mosquito bites; however, most infections occur through direct contact with the tissue, blood, or fluids of infected animals or their aerosolised blood during slaughter [52] (Figure 2). Exposure to raw milk from infected animals, either during milking or consumption, is also a risk factor for acquiring RVFV [53]. Animal-to-animal and human-to-human transmission of RVFV has not been documented, although vertical transmission readily occurs in animals and has been reported in humans [54, 55]. Numerous mosquito species, primarily in the Aedes and Culex genera, can transmit RVFV, while other arthropods, such as ticks, midges, and houseflies, have the potential to act as mechanical vectors [56, 57]. In interepidemic periods, RVFV is thought to remain dormant in transovarially-infected eggs of

floodwater-breeding Aedes mosquitoes in the dry soil of dambos or pans [58]. During periods of heavy rainfall, the infected eggs can hatch into infectious mosquitoes, resulting in RVFV transmission to nearby animals and humans [59]. RVFV can also be maintained in circulation by cycling between its vectors and wildlife and domestic animal hosts. Low-level circulation of RVFV in livestock and wildlife can occur without causing disease outbreaks [60, 61]. Additionally, mounting evidence suggests that low-level RVFV transmission to humans and animals occurs outside known epidemic periods [62].

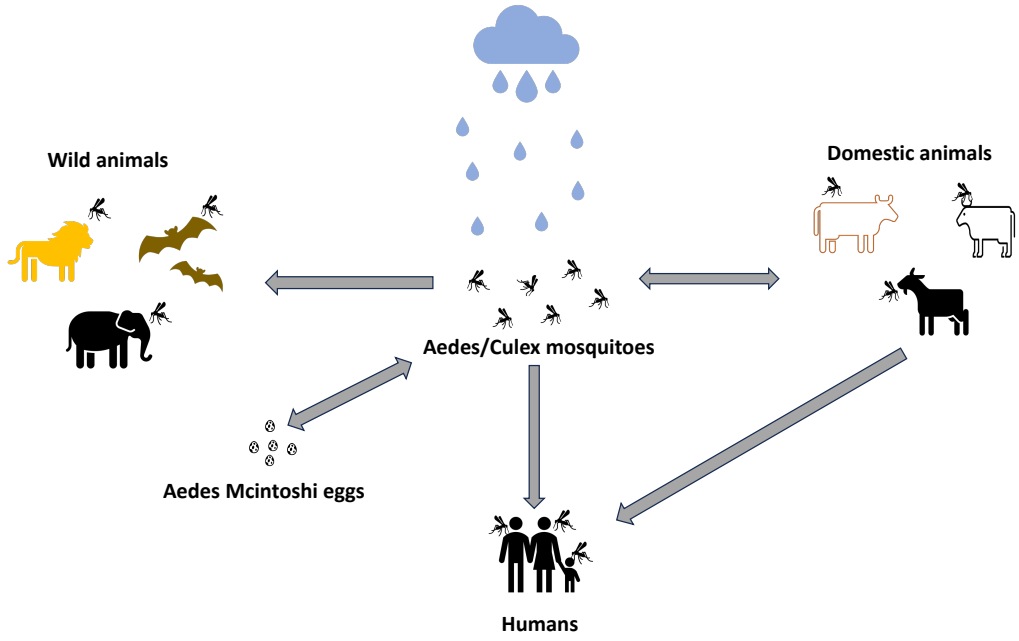

Figure 2: The RVFV transmission cycle

RVFV is transmitted in animals through mosquito bites. In humans, it may be transmitted by mosquitoes, but most infections occur through direct contact with the tissue, blood, or fluid of infected animals. During interepidemic periods, RVFV is maintained in transovarially-infected eggs of Aedes mosquitoes and wild animals, which can maintain low-level infections. Periods of heavy rainfall result in the hatching of infected Aedes eggs, leading to infection of animals, which may then spill over to humans.

2.2 Pathogenesis of Rift Valley fever

2.2.1 Animal infections with RVFV

Rift Valley fever infects several domestic and wild animals, including sheep, goats, cattle, camels, donkeys, elephants, lions, wildebeest, bats, gazelles, impala, and springbok [4]. Wild animals tend to experience mild or inapparent RVFV infections, whereas domestic animals are more susceptible to the disease [63]. The manifestation of RVF as a clinical disease in animals varies widely depending on the age and species of the infected animal. Among livestock, sheep are the most susceptible. Newborn lambs and goat kids less than a week old are highly susceptible to RVFV infection, with mortality often exceeding 90% within two days of the onset of illness [64]. In pregnant sheep and goats, RVFV infection results in nearly 100% foetal mortality, while in cattle, it is about 85% [4]. Rift Valley fever virus infection in susceptible, older non-pregnant animals is often asymptomatic. Abortion may be the only overt manifestation of the disease in a herd or flock, even though adult livestock are susceptible to peracute disease, resulting in death before any clinical signs appear [65]. When RVF symptoms appear in animals, they typically present as weakness, anorexia, diarrhoea, bloody nasal discharge, and jaundice [3].

2.2.2 Human infections with RVFV

Even though RVFV can be acquired through mosquito bites, most human RVF infections result from contact with tissue or fluids of infected animals [52]. After an incubation period typically lasting four to six days, most people infected with RVFV develop a self-limiting febrile illness characterised by severe chills [45], malaise, fever, severe headache, rigours [66], and flushed face [67]. Symptoms typically lessen after three days, with body temperature normalising by the fourth day. A few days after body temperature normalisation, some RVF patients may

experience a recurrence of high fever accompanied by a severe headache lasting several days [3]. The RVF virus can be detected in the blood during the three to four-day febrile period, whereas neutralising antibodies appear around the fourth day of symptom onset [68].

A small percentage of patients (<10%) develop a severe form of RVF disease characterised by three distinct syndromes: ocular complications, meningoencephalitis, or haemorrhagic fever [3]. Ocular complications are the most frequently reported symptom in severe RVF disease [65, 69]. Patients may experience reduced vision in one or both eyes, blind spots, photophobia, and retro-orbital pain [70]. Additionally, some patients also suffer from maculopathy or retinopathy. The affected eyes have macular oedema with exudates that contain a white mass covering the macular area with or without retinal haemorrhage, vasculitis, infarction, or vitreous haze [70]. Ocular lesions may develop one to three weeks after symptom onset, with macular or paramacular retinitis being the most common and specific type [71]. In many cases, incomplete recovery of vision and chorioretinal scarring can remain in macular and paramacular areas despite the resorption of exudates.

The meningoencephalitic form of RVF occurs in less than 1% of patients, and presents one to four weeks after symptom onset. It is characterised by intense headaches, hallucinations, disorientation, dizziness, insomnia, delirium, vertigo, convulsions, excessive salivation, weakness, and partial paralysis [72]. Although death from encephalitis in RVF patients is rare, neurological deficits may be prolonged or permanent [36].

The most severe form of human RVF disease is the haemorrhagic fever form. The first symptoms of this type of RVF disease include severe liver impairment such as jaundice, followed by haemorrhage signs such as hematemesis, passing blood in stool, ecchymoses (due to skin bleeding), bleeding from the nose or gums, and venepuncture sites. Elevated levels of the liver enzymes aspartate transaminase (AST) and alanine transaminase (ALT) also occur,

with the highest levels occurring in fatal cases [3]. Approximately 50% of patients with the haemorrhagic form of RVF die, typically three to six days after symptom onset [73].

2.3 Rift Valley fever diagnosis

2.3.1 Diagnosis in humans

The early stage of RVFV infection in humans is difficult to diagnose because of the non-specific nature of its symptoms. Typical symptoms such as fever, muscle pain, and headache resemble those of other hemorrhagic fevers and fever-causing infections such as malaria, shigellosis, typhoid, and yellow fever [17]. According to WHO, confirmation of RVFV infection requires the detection of RVFV RNA by reverse transcriptase-polymerase chain reaction (RT-PCR) in serum or plasma, and immunoglobulin M (IgM) and immunoglobulin G (IgG) detection by enzyme-linked immunosorbent assay (ELISA) [5]. Several molecular tests can be used to detect RVFV RNA, including one-step reverse transcription polymerase chain reaction (RT-PCR), real-time RT-PCR, and reverse transcription loop-mediated isothermal amplification (RT-LAMP). RT-LAMP is the most widely used molecular assay to detect RVFV infection in humans [74].

Serological tests for detecting RVFV infection include IgM and IgG ELISA, the virus neutralisation test (VNT), and, less commonly, indirect immunofluorescent assay (IFA) [74]. IgM ELISA can determine recent RVFV infection, as IgM is detectable for two to three months after infection [75]. In contrast, IgG ELISA can detect previous RVFV infections, as IgG persists for several years after infection [5]. ELISA-based seroprevalence testing may be complicated by low specificity, possibly due to cross-reactivity with other phleboviruses. In such cases, positive results–especially when the seroprevalence is low–should be confirmed using the highly specific VNT, which is generally considered the gold standard diagnostic assay [75].

The same methods used for RVFV detection in humans can also be applied to animals. In addition, a histopathologic examination of the liver can be performed to identify characteristic hepatic lesions, and immunohistochemical staining can be done to detect the presence of RVFV. Alternatively, RVFV can be identified through isolation in cell culture. For this, mammalian cell lines are preferred because RVFV induces a consistent cytopathic effect, characterised by minor cell rounding, followed by complete destruction of the cell layer within 12 to 24 hours [76].

2.4 The Rift Valley fever virus replication cycle

RVFV infects cells by receptor-mediated endocytic uptake and low pH-triggered membrane fusion. Infection is initiated by viral attachment to the host plasma membrane through the interaction between Gn and Gc displayed oligomannose-type glycans and the C-type lectins DC-SIGN and L-SIGN [77, 78]. This is followed by Gn-Gc caveolin-1-mediated endocytosis, which is facilitated by the acidic environment of the endosome [79]. Gn enables a pH-dependent host and virion membrane merger by adopting a class-II fusion protein fold [80]. In this process, a translational shift of Gn occurs, unshielding Gc to expose a nonpolar fusion loop segment. This segment inserts into the target membrane while Gc adopts an extended intermediate conformation, bridging the two membranes. The intermediate then collapses into a “hairpin” that brings the membranes into proximity [80]. After the fusion of viral and endosomal membranes, the viral nucleocapsid, composed of the three genomic segments, is released into the cytoplasm. Primary transcription of the genomic RNA into mRNA is then initiated by the RdRp, which is encoded by the L segment of the viral genome [81] (Figure 3). The RdRp synthesises complementary RNA strands, which serve as templates for producing new viral RNA genomes. The viral nucleoprotein and polymerase are synthesised in the cytoplasm, forming ribonucleoprotein complexes together with newly produced genomic RNA

[82]. The Gn and Gc precursor protein is translated at the ER, which is then cleaved by signal peptidase to yield the individual glycoproteins [83]. The nascent precursor polypeptide chain is translocated from the cytoplasm into the ER due to a signal peptide preceding Gn.

Two hydrophobic domains located in the C-termini of Gn and Gc within the Gn-Gc precursor serve as transmembrane domains of these glycoproteins. Additionally, a third hydrophobic domain separates Gn and Gc and acts as an internal Gc signal peptide, which is also cleaved by signal peptidase, thus separating Gn from Gc [83]. The Gn cytoplasmic tail is also involved in initiating the budding process and packaging ribonucleoproteins (RNPs) into virus particles [84]. After co-translational processing of the M segment-encoded polyprotein, Gn and Gc leave the ER and migrate to the Golgi apparatus, facilitated by a Golgi apparatus targeting signal located within the C-terminal sequence of Gn [32]. The Gc contains an ER retention signal, a basic dilysine motif in its short C-terminal domain [85]. Complex formation between Gn and Gc results in the masking of the Gc ER retention signal, thereby enabling the transportation of Gc to the Golgi. In the Golgi, correctly folded Gn-Gc heterodimers associate with RNPs via the cytoplasmic tails of Gn, facilitating the budding process. After the budding of new virions into the Golgi lumen is complete, virus-containing vesicles are transported to the plasma membrane, where the virions are released by exocytosis [86].

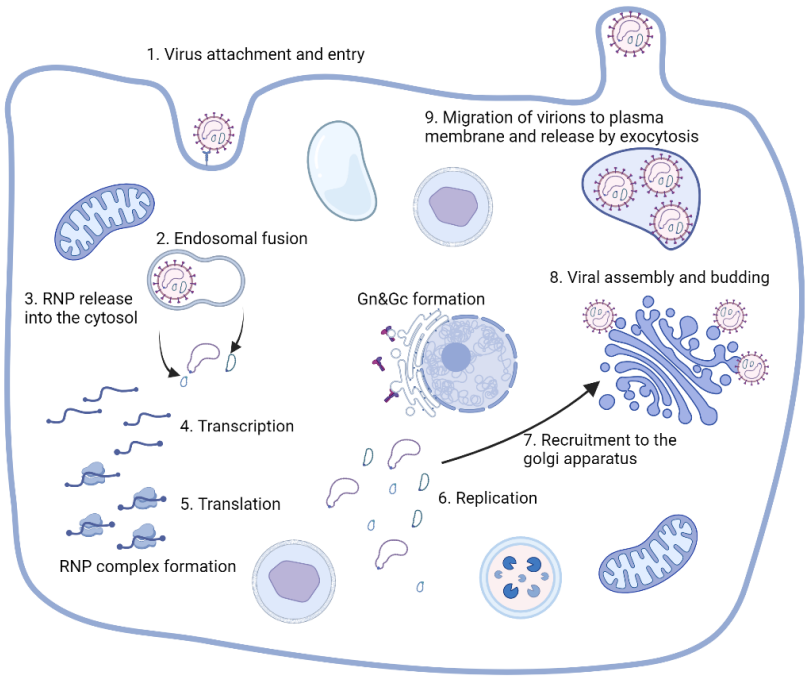

Figure 3: Rift Valley fever virus replication cycle

(1) Viral attachment and entry into the host cell by endocytosis. (2) Endosomal fusion. (3) Acid-activated release of RNPs from the endosomes into the cytoplasm. (4) Primary transcription of genomic RNA to mRNA by viral RdRp. (5) Translation of L and S-encoded mRNA in the cytoplasm and M segment mRNA by membrane-bound ribosomes in the ER. (6) Replication of RNPs in the cytoplasm. (7) Recruitment of newly replicated viral genomic segments and proteins to the Golgi apparatus. (8) Packaging and budding of virions into the Golgi lumen. (9) Migration of Golgi vesicles containing viruses to the cell surface and release by exocytosis. This figure was created using BioRender.

2.5 Rift Valley fever virus genome organisation and viral structure

The Rift Valley fever virus is a *Phlebovirus* belonging to the Phenuiviridae family and *Bunyavirales* order [87]. The virus has a predominantly negative-sense tripartite RNA genome consisting of large (L), medium (M), and small (S) segments, which are 6404, 3885, and 1690 nucleotides long, respectively (Figure 4). The negative-sense L segment encodes the RdRp, which synthesises both viral mRNA and genomic RNA. The negative-sense M segment encodes a polyprotein precursor that is cleaved into several nested polyproteins including: a 78-kDa protein (nt 21-2090), a 14-kDa non-structural protein NSm (nt 135-479), Gn (nt 480-2090) and Gc (nt 2091-3614) [83]. Synthesis of the M segment proteins involves leaky

ribosome scanning at five initiation codons at nucleotide positions 21, 135, 174, 411, and 426 in the NSm region [38]. The 78-kDa protein is synthesised from the first initiation codon and NSm from the second. The fourth initiation codon gives rise to Gn and Gc only [84]. These surface glycoproteins form heterodimers on the surface of the RVFV virion and are essential for virus attachment to initiate infection. The function of the 78-kDa protein is not fully understood, but it may aid in the transmission of RVFV from mosquitoes to ruminants, possibly affecting virus replication in the mosquito host [88]. The ambisense S segment encodes the 27-kDa nucleoprotein (N) and 30-kDa non-structural protein NSs [38]. The NSm and NSs proteins are essential for viral pathogenesis. The NSm is an anti-apoptotic protein [89], while the NSs is a major viral virulence factor that inhibits host innate immune responses [90, 91]. However, both proteins are dispensable for viral maturation, replication, and infection [92, 93].

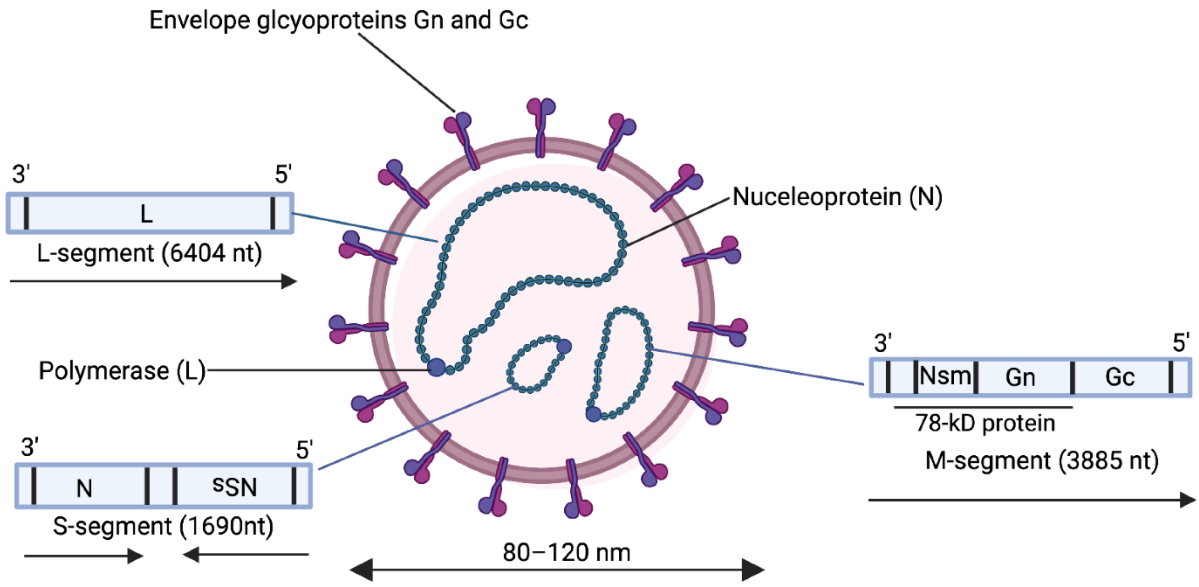

Figure 4: Rift Valley fever virus genome organisation

The Rift Valley fever virus has a tripartite genome consisting of a negative-sense large (L) segment, a negative-sense medium (M) segment and an ambisense small (S) segment. The segments are encapsidated by the nucleoprotein (N) into ribonucleoproteins that are associated with the viral polymerase (L). The surface of the virion is covered by Gn and Gc heterodimers. Adapted from Kitandwe, P. K., McKay, P. F., Kaleebu, P., & Shattock, R. J. (2022). An Overview of Rift Valley Fever Vaccine Development Strategies. *Vaccines*, *10*(11), 1794. https://doi.org/10.3390/vaccines10111794.

The RVFV virions are spherical, consisting of an envelope and an RNP with an average diameter of 95 ± 9 nm [38, 87]. The envelope of the RVFV consists of a lipid bilayer derived from the host cell membrane during viral budding. Embedded within this envelope are the Gn and Gc heterodimers, which form spikes protruding from the surface of the virion (Figure 4). The virion surface consists of 720 heterodimers made up of 110 cylindrical glycoprotein hexamers and 12 pentamers, forming 122 glycoprotein capsomeres arranged in an icosahedral lattice with a T = 12 configuration. The capsomers resemble hollow cylinders located at the five and six-sided capsomers [94-96]. Envelope surface projections 9 nm long form distinctive spikes that cover the virion surface embedded in a 7 nm lipid bilayer [38]. The Gn forms the capsomer spikes while Gc lies partially underneath, closer to the lipid membrane [82]. Inside the envelope, the viral RNA segments are encapsidated by the nucleoprotein (N), forming the nucleocapsid. Each RNA segment is individually associated with multiple N proteins, creating RNPs. The N protein protects the viral RNA and ensures its proper packaging into new virions. The L protein, or RdRp, is associated with the RNPs. It is responsible for the replication and transcription of the viral RNA genome, ensuring the production of new viral RNAs and proteins required for assembling new virions [97].

2.6 Immunity against Rift Valley fever virus infection

2.6.1 RVFV immune evasion mechanisms

RVFV employs various immune evasion strategies to counteract the host's immune responses, with the majority mediated by the NSs protein. This protein disrupts multiple cellular pathways crucial for interferon (IFN) production and signalling. By interacting with host Sin3A-associated protein 30 (SAP30), a component of the histone deacetylase complex, NSs maintains IFN-β signalling in a transcriptionally silent state, thereby promoting viral replication [98]. Additionally, NSs degrades double-stranded RNA (dsRNA)-dependent

protein kinase (PKR), which prevents the phosphorylation of eIF2α, thereby promoting viral translation and suppression of the host's immune defence [90]. NSs has also been shown to induce cell cycle arrest at the S or G0/G1 phase, disrupting cellular processes to facilitate RVFV replication [99, 100]. Another immune evasion strategy RVFV uses involves modifying its 5′ termini to avoid recognition by RIG-I [101]. RIG-I recognises uncapped 5′-triphosphate single stranded RNA (ssRNA) and short dsRNA formed during viral replication. This triggers downstream signalling that restricts the viral life cycle *in vitro* in the early stages after internalisation and before replication.

2.6.2 Innate immune responses to RVFV infection

The innate immune system provides the first line of defence against invading pathogens and is crucial in triggering adaptive immunity. It consists of external barriers such as skin and mucous membranes, immune cells such as macrophages, dendritic cells (DCs), natural killer (NK) cells, as well as other cell types like epithelial cells [102]. Invading pathogens, including viruses, are recognised by various pattern recognition receptors (PRRs) within host cells such as Toll-like receptors (TLRs), RIG-I-like receptors (RLRs), and NOD-like receptors (NLRs). These PRRs sense conserved structural and functional molecules of pathogens known as pathogen-associated molecular patterns (PAMPs) [103]. Through interactions with PAMPs, the PRRs activate several intracellular signalling pathways, thereby inducing the production of type I IFNs such as IFN-α and IFN-β, which play a critical role in inhibiting viral replication and spread by inducing an antiviral state in neighbouring cells [104]. Production of pro-inflammatory cytokines such as interleukin-6 (IL-6), tumour necrosis factor-alpha (TNF-α), and interleukin-1 beta (IL-1β) also occurs, resulting in the recruitment and activation of immune cells to the site of infection, aiding in viral clearance.

In human RVFV infection, the balance between anti- and pro-inflammatory cytokines and chemokines largely defines the disease outcome. Fatal RVFV infection cases were associated with higher levels of IL-10, an anti-inflammatory cytokine, compared to survivors and negative controls. Chemokines, along with both pro- and anti-inflammatory cytokines, were significantly altered, with some increasing (IL-8, CXCL9, MCP-1, IP-10, IL-10) and others decreasing (RANTES) when comparing fatal cases with infected survivors and uninfected controls [105]. In goats, where the infection course of RVFV was similar to that observed in other ruminants, the virus triggered the production of IFN-γ, IL-12, and other pro-inflammatory cytokines but not IFN-α. The virus targeted dendritic cells (DCs) and monocytes, inhibiting the IFN-α response and allowing rapid viral replication. Additionally, infection with insect cell-derived RVFV differed from mammalian cell-derived RVFV, with the former reaching peak viremia more quickly, inducing fever, and significantly impacting specific immune cell subpopulations [106]. This observation aligns with findings that insect cell-derived arboviruses, particularly those in the Alphavirus genus, were more infectious to monocyte-derived dendritic cells (MoDCs) than their mammalian cell-derived counterparts, potentially due to stronger recognition and binding to C-type lectin receptors [107, 108].

2.6.3 Adaptive immune responses to RVFV infection

Protection against RVFV infection is conferred by neutralising antibodies (nAbs), which are detectable within the first week of infection [109]. Passive serum transfer of neutralising antibodies in non-human primates and rodent models has confirmed the role of these antibodies in protecting against RVFV infection [110]. Therefore, the generation of neutralising antibodies is a good correlate of protection against RVFV infection. Following RVFV infection, neutralising antibodies produced are primarily directed against Gn, Gc, nucleoprotein N, and the non-structural protein NSs. Although Nucleoprotein N is the major

immunogen in bunyavirus infection, it does not elicit virus-neutralising activity [109]. Anti-Gn and anti-Gc antibodies are generated following RVF infection; however, it has been shown that anti-Gn alone is sufficient to provide protection. Gn-specific monoclonal antibodies (mAbs) isolated from a convalescent patient were protective and blocked virus binding to cells [111]. Studies have also shown that vaccination of rabbits with the ectodomain of Gn induces the production of mAbs that can protect mice against RVFV infection [112].

The role of T cells in controlling RVFV infection, particularly after natural exposure, remains unclear. In a mouse model, the control of RVFV replication *in vivo* and the prevention of the development of RVFV neurologic disease were found to rely on strong antibody responses and functional CD4+ T cells but not CD8+ T cells [113]. In another study in which African green monkeys were challenged with RVFV, the early proliferation of CD4+ and CD8+ T cells and expression of Th1 cytokines were associated with non-lethal outcomes [114]. This supports findings that higher concentrations of IL-10, a cytokine that suppresses Th1 response, are associated with fatal cases compared to non-fatal cases in humans [115].

2.7 Rift Valley fever vaccines

Currently, there is no licensed RVF vaccine for human use, although two inactivated vaccines–NDBR-103 and TSI-GSD-200–and a live attenuated vaccine, MP-12, have been tested and have had limited use in humans [18]. In contrast, a handful of live attenuated and inactivated RVF vaccines are licensed for veterinary use, but they have suboptimal safety and potency, respectively [19]. Additionally, nearly all currently licensed RVF vaccines lack the DIVA property, making their universal adoption in RVF-non-endemic countries problematic. Due to these limitations, substantial research has been ongoing to develop safer and more efficacious RVF vaccines for animal and human use.

2.7.1 Licensed RVF Vaccines

2.7.1.1 Licensed live attenuated vaccines

The first licensed RVF vaccine and one of the most widely used is the Smithburn vaccine, which was developed in 1949 by attenuating the neurotropic Smithburn RVFV Entebbe strain through 102 serial passages in mouse brain [116]. Despite its relatively low cost and ability to induce long-lasting immunity after a single dose, the Smithburn vaccine has been associated with numerous serious adverse events, including meningoencephalitis, foetal malformations, abortions, RVFV-associated pathologies, and mortality [117-120]. Consequently, the Smithburn vaccine is not recommended for use in RVF non-endemic countries [121].

Another widely used live attenuated RVF vaccine is the Clone 13 vaccine, developed using the RVFV strain 74HB59, which has a 69% natural deletion in the pathogenic NSs gene. This strain was isolated from a nonfatal human case of RVFV infection during the 1974 RVF outbreak in the Central African Republic [122]. While the vast majority of studies have shown that the Clone 13 RVF vaccine is safe, highly immunogenic, and protective against virulent RVFV infection, one study reported that when administered in an excessive dose to pregnant ewes in their first trimester, it can cause foetal infections, stillbirths, and malformations of the central nervous system or skeletal system [123].

2.7.1.2 Licensed inactivated RVFV vaccines

At least three inactivated RVF vaccines have been developed for veterinary use in RVF-endemic countries. These vaccines are the BEI-inactivated RVF ZH501 vaccine (BEI-inactivated ZH501-VSVRI), the formalin-inactivated vaccine based on the RVFV Menya strain (formalin-inactivated Menya/Sheep/258), and the formalin-inactivated vaccine derived from a field strain isolated from a cow in South Africa [124-126]. These vaccines are safe, but

their effectiveness is limited by the need for two initial doses to induce protective immunity and annual boosters to maintain it.

2.7.2 Candidate RVF vaccines

Significant research to develop safer RVF vaccine candidates has been ongoing–greatly aided by a better understanding of the molecular biology of the RVFV, the protective immune responses required, and advances in recombinant DNA technology. The use of reverse genetics to remove or mutate the virulence genes in wild-type and conventionally attenuated live RVFV has been a major strategy for developing safer live attenuated RVF vaccines. These genetically modified live attenuated vaccines have been shown to induce robust protective immune responses often similar to those induced by the Smithburn vaccine but with significantly milder and fewer adverse effects. RVF vaccines based on platforms such as DNA, viral vectors, recombinant subunit proteins, virus-like particles (VLPs), and replicon-deficient virus replicons have all been explored. A discussion on the development of these RVF vaccines is provided by Kitandwe et al. [20].

2.8 Self-amplifying RNA vaccines

2.8.1 Structure of self-amplifying RNA vaccines

Self-amplifying RNA (saRNA) vaccines are a type of mRNA vaccine that utilises the genome of a positive-sense, single-stranded RNA virus to replicate. They contain the essential elements of mRNA vaccines–a 5′ cap, a 5′ untranslated region (5′ UTR), a 3′ UTR, and a poly(A) tail. In addition, saRNA vaccines carry a large open reading frame (ORF) at the 5′ end that encodes four non-structural proteins (nsP1–4) and a subgenomic promoter. The nsP1-4 proteins are translated into the RdRp complex, enabling saRNA to replicate itself once delivered into the cell cytoplasm. The genomes most commonly used to make saRNA are those from

alphaviruses, usually Semliki Forest virus (SFV), Sindbis virus (SINV), and Venezuelan equine encephalitis virus (VEEV) [127, 128]. These genomes contain two ORFs encoding nsP1-4 and five structural proteins: capsid and glycoproteins E3, E2, 6K, and E1 at the 3′ end [129] (Figure 5).

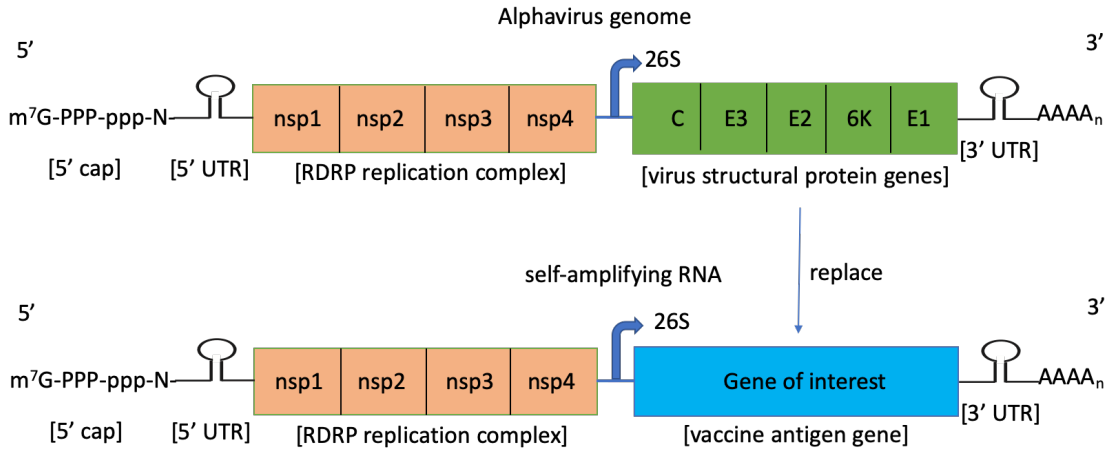

Figure 5: Adaptation of the alphavirus genome to make self-amplifying RNA

Figure 5 illustrates how the Alphavirus genome is adapted to make saRNA vaccines. The viral structural genes responsible for infectivity are replaced with those of the vaccine antigen under the control of the 26S subgenomic promoter. The four non-structural proteins (nsp1-4) make up the replication complex, which replicates the heterologous vaccine antigen genes. The rest of the backbone is similar to that of conventional mRNA.

As a result of encoding nsP1-4, saRNA is considerably larger (approximately 9–12 kb) than conventional non-amplifying mRNA. To try to overcome this problem, a two-vector trans-amplifying RNA (taRNA) system has been developed [130]. The first vector is an *in vitro*-transcribed mRNA encoding an alphavirus replicase, while the second vector is the trans-replicon (TR) RNA, which encodes the respective antigen under the control of the subgenomic promoter. The TR-RNA is amplified by the alphavirus replicase in trans as it contains the alphavirus 5′- and 3′- conserved sequence elements (CSEs) [131]. The taRNA vaccine candidate was shown to induce protective immune responses with less antigenic RNA compared to saRNA [130]. A novel bivalent taRNA vaccine candidate that utilises three RNAs,

with one encoding the replicase and two antigen-encoding TR-RNAs, has also been described. This vaccine candidate induced potent Chikungunya and Ross River virus-specific immune responses [132]. TaRNA vaccines offer enhanced safety, manufacturability, and optimisation potential compared to saRNA vaccines [133]. Their shorter RNA compared to saRNA makes their scaled-up production easier. However, two RNAs must be produced, and an effective *in vivo* delivery formulation has yet to be demonstrated.

2.8.2 Synthesis of saRNA

The synthesis of saRNA is a cell-free production process that is fast, easily standardised, and scalable, making it an ideal platform for producing vaccines against emerging pathogens [24]. To make saRNA, the alphavirus structural genes at the 3′ end are replaced by the vaccine antigen genes in the viral genome's complementary DNA (cDNA) clone. *In vitro* transcription (IVT) of the linearised cDNA clone using phage RNA polymerases such as T7, T3, or SP6 generates a saRNA replicon [129]. This is followed by the addition of a 5′ cap structure, which can also be done during transcription (co-transcriptional capping) or enzymatically after transcription. Enzymatic capping is more complex but provides much higher yields: capping efficiency is nearly 100% and all capped structures are added in the proper orientation [134]. Co-transcriptional capping, in which a cap analogue is provided in excess in the transcription reaction, is much simpler than enzymatic capping, but the overall yields tend to be lower. After IVT and 5′ capping, untranscribed DNA is removed by DNase digestion, and the saRNA is purified using a variety of methods.

2.8.3 Functions of the different components of saRNA

The 5′ cap structure is required for translation initiation as the eukaryotic initiation factor 4E (eIF4E) recognises and binds to it. It shields the saRNA from intracellular digestion by exonucleases and helps prevent its recognition by innate immune sensors. This structure is one

of the mechanisms by which eukaryotic cells differentiate between self and non-self mRNA [135]. Eukaryotic cells utilise a 7-methylguanosine (m7G) cap that links to the mRNA by a 5′-5′-triphosphate bridge (ppp) (m7GpppN structure) [136]. Further methylation of the 2′-hydroxy-groups of the first ribose moiety and the second ribose produces the cap-1 and cap-2 structures, respectively. Viral RNAs often contain cap-0 structures, which only contain the m7G cap, making it readily detectable by the innate immune system. Consequently, cap-1 and cap-2 structures are better suited for mRNA and saRNA vaccine synthesis compared to the cap-0 structure as they mark the exogenous mRNA as "self RNA", thereby evading intracellular immune surveillance mechanisms.

The 5′ and 3′ UTRs have numerous roles, including regulation of mRNA export from the nucleus, regulation of translation efficiency, orchestration of subcellular localisation and providing mRNA stability [137]. The poly(A) tail works synergistically with the cap structure to enhance translation efficiency and prevent mRNA decapping and degradation [138, 139]. A sufficiently long poly(A) tail is necessary to circularise the mRNA by allowing polyadenosine-binding proteins (PABPs) to bind both the poly(A) tail and the cap [140, 141]. The non-structural proteins nsP1-4 constitute the functional components of the RdRp or viral replicase. They are translated from the positive-sense genomic RNA and transcribe full-length negative-sense RNA. The negative-sense RNA then serves as a template for genomic RNA and 26S subgenomic mRNA. The 26S promoter located between the two ORFs on the negative-sense RNA is recognised by the non-structural proteins for transcription of sub-genomic mRNA, from which the vaccine antigen genes are translated [129].

2.8.4 Optimisation of the saRNA sequence

The sequence of saRNA can be optimised to improve its stability, translation efficiency, and immunogenicity. These optimisations can be made to the backbone (5′ UTR, 3′ UTR, poly A tail) and the ORF as discussed below.

2.8.4.1 5′ and 3′ UTR optimisation

The two main functions of the 5′ UTR are to stabilise mRNA and to facilitate scanning by the small ribosomal subunit to localise the start codon [142], while the 3′ UTR mainly regulates mRNA stability and translation efficiency [143]. Three approaches can be used to optimise 5′-UTR and 3′ UTR sequences used in mRNA vaccines. The first is to use the 5′ UTR from a highly expressed human gene such as the human α-globin and the 3′ UTRs of α- and β-globin. The second approach commonly used for saRNA vaccines is to use the native UTR of the virus such as VEEV or SINV. These first two strategies assume that naturally selected UTR sequences are sufficient for optimal expression in muscle cells. A third approach is to use the systematic evolution of ligands by exponential enrichment (SELEX), which has been used to optimise the 3′ UTR [144]. With this approach, it was shown that the mitochondrially encoded 12S rRNA (mtRNR1) element in combination with the Amino-enhancer of split (AES) or human β-globin outperformed the commonly used double β-globin in mRNA translation in human dendritic cells [144]. The Pfizer/BioNTech COVID-19 mRNA vaccine BNT162b2 used the first approach to design its 5′ UTR sequence and the third approach for the 3′ UTR sequence [142]. When rapid vaccine development is critical, such as during a pandemic, the first two approaches may be the most feasible. For saRNA vaccines, the 5′ and 3′ UTRs are based on the evolution of naturally occurring alphaviruses, but these can also be optimised to improve translation efficiency. In all strategies, a Kozak consensus sequence (typically

GCC(A/G)CCAUGG) is usually added in the 5′ UTR just before the start codon to improve translation efficiency [145].

2.8.4.2 Poly A tail optimisation

The length of the 3′-poly(A) tail affects mRNA stability and translation. It affects decapping and mRNA degradation because removal or shortening of the poly(A) tail to less than 12 residues results in degradation of the mRNA through cleavage of the 5′ cap structure and 5′ to 3′ exonucleolytic digestion or 3′ to 5′ degradation [146]. A gradual increase in the poly(A) tail length of IVT mRNA up to 120 bases commensurately increases the protein expression level [147]; nevertheless, highly expressed genes tend to have short poly(A) sequences and form loops efficiently [148]. For mRNA vaccines, a poly(A) tail of approximately 100 nucleotides is generally sufficient for efficient antigen expression and induction of immune responses in mRNA vaccines [149].

Poly(A) tails can be added to the mRNA sequence by encoding the poly(A) tail in the DNA template post-transcriptionally using recombinant poly(A) polymerase. However, post-transcriptional polyadenylation using recombinant poly(A) polymerase results in variable poly(A) tail length. Therefore, the preferred approach is to incorporate the poly(A) sequence in the DNA template [150].

2.8.4.3 Open Reading Frame Optimisation

Codon optimisation can be used to enhance the expression of the GOI by modifying the mRNA sequence without changing the encoded amino acids. Synonymous mutations are introduced to replace less efficiently translated rare codons with more common ones. Codon optimisation affects GC content and RNA secondary structure, both of which influence translation efficiency [151]. Codon optimisation thus includes replacing GC-poor codons in the ORF with

synonymous GC-rich codons, as this approach has been shown to enhance steady-state mRNA levels *in vitro*, boost protein expression *in vivo*, and decrease innate immunogenicity [152]. Codon optimisation also helps to minimise the formation of stable secondary structures readily formed through complementary self-interactions [153]. Highly stable secondary structures, particularly in the 5′ UTR and the first ten codons of the ORF reduce translation initiation efficiency and therefore overall protein expression [154]. Such structures in the mRNA sequence are generally undesirable as they can also be recognised as double-stranded RNAs by PRRs [155].

2.8.5 Purification of saRNA

Following the *in vitro* transcription step, saRNA must be purified to remove excess raw materials including the residual DNA template, RNA polymerase, and unincorporated nucleotides. In addition, IVT by-products such as short single-stranded RNA (ssRNA) produced by abortive initiation events and double-stranded RNA (dsRNA) should also be removed. Other impurities and contaminants may include endotoxins from bacterial cells used in plasmid DNA preparation and nucleases. Proper purification improves translation efficiency because clean mRNA leads to better ribosome binding by preventing competition with aberrant mRNA. It also minimises the inflammatory response to the mRNA as impurities can trigger innate immune sensors like Toll-like receptors [156].

For small-scale purification, salt precipitation using lithium chloride (LiCl), sodium acetate, or ammonium acetate can be used. LiCl precipitation is commonly used as it is a simple, rapid, and effective method to remove unincorporated nucleotides and most proteins. However, it does not efficiently precipitate DNA, protein, or carbohydrates [157]. mRNA can also be purified using organic extraction methods, such as phenol-chloroform extraction and isopropanol precipitation. This method relies on the phase separation between the higher-

density phenol-chloroform and water. Lipids are dissolved in the phenol-chloroform phase and the RNA in the aqueous phase, with the proteins remaining in the interfacial layer. The main challenge with this method is that both phenol and chloroform are hazardous reagents. In addition, there is a possibility of mRNA contamination by phenol-chloroform, which may negatively impact downstream assays [158]. mRNA can also be purified using silica membrane RNA binding columns. These simple purification methods can efficiently remove unincorporated nucleotides, proteins, and, to a lesser extent, short RNAs. The disadvantage of this method is that it is more expensive than salt precipitation or organic extraction.

When large-scale, highly pure Good Manufacturing Practice (GMP) grade mRNA is required, chromatographic approaches such as high-performance liquid chromatography (HPLC), anion-exchange chromatography (AEX), size-exclusion chromatography, and affinity chromatography are used [159]. HPLC is reported to eliminate residual inflammatory responses in nucleoside-modified mRNA and to increase translation efficiency by up to 1000 times in primary cells [160]. Size-exclusion chromatography separates molecules based on their size, and is the simplest chromatography method for purifying oligonucleotides [161]. A limitation of SEC is that it requires several additional purification steps such as protein removal using phenol-chloroform, desalination, and concentration. It is also inefficient at removing impurities of a similar size such as dsRNA [160]. AIEX chromatography utilises the polyanionic nature of mRNA molecules to remove impurities using an ion exchange matrix. RNA polymerase and unincorporated nucleotides are efficiently eluted from the column matrix while aberrant RNA transcripts and the excess DNA templates are fractionated over a shallow salt gradient [162]. This method is often used to purify oligonucleotides on a medium to large scale [163]. The most widely used affinity chromatography method involves using oligodeoxythymidine (oligo(dT)). The single-strand sequence of oligo(dT) binds to the poly(A) tail in mRNA, forming a stable hybrid under high-salt conditions. Removal of the salt

destabilises this hybrid, resulting in the release of the mRNA. This method is robust, straightforward, and produces high-quality industrial-scale GMP-grade RNA. However, it is limited by mRNA length and salt loading concentrations and has a relatively high cost [164].

While chromatographic methods are routinely used for mRNA purification, their suitability for saRNA remains poorly documented. The large molecular size of saRNA, (>10 kb), may present challenges with these methods [21].

2.8.6 Self-amplifying RNA vaccine delivery methods

The hydrophilicity, strong negative charge, and high molecular weight of saRNA (~10 kb) are significant barriers to its cellular uptake. In addition, like other forms of mRNA, saRNA is susceptible to ribonuclease degradation [165]. To overcome these barriers, saRNA must be formulated in good delivery vehicles. A good delivery vehicle should (i) protect the saRNA from ribonuclease degradation, (ii) facilitate efficient uptake by the target cell, (iii) allow dissociation from the delivery vehicle and escape from the endosome, (iv) be non-toxic, and (v) avoid excessive stimulation of innate immune responses [166].

In vivo saRNA delivery can be viral or non-viral. Viral saRNA delivery involves co-transfection in mammalian cell lines of *in vitro*-transcribed RNA from an expression vector and one or more helper RNA vectors encoding the viral structural genes, generating replication-defective virus replicon particles (VRPs) [128]. Viral delivery of saRNA faces two main challenges. The first is the development of anti-vector neutralising immunity, and the second is the difficulty in scaling up production due to limitations in the process of generating VRPs from packaging cell lines [167, 168].

Non-viral delivery of saRNA can be done using naked saRNA, a gene gun, electroporation, or formulation with an appropriate delivery vehicle. While it is possible to induce immune

responses using unformulated saRNA, the high doses required eliminate the advantage of using saRNA over non-replicating mRNA [21]. Physical methods of saRNA delivery using a gene gun and electroporation are difficult to scale, and the devices are bulky and expensive for mass deployment [165]. Given these challenges, synthetic formulations are preferred for *in vivo* saRNA delivery.

Non-viral delivery platforms can be divided into three main categories: (1) polymeric nanoparticles, (2) lipid nanoparticles, and (3) nanoemulsions. These platforms work on the same principle, whereby the anionic saRNA is condensed by a cationic carrier to form a nanoparticle approximately 100 nm in size that protects the saRNA from degradation and facilitates its cellular uptake [21].

Lipid nanoparticles (LNPs) are the most widely used non-viral saRNA delivery system. Several studies have shown that saRNA formulated in LNPs induces potent cellular and humoral immune responses by different administration routes [169]. LNPs typically comprise a complexing cationic amino lipid (either ionisable or non-ionisable), a phospholipid, cholesterol, and a poly(ethylene glycol)-lipid conjugate [170]. Examples of non-ionisable cationic lipids include 1,2-di-O-octadecenyl- 3-trimethylammonium propane (DOTMA) and 1,2-Dioleoyl-3-trimethylammoniumpropane chloride (DOTAP). Ionisable cationic lipids include 1,2-Dimethanoloxy-3-dimethylaminopropane (DLinDMA), and N1,N3,N5-tris (3-(didodecylamino)propyl) benzene-1,3,5-tricarboxamide (TT3). Ionisable cationic lipids have a positive charge when the pH is below the acid-base dissociation constant (pKa) and a near-zero charge at neutral pH [171]. This transient cationic charge aids in mRNA encapsulation during formulation and its release within the endosome's low pH environment, which enhances LNP stability and reduces toxicity [172]. The phospholipids (also known as helper lipids) such as 1,2-dioleoyl-sn-glycero-3-phosphoethanolamine (DOPE), 1,2- distearoyl-sn-glycero-3-

phosphocholine (DSPC), and cholesterol, stabilise LNP structures and facilitate endosome escape while the PEG-lipid stabilises the LNPs during preparation and provides a hydrophilic outer layer that increases their *in vivo* half-life [173].

Polymeric nanoparticle delivery platforms for saRNA can be classified into non-degradable and degradable polymers. Polyethyleneimine (PEI) is a non-degradable, cationic polymer that has been widely used to formulate saRNA. It is water-soluble, has a positive charge density associated with the amino groups, and is an efficient mRNA carrier for *in vitro* transfection. Unfortunately, PEI exhibits toxicity due to its high molecular weight (>25 kDa) which is thought to be caused by the adsorption of anionic serum proteins onto the polyplex surface [165]. Higher molecular weight PEI-based polymers have enhanced translation efficiency but like PEI, they tend to be toxic [174]. To overcome this challenge, bioreducible cationic polymers such as poly(CBA-co-4-amino-1-butanol) (pABOL) have been developed with enhanced translation efficiency without the toxicity associated with PEI [175]. pABOL includes a disulphide bond which enables its biodegradation by enzymatic reduction of intracellular esterases such as reduced glutathione (GSH) and thioredoxin reductases. A head-to-head comparison of pABOL and LNPs showed that the former resulted in higher protein expression, but the latter induced stronger humoral and cellular immune responses [176].

Cationic nanoemulsion (CNE) is a formulation that combines a cationic lipid with a nanoemulsion to deliver mRNA. Nanoemulsions utilise hydrophobic and hydrophilic surfactants to stabilise the oil core in the aqueous phase, generating nanoparticles. A commonly used nanoemulsion is MF59, an FDA-approved oil-in-water nanoemulsion adjuvant composed of naturally occurring oil (Squalene), sorbitan trioleate (Span 85), polyoxyethylene sorbitan monooleate (Tween 80), and citrate buffer. Incorporation of cationic lipids, such as DOTAP in the Squalene-based formulation creates positively charged CNE particles that can adsorb

negatively charged nucleic acids to the outer shell [177, 178]. The effectiveness of CNE in delivering saRNA has been demonstrated in various animal models, including mice, rats, rabbits, ferrets, and rhesus macaques [179].

The delivery route also plays a vital role in determining the type and magnitude of the induced immune response. The main delivery routes for IVT mRNA vaccines against infectious diseases are intramuscular (IM), intradermal (ID), and subcutaneous (SC) [166]. Although intradermal delivery enables preferential access to antigen-presenting cells (APCs), such as dendritic cells and macrophages, as well as lymphoid organs, it is limited by its small injection volume and a high risk of local adverse events such as swelling, pain, erythema, and pruritus [180]. Compared to intradermal delivery, subcutaneous injection permits a larger injection volume, resulting in less pain and lower pressure. Additionally, the larger injection volume may compensate for the less efficient draining activity in this layer of skin and the fewer immune cells compared to the dermis. The lower absorption rate of subcutaneous delivery may, however, lead to increased mRNA degradation [180]. The IM route is suitable for delivering mRNA to lymph node DCs. It enables the delivery of mRNA into deep muscle tissue, where an extensive network of blood vessels can help traffic various immune cells, such as the infiltrating APCs [181]. This delivery route allows for a larger injection volume compared to the ID route in humans. It is also associated with milder local side effects compared to both ID and SC routes. Most saRNA vaccines tested in mice, macaques, and humans have been administered via the IM route [179].

2.9 Immune responses to self-amplifying RNA vaccination

2.9.1. Innate immune responses to self-amplifying RNA vaccines

saRNA is considered self-adjuvanting due to its dsRNA structures, replicon intermediates, and other motifs that activate the innate immune system by stimulating several PRRs [182].

Whereas PRR stimulation can enhance vaccine-specific immune responses, it also induces an intracellular antiviral state that inhibits RNA replication and expression [183-185]. TLR3 detects double-stranded RNA (dsRNA) in the endosome while TLR7 and TLR8 recognise single-stranded RNA (ssRNA) [186, 187]. In the cytosol, dsRNA is detected by the cytosolic RNA sensors retinoic acid-inducible gene I (RIG-I) and melanoma differentiation-associated protein 5 (MDA5) [188], with the former also being activated by uncapped 5′-triphosphate ssRNA [189]. Additionally, the cytoplasmic nucleotide-binding oligomerisation domain 2 (NOD2) receptor is activated by ssRNA [190]. Activation of these PRRs initiates a complex series of interacting signalling pathways leading to the production of type I IFNs (α and β) and proinflammatory cytokines such as IL-6 and IL-12. These cytokines are transported to the extracellular environment where they can react with IFN-α/β receptors (IFNARs) in an autocrine or paracrine fashion, inducing the expression of interferon-stimulated genes (ISGs) protein kinase R (PKR) and 2′-5′-oligoadenylate synthetase (OAS). PKR expression hampers mRNA translation through phosphorylation of the eukaryotic translation initiation factor 2 alpha subunit (eIF2α), while OAS produces 2′-5′-linked oligoadenylates, which activate the endoribonuclease RNase L that degrades ssRNA [191, 192].

2.9.2. Modulation of innate immune responses induced by saRNA

Exogenous mRNA detection by the cellular PRRs can be masked by using nucleoside-modified messenger RNA (modRNA), in which standard nucleosides are replaced with other naturally modified nucleosides or synthetic nucleoside analogues. For example, uridine can be replaced with pseudouridine (Ψ) or N1-methyl-pseudouridine (m1Ψ) and cytosine with 5-methylcytosine. In the Pfizer/BioNTech BNT162b2 and the Moderna mRNA-1273 COVID-19 mRNA vaccines, uridine was replaced with N1-methyl-3′-pseudouridine [193]. Modified

nucleosides reduce PRR recognition by altering the secondary structure of the mRNA while still permitting effective translation [194, 195].

While nucleoside modification is effective for conventional mRNA vaccines, it poses unique challenges for saRNA due to its self-replicating nature. This is because modified nucleosides from *in vitro* transcription are replaced by the natural, unmodified nucleosides during amplification by RdRp. Additionally, modified nucleosides may not be compatible with T7 RNA polymerase, the cellular translation machinery, or the nsP genes that make up the RdRp replication complex [196]. Surprisingly, it was recently reported that saRNA encoding the modified nucleotides 5-methylcytidine and 5-methyluridine induced strong expression and immunogenicity in mice, while that encoding N1-methylpseudouridine lacked detectable expression [197, 198]. The lack of expression by saRNA incorporating N1-methylpseudouridine was attributed to the disruption of the replicase complex caused by this modified nucleoside.

Innate immune system activation of exogenous mRNA due to dsRNA contamination can be addressed using HPLC or cellulose chromatography [43, 160]. Cellulose chromatography purification drastically reduced the innate immune response and improved the expression and vaccination efficacy of a Zika virus saRNA vaccine [199]. Even though dsRNA contamination of saRNA formed during IVT can be eliminated through purification, this would not remove the dsRNA intermediates formed *in vivo* during self-replication.

To address these limitations, researchers have explored alternative strategies to suppress innate immunity in saRNA vaccines. One approach is to express proteins from viruses that avoid innate immune sensing. Beissert et al. demonstrated that co-administering the three vaccinia proteins E3, K3, and B18 using conventional mRNA along with saRNA achieved significant suppression of PKR and interferon pathway activation *in vitro* and enhanced expression of the

encoded genes of interest *in vitro* and *in vivo* [200]. Likewise, Blakney et al. showed that cis-encoded innate inhibiting proteins (IIPs) such as Middle East respiratory syndrome coronavirus (MERS-CoV) ORF4a could reduce the non-linear dose dependency and enhance the immunogenicity of saRNA, although the response was species-dependent [201]. The effectiveness of using this strategy in dampening the innate immune response of saRNA vaccines in humans is yet to be demonstrated.

2.9.3. Adaptive immune responses to saRNA vaccination

After vaccination, saRNA molecules are internalised via receptor-mediated endocytosis and transported through the endo-lysosomal compartment. A small fraction of the saRNA escapes the endosomes and binds to the ribosomes to produce the four functional components of RdRp. The RdRp first uses the positive-sense genome as a template to synthesise complementary negative-sense RNA, which then becomes a template for synthesising genomic and subgenomic positive-sense RNA. The subgenomic RNA is produced more than the viral genome, leading to high and sustained antigen expression levels [196].

Self-amplifying RNA vaccines also induce local immune responses at the injection sites, triggering the recruitment of antigen-presenting cells (APCs) such as dendritic cells and macrophages. Uptake and expression by these APCs result in antigen presentation on MHC class I, leading to the maturation of CD8+ T cells. In addition, these APCs process antigens through the MHC class II pathway, activating CD4+ T helper cells that are essential for developing humoral immunity.

2.9.3.1 B-cell Response to Vaccination

Proper B cell activation is vital for the induction and maintenance of humoral immunity. B cell activation is initiated when the B cell receptor (BCR) encounters an antigen in the extracellular

space and binds to it. The bound antigen is then internalised by endocytosis, digested and presented on MHC class II. The B cells then differentiate into short-lived plasma cells, which rapidly secrete low-affinity antibodies, or enter germinal centres (GCs), where they undergo somatic hypermutation and affinity maturation. The activated B cells entering the GCs present the antigen on MHC class II to T helper cells and receive co-stimulatory signals at the T and B cell borders. They then undergo somatic hypermutation in the dark zone of the GCs, proliferating and honing the specificity of their BCR against the antigen. The GC B cells move to the light zone where they undergo affinity maturation through interactions with follicular dendritic cells (DCs). Follicular DCs that received the antigens from B cells and DCs store the antigens in their non-degradative compartments and present them for long-term periods to B cells, helping their affinity maturation. A continuous affinity maturation process ensures the selection of B cells with high-affinity BCRs while clearing those with low-affinity BCR by apoptosis. The selected B cells with high BCR affinity exit the GCs and differentiate into long-lived plasma cells or memory B cells [202]. Upon secondary exposure to its cognate antigen, memory B cells rapidly produce antibodies, enabling a faster antibody-mediated immune response [203].

The presentation of endogenous antigen on MHC class II can be improved by engineering the mRNA sequence. For example, signal peptides which are short N-terminal sequences that facilitate the secretion and translocation of newly synthesised proteins to the specific intracellular compartment can be incorporated into the sequence [204]. Using optimised signal peptides instead of wild-type signal peptides may result in a stronger immune response and enhance the efficacy of mRNA vaccines [205, 206]. Alternatively, an mRNA sequence can be designed to express antigens in an extracellular form, either as secreted or transmembrane proteins [203]. Extracellularly expressed antigens can be recognised by APCs and effectively elicit CD4+ and CD8+ T cell responses by MHC class II presentation and cross-presentation,

respectively. Furthermore, considering the importance of germinal centres in antibody production, targeting mRNA vaccines to lymph nodes using efficient delivery vectors is another strategy that can be used to improve the potency of mRNA vaccines [207].

2.9.3.2 T-cell response to vaccination

Most licensed vaccines provide efficacy through humoral immunity with neutralising antibody titres often being used as the correlate of protection [208]. It is therefore standard practice to measure both vaccine antigen-specific and neutralising antibodies when evaluating the immunogenicity of candidate vaccines. In comparison, the contribution of T-cells in vaccine efficacy is less defined, even though the importance of CD8+ in killing virally infected cells and CD4+ cells in providing a helper role to B cells in antibody production is well established [209]. Accordingly, T-cell assays are often used to evaluate candidate vaccines and identify potential correlates of protection. T-cell parameters typically evaluated include T-cell phenotype, response breadth, cytokine secretion, cytotoxic killing, and proliferation ability.

The role of T-cell responses in RVFV vaccine-induced protection was reported for a recombinant pDNA and Modified Vaccinia Ankara virus vectored vaccine encoding RVFV Gn and RVFV Gc. In the absence of neutralising antibodies, BALB/c mice immunised with this vaccine were protected from virulent RVFV challenge by cellular responses that mainly targeted Gc epitopes [210]. Similarly, the measles live attenuated vaccine induces IFN-γ $CD4^+$ responses that protect 6-month-old infants against measles-associated mortality and morbidity in the absence of antibody responses [211].

3.0 CHAPTER THREE: METHODOLOGY

3.1 Generation of the consensus RVFV M segment sequence

3.1.1 Retrieval of RVFV M segment sequences from GenBank

RVFV M segment sequences were downloaded from GenBank (https://www.ncbi.nlm.nih.gov/genbank/) using the following search terms: 'Rift Valley fever virus M segment', 'Rift Valley fever phlebovirus', 'release date: 1930-01-01 to 2018-12-31', and 'molecule type: genomic DNA/RNA'. From this search, 341 RVFV M segment sequences were retrieved, of which 151 sequences (ranging from 3594 bp to 3952 bp) were selected. Sequences below 3594 bp were considered too short to produce a good alignment, as all were shorter than 859 bp. The coding sequences (CDS) of the selected sequences were exported to SnapGene software, version 4 (Dotmatics, Boston, MA, USA).

3.1.2 Retrieval of RVFV M segment sequences from ViPR

The Virus Pathogen Database and Analysis Resource (ViPR) is an open, publicly accessible bioinformatics database and analysis resource repository for viruses categorised as either A–C priority pathogens or viruses that adversely affect public health [212]. Rift Valley fever virus M segment sequences were downloaded from the ViPR database (https://www.viprbrc.org/brc/home.spg?decorator=vipr). The search criteria were as follows: 'Data to return: Genome segment', 'Collection year: 1930-2018', 'Segment: M Gn/Gc/Nsm', 'complete sequence only', and 'remove duplicate genome sequences'. A total of 123 sequences were obtained, of which 117 overlapped with those from GenBank. The six additional unique ViPR sequences were exported to SnapGene (version 4) and added to the 151 sequences retrieved from GenBank.

3.1.3 Alignment to obtain the RVFV wild-type consensus sequence

A DNA sequence alignment of the 157 sequences was performed in SnapGene (version 4) using Multiple Sequence Comparison by Log Expectation (MUSCLE) with eight iterations. The resulting aligned sequences were edited to remove gaps and trimmed to cover the coding region (3594 bp). This generated a consensus RVFV M segment coding sequence at a 50% threshold. This consensus sequence was translated and trimmed to start from the fourth methionine, yielding a consensus RVFV M segment amino acid sequence. A BLAST search of this consensus sequence was performed using the NCBI BLAST tool (https://blast.ncbi.nlm.nih.gov/Blast.cgi), revealing high identity percentages: 99.56% to 97.38% for nucleotide sequences and 100% to 99.16% for protein sequences, with an E-value of 0.0 for all 100 hits.

3.1.4 Phylogenetic analysis of the RVFV wild-type consensus sequence

Phylogenetic analysis was conducted to compare the RVFV M segment consensus sequence with the sequences used to generate it. This analysis was performed using the software Molecular Evolutionary Genetics Analysis (MEGA) X version 10.0.5 [213]. The RVFV M segment coding sequences downloaded from ViPR and GenBank were trimmed to start from the fourth methionine and aligned with the RVFV M segment consensus sequence using MUSCLE with eight iterations in SnapGene (version 4). Aligned sequences were exported to MEGA X, where a phylogenetic tree was constructed using the Maximum Likelihood algorithm. The Tamura 3-parameter substitution model with gamma distribution was selected using MEGA X's model selection function. The Partial Deletion option was applied to handle gaps and missing data. Branch reliability was estimated using bootstrap analysis with 1000 replicates.

3.2 Cloning the RVFV M segment consensus sequence into pcDNA3.1

The RVFV M segment consensus sequence was commercially synthesised and cloned into the plasmid expression vector pcDNA3.1(+) using GeneArt Gene Synthesis (Thermo Fisher Scientific, UK), which also codon-optimised the sequence for human expression after reverse translation. The consensus sequence was inserted between HindIII and NotI restriction enzyme sites in the multiple cloning sites of this vector. After construction, a maxiprep of this pcDNA3.1(+) plasmid cloned with the RVFV M segment consensus sequence was prepared. Briefly, the lyophilised pDNA was dissolved in 50 µl of nuclease-free water, and 1µl of this solution was added to 50 µl of *E. coli* DH5α cells thawed on ice. After a 20-minute ice incubation, the cells were heat-shocked at 42 ˚C for 45 seconds and incubated on ice for 2 minutes. Then, 500 µl of Super Optimal Broth with Catabolite Repression (SOC) outgrowth medium (Invitrogen, 1554-034) was added. The transformed cells were incubated with shaking at 37 ˚C for 30 minutes, spread on agar plates containing ampicillin (100 µg/mL), and incubated overnight at 37 ˚C. The following day, a bacterial colony was harvested from the agar plate and placed in a 5 mL culture medium comprising 50% Luria-Bertani (LB) broth (Sigma-Aldrich, L3522), 50% Terrific Broth (Sigma-Aldrich, T0918), and 0.5 µg of ampicillin. The bacterial culture was incubated at 37 ˚C with shaking at 225 rpm for 12–16 hours and then expanded in 100 mL of the same medium and conditions. The DNA was extracted using the QIAprep Spin Miniprep Kit (Qiagen, 27104) according to the manufacturer's instructions.

3.2.1 Preparation of glycerol stocks

Glycerol stocks for the long-term storage of the cloned pDNA were prepared as described below. Equal volumes of glycerol and PBS were thoroughly mixed, and 500 µL of this mixture was placed in a cryovial, followed by 500 µL of LB broth. A 20 mL cloning culture was transferred into a 50 mL centrifuge tube and centrifuged at 3000 rpm for 10 minutes. The

supernatant was poured off, and the cell pellet was resuspended in 1000 µL of PBS–glycerol–LB broth mix, which was then transferred to labelled cryovials and stored at -80 ˚C.

3.3 Introduction of the desired mutations into the RVFV M segment consensus sequence

Seven pDNA constructs expressing mutated RVFV glycoprotein sequences were generated using Gibson assembly cloning. Using SnapGene (version 4) software, unique restriction enzyme sites flanking the nucleotides to be mutated were identified, and DNA sequences containing 30 bp overlaps with the vector sequence upstream of the first (5′ end) restriction site and downstream of the second (3′ end) restriction site were designed. The sequences were then synthesised as double-stranded linear DNA fragments (GeneArt Strings) using GeneArt Gene Synthesis (Thermo Fisher Scientific, UK). The DNA fragments were cloned into the pDNA construct expressing the RVFV M segment consensus sequence, resulting in constructs with the desired RVFV Gn and Gc sequence mutations. Cloning was performed using the NEBuilder HiFi DNA assembly cloning kit (New England Biolabs, E5520S) following the chemical transformation protocol. Briefly, NEB 5-alpha Competent *E. coli* (NEB, 2987) were thawed on ice, and to this 2 µL of the assembled product was added and gently mixed by pipetting up and down. The mixture was then immediately placed on ice and incubated for 30 minutes. After incubation, the mixture was heat shocked at 42 °C for 30 seconds and immediately transferred to ice for 2 minutes. Room temperature SOC medium (950 µL) was added to the tube, which was then incubated at 37 °C for 60 minutes with shaking at 250 rpm. The transformed cells (100 µL) were placed on pre-warmed agar plates and incubated overnight at 37 °C. A transformation control pUC19, a NEBuilder positive control, and untransformed cells were used as the transformation control, positive control, and negative controls, respectively. After overnight incubation at 37 ˚C, five colonies were harvested from the agar plate, and each colony was inoculated into a mixture of 5 mL LB and 5 mL Terrific Broth culture medium. The culture

was incubated at 37 ˚C with shaking at 225 rpm for 12–16 hours, after which the pDNA was extracted using QIAprep Spin Miniprep according to the manufacturer's instructions. Successful clones were identified by diagnostic restriction digestion for some constructs, followed by Sanger sequencing for all constructs. Sanger sequencing was performed commercially by Eurofins Genomics (Ebersberg, Germany). Each of the five constructs sequenced was aligned with the reference sequence using SnapGene (version 4) to identify those that had been successfully cloned. The 5 mL clone culture containing the successfully cloned pDNA construct was then expanded by overnight culture in 100 mL culture medium (50% LB broth and 50% Terrific Broth with 10 μg of ampicillin) at 37 °C with shaking at 225 rpm. Following the manufacturer's instructions, the plasmid DNA was extracted using the QIAGEN Plasmid Plus Maxi Kit (Qiagen, 12963). Glycerol stocks of the cloned pDNA were prepared as described in Section 3.2.1.

3.3.1 Diagnostic restriction digestion

Using SnapGene (version 4), the appropriate restriction enzymes were selected, and a restriction enzyme digestion map was generated. To a microcentrifuge tube was added restriction enzymes (20 units per enzyme), followed by 2 μL of CutSmart buffer (NEB, B7204) and nuclease-free water to bring the final volume to 20 μL after the addition of the pDNA. The mixture was then incubated at 37ºC for one hour. During incubation, a 1.0% agarose gel in TAE buffer was prepared, and a DNA gel stain was added at a ratio of 1:10,000. The digest (7.5 μL) was mixed with 1.5 μL of Gel Loading Dye Purple (NEB, B7024S) and loaded into the gel well. A DNA ladder was added to the first well of the gel, and the gel was run at 100 V for one hour. An image of the gel was then captured using a gel documentation system, and pDNA clones that were successfully digested were identified.

3.3.2 Description of the constructs made for this study

A description of the constructs made for this study is provided below and in Figure 6.

1. Rift Valley fever virus wild-type consensus construct

A construct containing a consensus Gn and Gc polyprotein sequence.

2. K1064A construct

A construct with a lysine-to-alanine amino acid substitution at position 1064 in the cytoplasmic tail of Gc (K1064A), reported to increase the expression of Gn at the plasma membrane. Gc contains an ER retention signal, a basic di-lysine motif in its C-terminal domain [85]. Carnec et al. showed that replacing either of these lysines causes a mislocalisation of Gn to the cell surface [84].

3. K1050del construct

A construct with a deletion of the Gc cytoplasmic tail reported to increase plasma membrane expression of the Gn and Gc glycoproteins. Phleboviruses have an endoplasmic reticulum retrieval signal of approximately five amino acids in their Gc cytoplasmic tails. Removal of this signal in the Gc of Uukuniemi Phlebovirus results in an accumulation of expressed Gn/Gc at the Golgi apparatus and plasma membrane [214]. Similarly, removing this signal in mutant RVFV MP-12 led to the accumulation of Gn and Gc at the Golgi apparatus, with some mutant glycoprotein being translocated to the plasma membrane [215].

4. Furin-T2A construct

A construct with cytoplasmic tail deletions in the Gn and Gc glycoproteins separated by a furin cleavage site and a T2A self-cleaving peptide (RRRRRRGSGEGRGSLLTCGDVEENPGP). The Golgi localisation signal in Gn is found within a 47-amino-acid segment encompassing the transmembrane domain and 28 amino acids of the cytosolic tail [216]. Removal of this region prevents the accumulation of Gn and Gc in the Golgi and induces their plasma membrane expression. The use of a furin cleavage site and a T2A peptide was intended to

promote cleavage of the Gn and Gc proteins during translation. The T2A peptide (EGRGSLLTCGDVEENPGP) is a 2A “self-cleaving” peptide derived from *Thosea asigna* virus 2A. 2A peptides are 18–22 amino-acid long viral oligopeptides that mediate cleavage of polypeptides during translation in eukaryotic cells [217]. Peptide cleavage occurs by breaking the peptide bond between proline and glycine in the C-terminus of the 2A peptide via ribosomal "skipping" [218]. The addition of the optional linker glycine-serine-glycine (GSG) on the N-terminal of a 2A peptide increases cleavage efficiency [219].

Furin is a ubiquitously expressed type-I transmembrane protein found in all vertebrates and many invertebrates that cleaves specific sections of newly synthesised proteins and activates them [220]. It cleaves proteins having a target sequence canonically Arg-X-(Arg/Lys)-Arg'. Incorporating furin-specific cleavage sites in the carboxy and/or amino termini of the expressed protein provides an efficient means for the secretion of poorly expressed proteins at the cell surface [221].

5. H727A construct

A construct with a histidine-to-alanine amino acid substitution at position 727. This mutation stabilises the Gn and Gc glycoprotein dimer in its - conformation, preventing the formation of a fusion loop required for viral infection [80]. The protonation of histidines is essential for triggering conformational changes in viral fusion proteins. Located near positively charged residues in the prefusion conformation, histidines form salt bridges with negatively charged residues in the post-fusion conformation [222]. In RVFV, it has been shown that the histidine at position 727 is essential for acid-induced rearrangement of Gc into higher-order structures. The formation of the stable Gc oligomer induced by protonation of this histidine is essential for virus entry into the host cell. Its replacement with the non-polar amino acid alanine stabilises the Gn and Gc glycoprotein dimer in its pre-fusion conformation, thereby preventing

the formation of a fusion loop required for viral infection [80]. Therefore, a construct with this mutation is expected to induce antibodies against the pre-fusion conformation, abrogating virus fusion and entry.

6. Gn-S-S-Gc construct

A construct with a disulfide bond created between Gn and Gc at positions 72 and 672, achieved by replacing lysine and phenylalanine with cysteine, respectively. Disulfide bonds are covalent bonds formed by the oxidation of thiol groups (SH) between two cysteine residues essential for the native structure and biological activity of many secreted and outer membrane proteins [223]. They confer stability when secreted proteins are exposed to the extracellular medium or when membrane proteins are recycled through acidic endocytic compartments. The greater the number of disulfide bonds a protein has, the less susceptible it is to denaturation. Cysteine residues in Gn and Gc were introduced at positions 072 (Gn) and 672 (Gc), replacing leucine and phenylalanine, respectively, in order to introduce a disulfide bond between these two amino acids and stabilise their tertiary structure.

7. Gn-s-s-Gc-H727A construct

A construct that combines both a disulphide bond between Gn and Gc and the H727A mutation described above.

8. RV-Gn construct

A construct having only Gn, with its signal peptide at the N-terminus was replaced with an optimised artificial signal peptide. The Gn protein consists of an N-terminal ectodomain and a C-terminal transmembrane domain followed by a cytoplasmic tail. It has been shown that the Gn ectodomain is the main target for neutralising antibodies [224] and that rabbit and human-derived monoclonal antibodies against glycoprotein Gn alone protect mice against Rift Valley fever infections [111, 112]. Subsequently, a Gn-only construct was made. This construct was

designed for optimal extracellular excretion by excluding the transmembrane and cytoplasmic regions and by replacing the native signal peptide with an artificial signal sequence *MDRAKL$_{10}$PQAQA*.

All constructs started from the fourth start codon of the M segment polyprotein to include the signal peptide. Transcription initiation from this codon produces only Gn and Gc glycoproteins [83]. Figure 6 provides a map and a summary description of the constructs made.

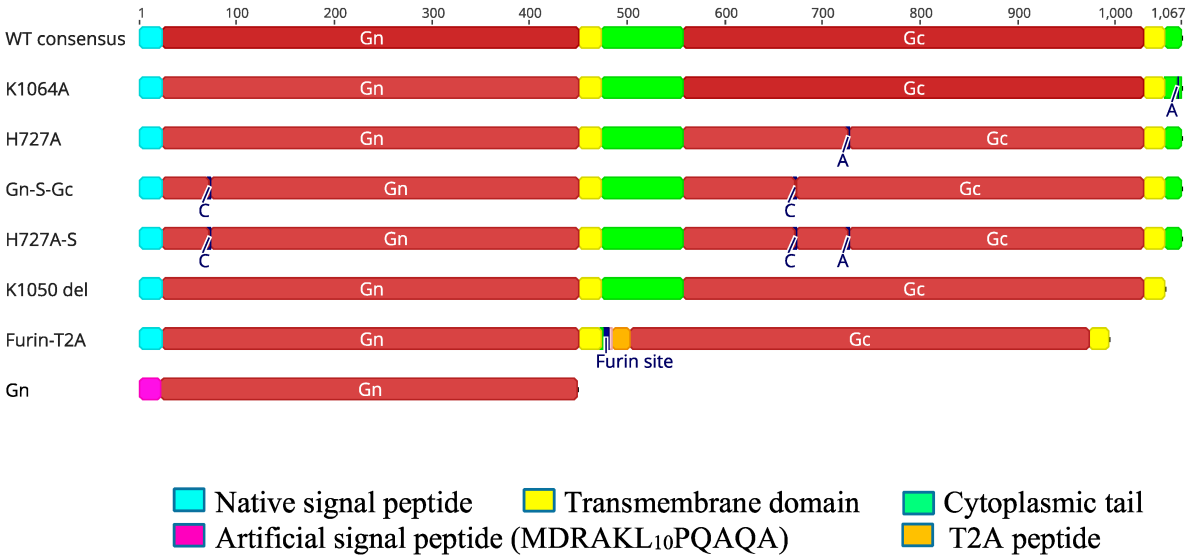

Figure 6: Mutations made to the RVFV medium (M) segment consensus sequence

Site-directed mutations were introduced into the RVFV M segment to enhance the expression and immunogenicity of the viral surface glycoproteins Gn and Gc: (1) WT consensus, the unmodified M segment consensus; (2) K1064A, lysine-to-alanine substitution at position 1064, reported to cause mis-localization of Gn to the plasma membrane; (3) H727A, histidine-to-alanine substitution at position 727 reported to stabilise the Gn-Gc heterodimer in its prefusion conformation; (4) L202C_F672C (Gn-S-Gc), leucine-to-cysteine and phenylalanine-to-cysteine substitutions introducing disulfide bonds between Gn and Gc; (5) L202C_F672C_H727A (H727A-S), combining mutations in constructs 3 and 4; (6) K1050del, deletion of the Gc cytoplasmic tail which enhances plasma membrane translocation of Gn and Gc; (7) Furin-T2A, cytoplasmic tail deletions in both glycoproteins, combined with a furin cleavage and a T2A peptide for increased plasma membrane expression and cleavage; (8) Gn, encoding Gn only, with its native signal replaced by an artificial signal peptide (MDRAKL$_{10}$PQAQA) to enhance extracellular expression. All constructs started from the fourth methionine of the RVFV M segment to translate Gn and Gc only.
Adapted from Figure 1 in Kitandwe, P. K., Rogers, P., Hu, K., Nayebare, O., Blakney, A. K., McKay, P. F., Kaleebu, P., & Shattock, R. J. (2024). A Lipid Nanoparticle-Formulated Self-Amplifying RNA Rift Valley Fever Vaccine Induces a Robust Humoral Immune Response in

Mice. *Vaccines*, *12*(10), 1088. https://doi.org/10.3390/vaccines12101088, under the Creative Commons Attribution 4.0 International (CC BY 4.0) license.

3.4 Transfection of HEK 293 F cells with RVFV pDNA vectors

Plasmid DNA vectors encoding RVFV surface glycoproteins Gn and Gc were transfected into FreeStyle™ 293-F cells (Gibco, R79007) using 293fectin™ transfection reagent (Invitrogen, 12347019) following the manufacturer's instructions. The FreeStyle™ 293-F cell line is derived from the human embryonic kidney (HEK) 293 cell line and is intended for suspension culture in the FreeStyle™ Expression Medium (Invitrogen, 12338018). Briefly, the viable cell count of the HEK 293-F cells to be transfected was determined using the trypan blue dye exclusion method. The volume required to obtain 5 μg of each plasmid was calculated and diluted in Opti-MEM™ I Reduced Serum Medium (Invitrogen, 31985062) to a total volume of 167 μL per plasmid. 293fectin™ (10 μL) was diluted with 157 μL of Opti-MEM™ I Reduced Serum Medium, mixed, and incubated for 5 minutes. The diluted 293fectin™ was added to the diluted pDNA, mixed, and incubated for 30 minutes. The 293-F cells required to achieve $1.0x10^6$ cells/mL in a total volume of 5 mL were added to each well of a 6-well sterile tissue culture plate. To each well, 334 μL of the pDNA–293fectin™ complex was added, followed by FreeStyle™ Expression Medium to bring the final volume to 5 mL. The cells were incubated at 37 °C with 8% CO_2, and shaking at 125 rpm for 24–72 hours.

3.5 Assessment of *in vitro* expression of RVFV pDNA using western blot

Human embryonic kidney 293-F cells were transfected with the various RVFV pDNA constructs described in Section 3.4 above. After incubation, the cells were harvested and centrifuged at 400 × g for 5 minutes, and the cell pellet was resuspended in 1 mL phosphate-

buffered saline (PBS). The cells were centrifuged at 700 × g for 5 minutes, lysed in 200 µl of Pierce™ Lysis Buffer (Thermo Fisher Scientific, 87787) in the presence of a protease inhibitor cocktail (Abcam, ab65621), and incubated for 10 minutes on ice. After lysis, the lysate was centrifuged at 10,000 × g for 10 minutes at 4 ˚C. For the reduced western blot samples, the cell lysate (65 µl) was resuspended in 35 µl of 1× LDS sample buffer (Thermo Fisher Scientific, B0007) mixed with sample reducing agent (Thermo Fisher Scientific, B0009) and heated at 70 ˚C for 10 minutes. For the non-reduced western blot samples, the sample reducing agent was replaced with water, and the samples were not heated. The sample (15 µl) and 10 µl of pre-stained protein ladder Page Ruler™ Plus (Thermo Fisher Scientific, 26619) were loaded on an SDS-polyacrylamide gel Invitrogen Bolt 4-12% Bis-Tris Plus (Thermo Fisher Scientific, NW04125B0X) placed in an electrophoresis tank. The tank was filled with Bolt™ MOPS SDS running buffer (Thermo Fisher Scientific, B0001), and the gel was run at 200 V for 35 minutes. The gel was removed from its cassette and placed onto a Polyvinylidene fluoride (PVDF) transfer membrane, Invitrolon™ PVDF/filter paper sandwiches (Thermo Fisher Scientific, LC2005), pre-activated for 30 seconds in 100% methanol. The gel and membrane were sandwiched between filter papers and sponges and run at 35 V for one hour in Novex Bolt™ SDS transfer buffer (Thermo Fisher Scientific, BT00061). After transfer, the membrane was blocked for one hour at room temperature in 5% non-fat dried milk powder in PBS+0.05% Tween 20. The membrane was incubated at 4 ˚C overnight with one of the following antibodies: rabbit anti-RVFV Gn immunoglobulin G (IgG) monoclonal antibody RV-Gn1, mouse anti-RVFV Gn IgG monoclonal antibodies clone 3C10 (BEI Resources, NR-43186) or 4D4 (BEI Resources, NR-43190) or mouse anti-RVFV Gc monoclonal antibodies clone 1G4 (BEI Resources, NR-43738) or 9C10 (BEI Resources, NR-43187). The mouse anti-RVFV Gn and anti-RVFV Gc monoclonal antibodies were obtained from the Joel M. Dalrymple–Clarence J. Peters USAMRIID antibody collection through BEI Resources, NIAID, NIH. The anti-β actin

mouse monoclonal antibody (Invitrogen, MA5-15739) was used as the loading control. All antibodies were diluted to a concentration of 1 μg/mL in 5% non-fat dried milk powder PBS+0.05% Tween 20. The membrane was then washed three times for 5 minutes each in PBS+0.05% Tween 20 and incubated on a rocker for one hour at room temperature with secondary antibody anti-rabbit IgG horseradish peroxidase (HRP) (Invitrogen, 65-6120) diluted 1: 10,000 in 5% milk powder PBS+0.05% Tween 20. After washing, the membrane was developed for 3 minutes in Immobilion Crescendo western HRP substrate (Millipore, WBLUR0500) and imaged using the Biostep Celvin S chemiluminescence reader.

3.6 Assessment of plasma membrane expression of RVFV pDNA using flow cytometry

Human embryonic kidney 293-F cells were transfected with the different RVFV pDNA constructs as described in Section 3.4 above. After incubation, the HEK293-F cells were counted using the trypan blue dye exclusion method and 1.0 x10^6 cells per transfection were stained with Live/Dead™ fixable violet dead cell stain kit (Thermo Fisher Scientific, L34964) diluted 1:400 in PBS. After incubation for 20 minutes at room temperature, the cells were washed by centrifugation in 1 mL PBS and stained with the same primary antibodies used for western blot diluted 1:100 in PBS. After another 20 minutes of incubation on ice, the cells were washed in 1 mL PBS and incubated with either goat anti-rabbit IgG PE (Santa Cruz Biotechnology, sc-3739) or goat anti-mouse IgG PE (Abcam, ab97024) secondary antibody diluted 1:100 in PBS. The cells were then incubated for 20 minutes on ice, washed by centrifugation in 1 mL PBS, and resuspended in 400 μL of PBS. The cells were then acquired on a BD LSRFortessa™ flow cytometer (BD Biosciences, San Jose, CA, USA), and the expression of Gn and Gc was measured as median fluorescence intensity (MFI) using FlowJo software (TreeStar Inc).

3.7 Generation of RVFV saRNA constructs

3.7.1 Selection of constructs for *in vitro* transcription into saRNA

This study tested the hypothesis that increasing cell surface expression of Gn and Gc enhances the immunogenicity of the RVFV envelope. Therefore, the wild-type consensus and one other construct with the highest *in vitro* cell surface expression of Gn or Gc were preselected for synthesis into saRNA. While the Furin-T2A and the H727A constructs had the highest Gn and Gc expression respectively, the Furin-T2A and the wild-type consensus were selected for synthesis into saRNA. This decision was based on previous findings that Gn-specific monoclonal antibodies exhibit significantly higher neutralising activity *in vitro* and protective efficacy compared to Gc-specific monoclonal antibodies [111].

3.7.2 Cloning of the RVFV Gn/Gc sequences into the VEEV vector

Following procedures similar to those described in Section 3.3, synthetic linear DNA fragments encoding the RVFV wild-type consensus and the Furin-T2A sequences were synthesised using GeneArt Strings and cloned into a VEEV plasmid DNA vector using the NEBuilder HiFi DNA Assembly Kit, according to the manufacturer's instructions. The vector used was based on the Trinidad donkey VEEV genome in which structural genes driven by the 26S subgenomic promoter were replaced with the firefly luciferase (Fluc) gene. Briefly, the vector was digested with NotI and NdeI restriction enzymes to excise the Fluc gene, which was replaced with the synthetic linear DNA fragments encoding the RVFV Gn–Gc sequences using the NEBuilder HiFi DNA Assembly Kit. The assembled product was cloned into *E. coli* DH5α cells by chemical transformation, and after overnight incubation at 37 °C, 225 rpm, it was purified using a QIAprep Spin Miniprep Kit. The concentration and purity of the plasmid DNA were measured using a NanoDrop One spectrophotometer (Thermo Fisher Scientific, UK), and the success of the cloning was confirmed using Sanger sequencing.

3.7.3 Generation of saRNA constructs by *in vitro* transcription

Self-amplifying RNA constructs were synthesised by cell-free *in vitro* transcription of the VEEV pDNA vectors containing RVFV wild-type consensus and the furin–T2A sequences. To do this, the VEEV pDNA vectors (2.5 µg) were first linearised by incubation with 2 µL of MluI restriction enzyme (NEB, R3198L) for 3 hours at 37 °C. The linearised pDNA was then *in vitro* transcribed into saRNA using the MEGAscript™ T7 RNA polymerase transcription kit (Invitrogen, AM1334) following the manufacturer's protocol. In brief, 8 µL of the linearised pDNA (0.9 µg) was added to a master mix containing 2 µL of each of the nucleotides adenosine triphosphate (ATP), cytidine triphosphate (CTP), guanosine triphosphate (GTP), uridine triphosphate (UTP), and 2µL reaction buffer. Then, 2 µL of the T7 RNA polymerase was added, and the mixture was incubated at 37 °C for two hours. Immediately after transcription, an equal volume of lithium chloride (LiCl) solution was added and the reaction mixture was incubated overnight at -20 °C to enable the saRNA to precipitate out of the solution. The following day, the mixture was centrifuged at 14,000 rpm for 20 minutes at 4 °C to sediment the saRNA pellet. The supernatant was removed and the saRNA pellet was resuspended in 900 µL of 70% ethanol and centrifuged at 14,000 rpm for 5 minutes at 4 °C. After centrifugation, the supernatant was removed and the saRNA pellet was air-dried for 5 minutes. The pellet was then gently resuspended in 70 µL of nuclease-free water, and its concentration was measured on a NanoDrop spectrophotometer.

3.7.4 Capping of saRNA transcripts

The saRNA transcripts were capped using the ScriptCap™ Cap 1 Capping System Kit (Cellscript Inc., CSCCS1710). To do so, the saRNA was first denatured by heating at 65 ˚C for 10 minutes and then immediately placed on ice. A 100 µL master mix (per reaction) was prepared, consisting of 2.5 µL of *S*-adenosyl-methionine (1 mM), 10 µL of buffer (0.5 M Tris-

HCl, pH 8.0, 60 mM KCl, and 12.5 mM $MgCl_2$), 10 µL of guanosine triphosphate (1 mM), 2.5 µL of RNase inhibitor (100 U), and 4 µL of ScriptCap™ 2'-O-Methyltransferase (400 U). Then, 67 µL of heat-denatured saRNA (100–150 µg) was added, followed by 4 µL of ScriptCap™ Capping Enzyme (40 U), and the mixture was gently mixed and incubated at 37 °C for two hours. After incubation, the capped transcripts were purified by LiCl precipitation as described in Section 3.7.3, but precipitation was carried out for more than 2 hours instead of overnight. The purified saRNA was resuspended in 100 µL of RNA storage buffer (10 mM HEPES, 0.1 mM EDTA, and 100 mg/mL trehalose) and stored at -80 °C until further use.

3.8 Assessment of saRNA quality using a denaturing agarose gel

The integrity of the saRNA was assessed using a denaturing agarose bleach gel following the protocol described by Aranda *et al*., 2012 [225]. In brief, agarose (1% w/v) was added to 1× TAE buffer, followed by bleach (1% v/v), and the mixture was incubated for 5 minutes at room temperature with occasional swirling. The mixture was then heated in a microwave oven to melt the agarose and left to cool. During cooling, GelRed™ stain (Biotium, 41003) was added in a ratio of 1:10,000, and the solution was poured into a gel mould to solidify. The saRNA (1 µg) was mixed with DNA loading buffer and loaded onto the gel along with a DNA ladder. The gel was electioletrophoresed in 1× TAE buffer at 100 V for 35 minutes before being visualised by ultraviolet transillumination.

3.9 Transfection of HEK293T/17 cells with saRNA encoding RVFV Gn and Gc

HEK293T/17 cells obtained from American Type Culture Collection (ATCC) were suspended in complete Dulbecco's Modified Eagle's Medium (DMEM) [DMEM supplemented with 10% foetal bovine serum (Sigma, 806544), 2 mm L-glutamine (Sigma, G7513) and 1% penicillin–streptomycin (Sigma, P4333)]. The cells were then plated onto 6-well tissue culture plates at a

concentration of 7.5×10^5 cells per well. The cells were then incubated at 37 °C with 5% CO_2 for 24 hours to reach 70–90% confluence. The following day, 3.75 µl of Lipofectamine MessengerMAX™ reagent (Thermo Fisher Scientific, LMRNA001) was diluted in 125 µl Opti-MEM™ I reduced serum medium, vortexed briefly, and incubated for 10 minutes. Self-amplifying RNA (2.5 µg) was diluted in 125 µl Opti-MEM™ I reduced serum medium, added to the diluted Lipofectamine MessengerMax™ reagent, and incubated for 5 minutes. The Lipofectamine–saRNA mixture (250 µl) was then added to the HEK293T/17 cells and incubated at 37 °C, 5% CO_2, for 24 hours.

3.10 Assessment of *in vitro* expression of RVFV saRNA using western blot

Human embryonic kidney 293T/17 cells were transfected as described in Section 3.8 above with saRNA encoding either the wild-type consensus or the Furin-T2A sequences. After 48 hours, the cells were harvested using 500 µl/well of TrypLE™ Express Enzyme (Gibco, 12605010) and washed with 1 mL DMEM. Briefly, the spent medium was aspirated from the wells using a Pasteur pipette and discarded. Each well was washed with 1 mL PBS, after which 1 mL TrypLE™ Express Enzyme, prewarmed to 37 °C was added to the 6-well plate and incubated at 37 °C for two minutes to allow for complete cell detachment from the plate surface. Complete DMEM (2 mL) was then added to each well, and the cells were aspirated into a 15 mL centrifuge tube and centrifuged at 400 × g for 5 minutes. The supernatant was discarded, and the cells were resuspended in 1 mL PBS. A reduced western blot procedure was performed on the cells using the method described in Section 3.5.

3.11 Assessment of plasma membrane expression of saRNA using flow cytometry

Human embryonic kidney 293T/17 cells were transfected as described in Section 3.8 with saRNA encoding either the wild-type consensus sequence or the Furin-T2A sequence. After

24 hours, the cells were harvested as described in Section 3.9, and flow cytometry was performed as described in Section 3.6.

3.12 Formulation of RVFV saRNA

The saRNA vaccines used in the murine immunogenicity studies were delivered non-virally after being formulated in either LNPs or the lipid-based in vivo mRNA transfection reagents *in vivo* jet-RNA and *in vivo*-jetRNA+. *In vivo*-jetRNA+ is an improved version of *in vivo*-jetRNA. The manufacturer reports that *in vivo*-jetRNA+ is stable for up to 72 hours at room temperature, can encapsulate mRNA up to a concentration of 0.3 µg/µL, and achieves an encapsulation efficiency of up to 100% [226]. In contrast, *in vivo*-jetRNA was reported to be stable for only one hour at room temperature and to formulate mRNA up to a concentration of 0.1 µg/µl. The manufacturer and available publications do not provide information on the formulation efficiency of *in vivo*-jetRNA. The procedure for the formulation of mRNA with *in vivo*-jetRNA and *in vivo*-jetRNA+ is similar except that for the former, the ratio of *in vivo*-jetRNA to saRNA was 1:1 while for the latter, it is 1:2. Unlike LNPs, both *in vivo*-jetRNA and *in vivo*-jetRNA+ do not require specialised formulation equipment.

3.12.1 Formulation of saRNA using LNPs

The saRNA was formulated in LNPs using a self-assembly process whereby an aqueous solution of saRNA was rapidly mixed with an ethanolic solution of the LNPs. The LNPs used and their formulation method were similar to those described by McKay et al., 2020 [227]. They contained an ionisable cationic lipid (proprietary to Acuitas), phosphatidylcholine, cholesterol, and polyethylene glycol lipid. The proprietary cationic ionisable lipid and LNP composition is described in US patent US10,221,127. Formulation of saRNA was performed

by Dr. Anna K. Blakney and Dr. Paul McKay who were staff members of the Robin Shattock Laboratory at Imperial College London St Mary's Campus.

3.12.2 Formulation of saRNA using *in vivo*-jetRNA and *in vivo*-jetRNA+

In vivo-jetRNA (or *in vivo*-jetRNA+), mRNA, and mRNA buffer were equilibrated at room temperature. The saRNA was then diluted to the recommended concentration of 1–2 μg/μl using RNase-free water. The desired volume of the mRNA was then added to the mRNA buffer and mixed by pipetting up and down. *In vivo*-jetRNA (or the *in vivo*-jetRNA+) was vortexed for 5 seconds and added to the mRNA buffer solution in a ratio of saRNA to formulation reagent of 1:1 and 1:2 (μg saRNA:μl formulation reagent) for *in vivo*-jetRNA and *in vivo*-jetRNA+ respectively and gently mixed by pipetting up and down. The saRNA–*in vivo*-jetRNA/*in vivo*-jetRNA+ formulation was then left to incubate at room temperature for 15 minutes before administration to the study mice.

3.12.3 Measurement of encapsulation efficiency

The encapsulation efficiency of the saRNA after formulation was measured using the Quant-iT RiboGreen RNA assay. In brief, 20× TE buffer (10 mm Tris-HCl, 1 mm EDTA, pH 7.5) was diluted with nuclease-free water to make 1× TE buffer. A 2% Triton X-100 solution and an RNA standard solution (20 μg/mL) were prepared by dilution in 1× TE buffer. To four rows of a 96-well microplate, 50 μL per well of 1× TE was added, and to another four rows, 50 μL of 2% Triton X-100 was added per well (two wells per formulation and two wells per blank). In rows 11 and 12 was also added 50 μL of 2% Triton X-100 per well for quantification of the RNA standard. A total of 15 μL of each saRNA was diluted in 1× TE, and 50 μL of this dilution was added to each of its two wells. Decreasing volumes of 1× TE buffer (50 μL, 49 μL, 47.5 μL, 45 μL, 40 μL, 30 μL, and 25 μL) were added to wells in A to H in columns 11 and 12

followed by increasing volumes of the RNA standard (0 µL, 1 µL, 2.5 µL, 5µL, 10 µL, 20 µL, and 25 µL). To all the wells was then added 100 µL of RiboGreen reagent to give a total volume of 150 µL per well (2% Triton X-100 + 1× TAE + RiboGreen reagent). The plate was incubated for 3 minutes and then read on a fluorescence reader, with the excitation filter and emission filters set at 485 nm and 520 nm, respectively. The mean fluorescence of the blank wells was subtracted from each of the saRNA sample wells, and linear regression was used to interpolate the concentrations of the saRNA using a standard curve. The encapsulation efficiency was then measured using the formula below:

$$\text{Encapsulation efficiency (\%)} = \frac{[\text{total saRNA (Triton treated)} - \text{free saRNA (TE buffered)}]}{\text{total saRNA}} \times 100$$

3.13 Immunisation of mice with candidate saRNA RVF vaccines

Three preclinical studies assessed the immune response induced in mice by the candidate saRNA RVF vaccines (Table 1). The first study, conducted at Imperial College London, St Mary's Campus, evaluated the humoral immune responses of the candidate vaccines after their formulation in LNPs. The second and third studies were conducted at the College of Veterinary Medicine, Animal Resources and Biosecurity (CoVAB). These studies evaluated the same candidate saRNA RVF vaccines after their formulation with the *in vivo* transfection reagents *in vivo*-jetRNA (Polyplus, 101000021) and *in vivo*-jetRNA+ (Polyplus, 101000122) for the second and third studies, respectively.

Mouse immunisations and sample collections at Imperial College London were performed by staff from Robin Shattock's laboratory, while those conducted at CoVAB were carried out by CoVAB staff.

3.13.1 Immunisation of mice with LNP-formulated saRNA RVF vaccines

For the first preclinical study, 35 six-week-old BALB/c mice were randomly assigned to seven groups of five mice each. After a one-week acclimation period, each mouse was immunised intramuscularly with 50 µl of either 0.1 µg, 1.0 µg, or 10 µg of the candidate saRNA RVFV vaccine encoding the wild-type consensus or the Furin-T2A sequence. Mice in the negative control group received 10 µg of saRNA RVFV vaccine encoding the rabies glycoprotein. After 28 days, the mice were given a booster immunisation using the same dose and administration route. Tail vein blood was collected from the mice on days 14, 28, and 35 to measure RVFV-Gn binding antibodies and RVF pseudovirus-neutralising activity in serum. Immunisation of the mice and collection of samples were performed by the staff of the Robin Shattock Lab at Imperial College London, St Mary's Campus.

3.13.2 Mice immunisation with *in vivo*-jetRNA and *in vivo*-jetRNA+ saRNA RVF vaccines

For the second preclinical study which used the *in vivo*-jetRNA formulation, 42 six-week-old BALB/c mice were randomly assigned to seven groups of six mice each. After a one-week acclimation period, each mouse was immunised intramuscularly with 50 µl of either 1 µg, 5 µg, or 10 µg of the candidate saRNA RVFV vaccine encoding the wild-type consensus or the Furin-T2A sequence depending on its group allocation. Mice in one of the groups served as the negative control and were not immunised.

For the third preclinical study that used *in vivo*-jetRNA+ formulation, 48 six-week-old BALB/c mice were randomly assigned to eight groups of six mice each. After a one-week acclimation period, each mouse in each group was immunised intramuscularly with 50 µl of either 1 µg, 5 µg, or 10 µg of the candidate saRNA RVFV vaccine encoding either the WT consensus or the Furin-T2A sequence. Mice in one of the groups served as the negative control and were not

immunised. Mice in a second control group were immunised with *in vivo*-jetRNA+ only to control for background immune responses that this formulation could induce.

For both the second and third studies, the mice were given a booster immunisation using the same dose and administration route on days 21 and 42 (*in vivo*-jetRNA) and day 63 (*in vivo*-jetRNA+). Tail vein blood was collected from the study mice to measure RVFV-specific IgG antibodies, RVF pseudovirus-neutralisation activity, and serum cytokine levels (Table 1). At the final sample collection time point, the mice were euthanised, and their spleens were harvested to measure T-cell immune responses. Immunisation of the mice and sample collection were performed by CoVAB staff.

Table 1. Schedule of procedures for the mice immunogenicity studies

	Study 1 (LNPs)				**Study 2 (*in vivo*-jetRNA)**				**Study 3 (*in vivo*-jetRNA+)**				
Day	**0**	**14**	**28**	**35**	**0**	**21**	**42**	**56**	**0**	**21**	**42**	**63**	**77**
Vaccination	X		X		X	X	X		X	X		X	
Blood collection		X	X	X	X	X	X	X	X	X	X		X
Spleen harvest								X					X
IgG ELISA		X	X	X	X	X	X	X	X	X	X		X
Pseudovirus neutralisation				X									X
Multiplex cytokine analysis													X
IFN-γ elispot													X

3.14 Study ethics approvals

The first study, conducted at the Imperial College London, St Mary's Campus was carried out after obtaining ethics approval from its Animal Welfare and Ethics Review Board. It was conducted following the UK Home Office Animals (Scientific Procedures) Act 1986 under the

project licence (PPL) number P63FE629C. This study also received ethics approval from the LSHTM Animal Welfare and Ethics Review Board LSHTM AWERB reference: 2023-01.

The preclinical studies that were done at CoVAB received ethics approvals from the CoVAB SVAR Institutional Animal Care and Use Committee (IACUC), approval number SVAR-IACUC/115/2022 and from the Uganda National Council for Science and Technology (UNCST), registration number HS2408ES. Approval was also obtained from the LSHTM AWERB (LSHTM AWERB reference: 2022-05).

3.15 RVFV Gn and Gc IgG ELISA

Rift Valley fever virus surface antigen IgG titres in mouse sera were assessed by indirect ELISA. In brief, ELISA plates were coated with 100 µl per well (1 µg/mL in PBS) of recombinant RVFV strain MP12 Gn (ABD38821.1) (Sino Biological, 40338-V08B) and Gc (ABD38821.1) (Sino Biological, 40338-V07B1) protein. For the standard, 100 µl per well (1 µg/mL in PBS) of goat anti-mouse IgG kappa (Southern Biotech, 1060-01) and lambda chains (Southern Biotech, 1050-01) were used. After overnight incubation at 4 °C, the plates were washed four times with PBS+0.05% Tween 20 and blocked for one hour at 37 °C with 200 µl per well of assay buffer (PBS+0.05% Tween 20 with 1% bovine serum albumin). After washing the plates as before, 50 µl of mice sera diluted 1:100, 1: 1,000, and 1: 10,000 in assay buffer, and a fivefold dilution series of the IgG standard (Southern Biotech, 0107-01) were added per well in triplicate starting with a 1000 ng/mL dilution. The plates were then incubated for one hour at 37 °C, washed as before, and 100 µl per well of goat anti-mouse IgG human adsorbed, HRP-conjugated antibody (Southern Biotech, 1030-05) was added at a 1:2000 dilution in assay buffer. After incubation at 37 °C for one hour, the plates were washed as before and 50 µL of KPL sure Blue 3,3′,5,5′-Tetramethylbenzidine microwell peroxidase substrate (Sera care, 5120-0077) was added per well. After 5 minutes, the reaction was stopped

using 50 μL per well of 0.12 N HCl acid stop solution (Sera care, 5150-0020), and the absorbance of each well was measured spectrophotometrically at 450 nm. Statistical analysis was performed using GraphPad Prism (version 10), applying two-way ANOVA with Dunnett's multiple comparisons test and a single pooled variance.

3.16 RVFV pseudovirus neutralisation assay

The RVFV pseudovirus assay was conducted at Imperial College London by Dr. Hu Kai and at UVRI by me, using pseudoviruses prepared according to the procedure described below and those commercially synthesised by Creative Diagnostics, respectively.

3.16.1 Pseudovirus production

The RVFV pseudotyped viruses were produced by co-transfection of 293T/17 cells with an HIV-1 gag-pol plasmid (pCMV-Δ8.91, a kind gift from Prof. Julian Ma, St George's University of London), a firefly luciferase reporter plasmid (pCSFLW, a kind gift from Prof. Julian Ma, St George's University of London) and a plasmid encoding the RVFV wild-type consensus sequence at a ratio of 1:1.5:1. Briefly, HEK 293T/17 cells were seeded into a T175 flask at a cell density of $4x10^6$ cells/mL and cultured for 24 hours at 37 °C. The HIV-1 gag-pol plasmid pCMV-Δ8.91 (12 μg), the firefly luciferase reporter plasmid pCSFLW (18 μg), and the RVFV wild-type consensus sequence plasmid (12 μg) were diluted with 3.5 mL transfection medium (DMEM supplemented with 2mM L-glutamine). PEI (126 μg) was mixed with the transfection medium and added to the diluted plasmids. The mixture was vortexed and incubated for 20 minutes at room temperature, followed by the addition of 17 mL of transfection medium. The culture medium was then removed from the HEK 293T/17 cells, replaced with the PEI-DNA mixture, and incubated for five hours. The PEI-DNA mixture was then removed from the cell culture, replaced with 40 mL complete DMEM cell culture medium and cultured at 37 °C for

48 hours. After incubation, the conditioned cell culture medium was collected and centrifuged at 1750 rpm for 5 minutes to remove cell debris. The supernatant was then filtered using a 0.45 μm syringe filter, aliquoted, and stored at -80 °C until use.

3.16.2 RVFV pseudovirus titration

Following the production of the RVFV pseudoviruses, their concentration was determined by titration. To do this, complete DMEM (100 μl) was added to each well of a 96-well plate. RVFV pseudovirus (50μl) was then added to the wells of the first column (A1 to D1) which were then mixed and transferred sequentially to the next wells. This 1:3 serial dilution was repeated until column 11 (A11 to D11). A total of 100 μl of HEK 293T/17 cells (100,000 cells/mL) was then added to each well of the plate and incubated for 48 hours. After the 48-hour culture, complete DMEM (115 μL) was gently removed from each well and replaced with 75 μL of Bright-Glo luciferase substrate (Promega, E2620). The plate was gently tapped to ensure proper mixing, and the cells were left to lyse for 5 minutes at room temperature. The mixture was then gently pipetted up and down and transferred onto a white polystyrene plate starting from column 12 to column 1, and the luciferase activity was read. The $TCID_{50}$ of the RVFV pseudovirus was then established using the Reed-Muench method [228]. The cut-off was set at 2.5 times the background.

Reed-Muench calculation

$TCID_{50}$ = log10 of the dilution above 50%+ (-PD x log10 of the dilution factor)

$TCID_{50}$/mL = $TCID_{50}$/virus inoculation volume

$$\text{PD (proportional distance)} = \frac{\text{\% positive above 50\%-50\%}}{\text{\% positive above 50\%-\% positive below 50\%}}$$

3.16.3 RVFV pseudovirus neutralisation

For the neutralisation assay, heat-inactivated sera were serially diluted and incubated with 100 $TCID_{50}$ of RVFV pseudovirus for one hour at 37 °C. Human embryonic kidney (HEK) 293T/17 cells ($1.0x10^5$) were added to the serum-virus mixture and cultured at 37 °C in 5% CO_2 for 48 hours. The cells were then lysed, and their luciferase activity was measured using the Bright-Glo luciferase assay system (Promega, E2620), and the half-maximal inhibitory concentration (IC50) neutralisation was calculated by non-linear regression in GraphPad Prism (version 10) as described by Ferrara & Temperton [229]. Statistical analysis was performed in GraphPad Prism using the Kruskal–Wallis test followed by Dunn's post hoc test with correction for multiple comparisons.

3.17 Enumeration of interferon-gamma production using ELISpot assay

The enzyme-linked immunospot (ELISpot) assay was used to detect mouse IFN-γ in the splenocytes of vaccinated mice. Briefly, the PVDF membranes of the ELISpot plates (Millipore, MAIPS4510) were first preactivated by adding 50 µL of 70% ethanol to each well, and the plates were incubated for 30 seconds. They were then washed with sterile PBS and coated with 100 µL/well of anti-mouse IFN-γ monoclonal antibody (BD, 51-2525KZ) at a concentration of 5 µg/mL. After overnight incubation at 4 °C, the plates were washed three times with sterile PBS solution, and 200 µL/well of R10 medium was added to block the plate. The plates were then incubated at 37 °C, 5% CO_2 for 2 hours. After incubation, the plates were inverted to decant the R10, after which 100 µL of splenocytes ($3.5×10^6$ cells/mL) were added to each well in triplicate for each mouse and peptide (Figure 8). Next, the RVFV Gn peptide SYAHHRTLL and Gc peptides SYKPMIDQL and GGPLKTILL were added. The positive controls, phytohaemagglutinin (PHA) and Concanavalin A (Con A), were also added to the appropriate wells at a concentration of 5 µg/mL and volume of 100 µL/well. The plates were

then incubated at 37 °C, 5% CO_2 for 18 hours in a humidified incubator. After incubation, the plates were washed six times with 200 µL of PBS+0.05% Tween 20 solution, after which 100 µL of biotinylated anti-mouse IFN-γ detection antibody (BD, 51-1818KA) diluted to 2 µg/mL in 0.5% BSA/PBS was added to each well. Following a two-hour incubation, the ELISpot plates were washed six times with PBS+0.05% Tween 20 solution, and 100 µL of peroxidase avidin-biotin complex (Vector Labs, PK6100) prepared according to kit instructions was added. After a one-hour incubation at room temperature, the plates were washed three times with PBS+0.05% Tween 20 and three times with PBS. Then, 100 µL of 3-amino-9-ethylcarbazole (AEC) substrate solution was added to each well. The AEC substrate solution was prepared by dissolving one AEC tablet (Sigma, A6926) in 2.5 mL of dimethylformamide (DMF) and allowing it to incubate for 5 minutes to ensure complete dissolution. This solution was then added to a buffer consisting of 180 µL of 2 M acetic acid and 280 µL of 3 M sodium acetate in 47 mL of deionised water. Immediately before application to the ELISpot plate, 25 µL of hydrogen peroxide was added to activate the substrate. The plates were then incubated for 4 minutes at room temperature, and the reaction was stopped by rinsing under gently running tap water. The plates were then dried overnight in the dark on paper towels before enumerating the IFN-γ spots in each well using an automated AID ELISpot plate reader (Autoimmun Diagnostika GmbH). Interferon (IFN)-γ production was quantified as spot-forming units (SFU) per million splenocytes, and responses were normalised by subtracting the mock (no peptide) response. GraphPad Prism (version 10) was used to perform statistical analysis, applying the Kruskal–Wallis test followed by Dunn's post hoc test with correction for multiple comparisons.

3.18 Cytokine quantification using the LEGENDplex™ mouse Th cytokine panel

Cytokine production by splenocytes from vaccinated mice was quantified using a 12-plex LEGENDplex™ Mouse Th Cytokine Panel. This bead-based immunoassay is based on same basic principle as the sandwich immunoassay.

3.18.1 Principle of the LEGENDplex assay

Capture beads are differentiated by size and internal fluorescence intensities; each bead set is conjugated with a specific antibody on its surface and serves as the capture bead for that particular analyte. When the capture beads are mixed with a sample containing target analytes, the antibodies on the beads bind to their respective analytes. After washing, a biotinylated detection antibody cocktail is added, and each detection antibody in the cocktail binds to its specific analyte on the capture beads, thus forming capture bead-analyte-detection antibody sandwiches. Streptavidin-phycoerythrin (SA-PE) is then introduced, binding to the biotinylated detection antibodies and producing a fluorescent signal whose intensity is directly proportional to the amount of analyte bound to the beads. The flow cytometer distinguishes each bead population based on size and internal fluorescence, allowing the detection and quantification of PE fluorescence for specific analytes. Analyte concentrations are calculated using a standard curve generated in the same assay, ensuring accurate quantification.

3.18.2 Procedure for running the LEGENDplex assay

The lyophilised mouse Th panel standard cocktail was reconstituted with 250 µL of assay buffer, and serially diluted 1:4 in assay buffer to make six dilutions (1:4 to 1:4096). Assay buffer and undiluted standard were used as the zero and top standards, respectively. Assay buffer (25 µL) was added to a 96-well V-bottom plate, followed by 25 µL of standard or cell culture supernatant. Vortexed beads (25 µL) were then added to each well, and the plate was sealed with aluminium foil and incubated for 2 hours at room temperature with shaking at 800

rpm. The plate was centrifuged at 250 × g for 5 minutes, and the supernatant was poured off. The plate was then washed twice with 200 µL of wash buffer, followed by the addition of 25 µL of detection antibody. The plate was then sealed with aluminium foil and incubated for one hour at room temperature with shaking at 800 rpm. Next, 25 µL of SA-PE was added to each well, and the plate was sealed with aluminium foil and incubated for 30 minutes at room temperature with shaking at 800 rpm. The plate was then centrifuged at 250 × g for 5 minutes, as previously described. The supernatant was discarded, and the wells were washed with 200 µL of wash buffer. The beads were then resuspended in 150 µL of wash buffer and read on a Beckman Coulter CytoFLEX flow cytometer. Cytokine levels were calculated from a standard curve using Qognit software (BioLegend), and statistical analysis was conducted in GraphPad Prism (version 10) using the Kruskal-Wallis test with Dunn's correction for multiple comparisons.

CHAPTER FOUR RESULTS: GENERATION AND OPTIMISATION OF RVFV M SEGMENT CONSTRUCTS

4.1 Introduction

The Rift Valley fever virus (RVFV), a zoonotic arbovirus, poses a significant threat to human and animal health, particularly in Africa and the Middle East. This virus causes widespread disease outbreaks, leading to severe morbidity and mortality in humans and livestock [42]. Despite the public health and economic burden of RVF, there are currently no licensed vaccines for human use to control or prevent it, and the available livestock vaccines have suboptimal safety or immunogenicity [20]. This underscores the importance of developing novel RVF vaccines using vaccine platforms capable of addressing the limitations of current vaccines.

The RVFV's medium (M) segment encodes two envelope glycoproteins, glycoprotein n (Gn) and c (Gc), which are essential for viral entry and immune recognition. These glycoproteins are critical targets for neutralising antibodies, the most widely recognised correlate of protection against RVFV infection [31]. These glycoproteins are, however, not efficiently delivered to the cell surface due to a Golgi apparatus localising signal and endoplasmic reticulum retention motif located in their cytoplasmic tails [32]. Site-directed mutations in the RVFV M segment have been shown to increase the plasma membrane expression of these glycoproteins [33, 34]. However, it remains to be demonstrated if increasing the cell surface expression of Gn and Gc through such mutations enhances their immunogenicity.

This chapter focuses on designing various RVFV M segment sequence constructs with mutations that enhance plasma membrane expression of Gn and Gc and evaluating the *in vitro* expression of these constructs.

A consensus RVFV M segment sequence was first generated using sequences available in the Genbank and ViPR databases. Site-directed mutations were introduced to enhance the

expression of these constructs and potentially improve immune responses. The constructs were cloned into plasmid DNA (pDNA) vectors and assessed for their ability to express Gn and Gc *in vitro* using SDS-PAGE and western blot, and flow cytometry. The optimised constructs were the foundation for saRNA RVF vaccine candidates, enabling their evaluation in subsequent chapters.

This chapter presents data on the generation and evaluation of RVFV M segment constructs, the first step in developing a saRNA vaccine against RVF. By identifying constructs with enhanced glycoprotein expression, this work supports the goal of developing a safe and effective vaccine platform for this high-priority disease.

4.2 Generation of the RVFV M segment consensus sequence

The RVFV M segment encodes Gn and Gc, the prime antigens for vaccine development, as they elicit neutralising antibodies. This segment encodes a polyprotein precursor that is cleaved into several nested polyproteins, including a 78-kDa protein, a 14-kDa non-structural protein NSm, Gn, and Gc [83]. Synthesis of these proteins involves leaky scanning at five initiation codons at nucleotide positions 21, 135, 174, 411, and 426 in the NSm region, with the fourth initiation codon giving rise to Gn and Gc only [38, 84]. Therefore, we generated an RVFV M segment consensus sequence that was truncated to start from the fourth initiation codon to express only Gn and Gc.

Using a consensus sequence ensured greater cross-strain applicability, which is essential for developing a more globally applicable vaccine. The viral strains used to produce current RVF livestock vaccines and those used by other groups to develop RVF vaccines may not represent strains that have dominated more recent epidemics. A consensus sequence would also be more suitable for use in areas where diverse RVFV strains co-circulate. Furthermore, as it includes

conserved regions from multiple strains, a consensus sequence may induce broader immune responses by targeting shared epitopes.

To generate the RVFV M segment consensus, the coding sequence of all complete and near-complete RVFV M segment sequences deposited in GenBank and the Virus Pathogen Database and Analysis Resource (ViPR) as of 31 December 2018 were aligned using the MUSCLE algorithm. After removing gaps and trimming overly long sequences, a consensus RVFV M segment coding sequence was produced using a 50% consensus threshold. This sequence was translated and truncated to start from the fourth methionine (Figure 7).

```
MAGIAMTVLPALAVFALAPVVFAEDPHLRNRPGKGHNYIDGMTQEDATCKPVTYAGACSS
FDVLLEKGKFPLFQSYAHHRTLLEAVHDTIIAKADPPSCDLQSAHGNPCMKEKLVMKTHC
PNDYQSAHYLNNDGKMASVKCPPKYELTEDCNFCRQMTGASLKKGSYPLQDLFCQSSEDD
GSKLKTKMKGVCEVGVQALKKCDGQLSTAHEVVPFAVFKNSKKVYLDKLDLKTEENLLPD
SFVCFEHKGQYKGTMDSGQTKRELKSFDISQCPKIGGHGSKKCTGDAAFCSAYECTAQYA
NAYCSHANGSGIVQIQVSGVWKKPLCVGYERVVVKRELSAKPIQRVEPCTTCITKCEPHG
LVVRSTGFKISSAVACASGVCVTGSQSPSTEITLKYPGISQSSGGDIGVHMAHDDQSVSS
KIVAHCPPQDPCLVHGCIVCAHGLINYQCHTALSAFVVVFVFSSIAIICLAILYRVLKCL
KIAPRKVLNPLMWITAFIRWVYKKMVARVADNINQVNREIGWMEGGQLALGNPAPIPRHA
PIPRYSTYLMLLLIVSYASACSELIQASSRITTCSTEGVNTKCRLSGTALIRAGSVGAEA
CLMLKGVKEDQTKFLKIKTVSSELSCREGQSYWTGSFSPKCLSSRRCHLVGECHVNRCLS
WRDNETSAEFSFVGESTTMRENKCFEQCGGWGCGCFNVNPSCLFVHTYLQSVRKEALRVF
NCIDWVHKLTLEITDFDGSVSTIDLGASSSRFTNWGSVSLSLDAEGISGSNSFSFIESPG
KGYAIVDEPFSEIPRQGFLGEIRCNSESSVLSAHESCLRAPNLISYKPMIDQLECTTNLI
DPFVVFERGSLPQTRNDKTFAASKGNRGVQAFSKGSVQADLTLMFDNFEVDFVGAAVSCD
AAFLNLTGCYSCNAGARVCLSITSTGTGTLSAHNKDGSLHIVLPSENGTKDQCQILHFTV
PEVEEEFMYSCDGDERPLLVKGTLIAIDPFDDRREAGGESTVVNPKSGSWNFFDWFSGLM
SWFGGPLKTILLICLYVALSIGLFFLLIYLGRTGLSKMWLAATKKAS
```

Signal sequence
Transmembrane
Cytoplasmic tail
AS – cleavage

Figure 7: RVFV M segment consensus sequence

This figure shows the amino acid sequence of the RVFV medium (M) segment consensus sequence obtained by aligning all complete and near complete RVFV M sequences that were available in GenBank (151 sequences) and the Virus Pathogen Resource (ViPR) database (6 out of the 123 sequences that were not overlapping with those in GenBank) as of 31st December 2018. Sequence alignment was performed using the MUSCLE algorithm (8 iterations) in SnapGene software version 4.2.0 (Dotmatics, Boston, MA, USA). The sequence was truncated to start from the fourth methionine of the complete M segment sequence, which leads to the translation of glycoprotein n (Gn) and c (Gc) only. All other constructs reported in this thesis were mutated from this reference sequence with mutation positions referenced to it.

Phylogenetic analysis was performed to validate the consensus RVFV M segment sequence, assess its diversity relative to the sequences used to construct it, and compare it with other live-attenuated RVFV vaccine strains. This analysis was done in MEGA X software (version 10.0.5) using the Tamura 3-parameter substitution model with gamma distribution. Classification followed that used by Samy et al. [42].

The phylogenetic analysis showed that the RVFV M segment consensus sequence clustered with RVFV strains isolated from East Africa (Uganda, Kenya, Tanzania), Sudan, Madagascar, and Saudi Arabia (Figure 9). These strains were all isolated from RVFV outbreaks that occurred at the turn of the century. A comparison of the consensus with the live attenuated RVFV vaccine strains showed that they all clustered in different clades. The consensus, MP-12, clone 13, and Smithburn vaccine strains clustered in clades I, A, K, and E, respectively. These results show that the consensus vaccine more closely represents RVFV strains from recent outbreaks compared to those used to make current live-attenuated vaccines from the 1940s (Smithburn) and 1970s (Clone 13 and MP12). Therefore, a vaccine based on a wild-type consensus sequence is more likely to induce neutralising antibodies and T-cell responses that are effective against currently circulating RVFV strains.

Figure 8: Phylogenetic analysis of the RVFV M segment consensus sequence

This figure illustrates the evolutionary relationships between the consensus sequence and all complete RVFV M segment sequences deposited in GenBank and Virus Pathogen Resource (ViPR) by 31st December 2018, which were used to generate it. The tree was constructed using the Maximum Likelihood method with the Tamura 3-parameter substitution model and gamma distribution in MEGA X (version 10.0.5). The tree is unrooted and drawn to scale, with branch lengths representing substitutions per site. Branch reliability was evaluated with 1,000 bootstrap replicates. Sequence tips are labelled with strain name, GenBank accession number, country, and isolation date, with similar strains collapsed into triangular tips for clarity. Adapted from Figure 2 in Kitandwe, P. K., Rogers, P., Hu, K., Nayebare, O., Blakney, A. K., McKay, P. F., Kaleebu, P., & Shattock, R. J. (2024). A Lipid Nanoparticle-Formulated Self-Amplifying RNA Rift Valley Fever Vaccine Induces a Robust Humoral Immune Response in Mice. *Vaccines*, *12*(10), 1088. https://doi.org/10.3390/vaccines12101088, under the Creative Commons Attribution 4.0 International (CC BY 4.0) license.

4.3 Mutation of the RVFV M segment consensus

Site-specific mutations were introduced into the RVFV M segment consensus sequence to enhance the expression and immunogenicity of the viral surface glycoproteins. The rationale for each mutation was based on previously reported studies and structural insights into glycoprotein function. Eight constructs were generated to increase the plasma membrane expression of Gn and Gc or to alter their conformation as a strategy to increase the immunogenicity of these glycoproteins.

To introduce these mutations, the RVFV M segment consensus sequence was first cloned into the mammalian expression vector pcDNA3.1(+) using GeneArt gene synthesis (Thermo Fisher Scientific, Cambridge, UK). The desired mutations were introduced into the RVFV M segment sequence using Invitrogen GeneArt Strings DNA Fragments (Waltham, MA, USA). These custom-made DNA fragments (GenArt Strings) were cloned into the pcDNA3.1(+) vector carrying the consensus RVFV M segment sequence using the NEBuilder HiFi DNA Assembly kit (New England Biolabs, Ipswich, MA, USA), resulting in plasmids with the intended mutations. Cloning success was verified using restriction enzyme digestion gel electrophoresis for some constructs, followed by Sanger sequencing for all constructs (Figure 9).

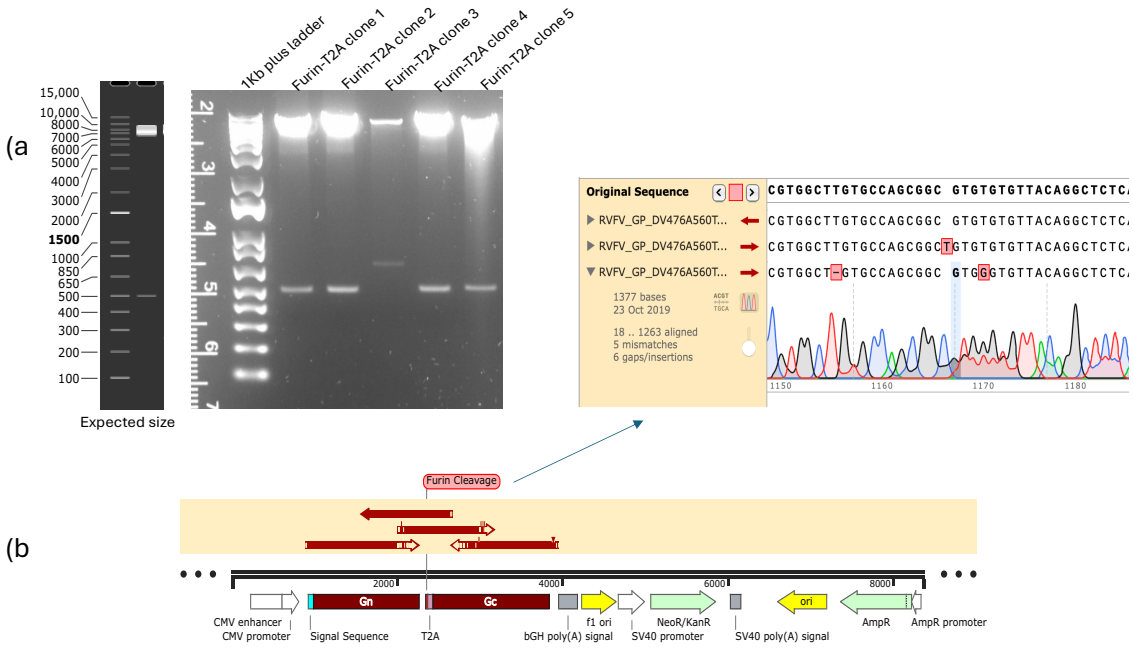

Figure 9: Verification of cloning of RVFV M segment sequences into pcDNA3.1(+)

This figure shows how the introduction of mutations into the RVFV medium (M) segment by Gibson Assembly cloning was verified. Restriction enzyme digestion was performed for some clones, followed by Sanger sequencing for all clones. (a) Agarose gel electrophoresis of the Furin-T2A pcDNA3.1(+) construct following digestion with the restriction enzymes PshAI and PmlI. All clones except clone 3 are of the expected size. (b) Sanger sequencing map of Furin-T2A pcDNA3.1(+). Sequencing was done by Eurofins Genomics and verified by aligning the sequences covered by each primer (red arrows) to the reference sequence using SnapGene software version 4 (Dotmatics, Boston, MA, USA).

4.4 Expression of Gn and Gc using SDS-PAGE and western blot

The expression of Gn and Gc from cell lysates of HEK293 cells transfected with plasmid DNA vectors (pcDNA3.1+) cloned with the RVFV M segment sequences was assessed using SDS-PAGE and western blot. The expression of Gn and Gc was evaluated in reduced and non-reduced samples to obtain insights into their folding, disulfide bond formation, and oligomerisation. Reduced samples were treated with dithiothreitol (DTT) to break the disulfide bonds and ensure that the glycoproteins Gn and Gc were resolved as monomers during electrophoresis.

For the reduced cell lysates, Gn was readily detected in all constructs (predicted size, 61 kDa) (Figure 11A). The size of Gn expressed from the Gn only and the Furin-T2A construct was smaller than that of the other constructs, as expected from their amino acid truncations (Figure 6) and in conformity with their predicted sizes of 49 kDa and 51 kDa, respectively. These results confirmed that Gn is expressed as a monomer under reducing conditions. For the non-reduced cell lysates, strong Gn detection was observed for the WT consensus, K1064A, K1050del, and H727A constructs, while low Gn detection was observed for Furin-T2A and very low Gn detection for the Gn-S-Gc and H727A-S constructs (Figure 11B). The very weak Gn detection from these two constructs suggests that the cysteine mutations introduced to induce disulfide bonds between Gn and Gc could have disrupted the folding or stability of Gn or Gc, leading to aggregation or degradation that may have hindered efficient immunoblot transfer during western blotting. This misfolding could also have led to the loss of antibody accessibility through obscuring the epitopes recognised by the anti-Gn monoclonal antibody.

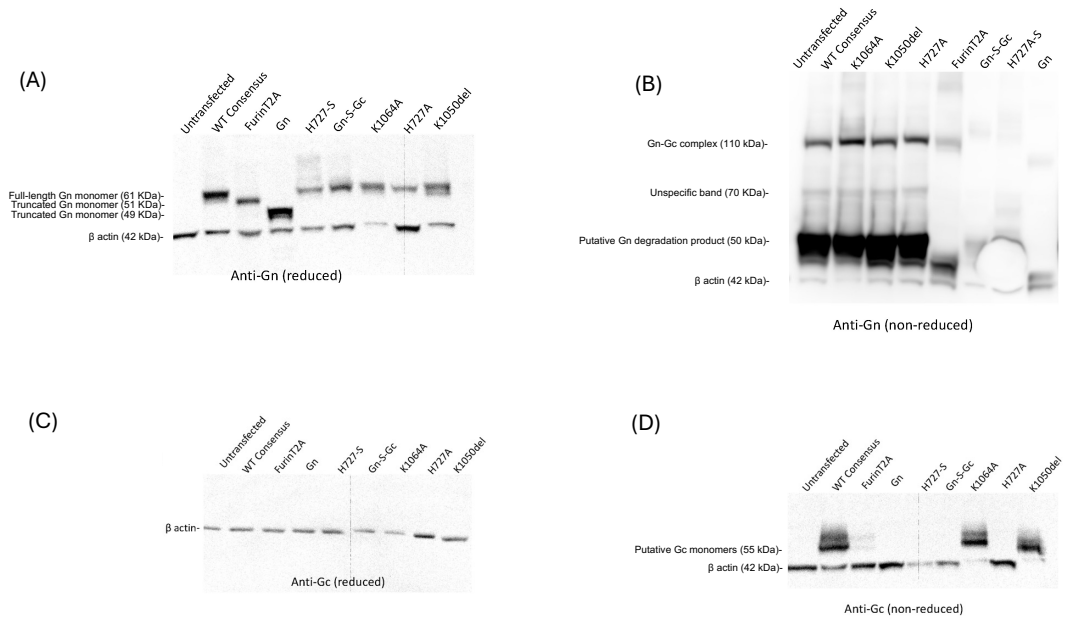

Figure 10: Gn and Gc expression from whole-cell lysates using SDS-PAGE and western blot

Expression of RVFV glycoproteins n (Gn) and c (Gc) from HEK293T/17 cell lysates transfected with plasmid DNA vectors encoding the various RVFV M segment sequences. Detection was achieved using mouse RVFV Gn and Gc IgG monoclonal antibodies and an HRP-conjugated secondary antibody. (A) Reduced Gn lysates. The bands at ~61 kDa correspond to full-length Gn monomers. Truncated bands at ~49 kDa (Gn-only) and ~51 kDa (Furin-T2A) align with expected sizes due to cytoplasmic tail deletions. (B) Non-reduced Gn. Bands at ~110 kDa likely represent Gn-Gc complexes, consistent with non-reduced conditions preserving disulfide bonds. Weak/no bands for Furin-T2A and Gn-S-Gc suggest misfolding or aggregation. Bands at ~50 kDa possibly represent Gn degradation products. ~70 kDa bands are non-specific. (C) Reduced Gc. Gc was not detected, possibly due to antibody limitation under denaturing conditions. (D) Non-reduced Gc. Putative Gc monomer (~55 kDa) seen in WT consensus, K1064A, and K1050del constructs, but this is inconclusive due to antibody detection limitations. Adapted from Figure 3 in Kitandwe, P. K., Rogers, P., Hu, K., Nayebare, O., Blakney, A. K., McKay, P. F., Kaleebu, P., & Shattock, R. J. (2024). A Lipid Nanoparticle-Formulated Self-Amplifying RNA Rift Valley Fever Vaccine Induces a Robust Humoral Immune Response in Mice. Vaccines, 12(10), 1088. https://doi.org/10.3390/vaccines12101088, under the Creative Commons Attribution 4.0 International (CC BY 4.0) license

The detection of Gc for reduced and non-reduced cell lysates was much less than that of Gn. Under reducing conditions, there was no Gc detection from the cell lysates of all constructs (Figure 11C). However, when the samples were not reduced, Gc was detected for the WT consensus, K1064A, and K1050del constructs (Figure 11D). Failure to detect Gc under reducing conditions could have resulted from poor antibody recognition under reducing conditions. Such conditions lead to Gc losing its tertiary structure, exposing linear epitopes not recognised by antibodies specific for conformational epitopes. Notably, the two mouse anti-Gc monoclonal antibodies (Clone 9C10 and Clone 1G4, BEI Resources) that were separately in this assay are not reported to be reactive in western blot, further supporting the possibility of failed detection due to poor antibody compatibility.

Interestingly, Gc was detected in three constructs (WT consensus, K1064A, and K1050 del) under non-reducing conditions (Figure 11D). However, the detected protein had a much smaller molecular weight (~55 kDa) than the ~100 kDa protein detected by anti-Gn under the same non-reducing conditions (Figure 11B).

4.5 Cell surface expression of Gn and Gc by flow cytometry

To assess the effects of the various RVFV M segment mutations on plasma membrane expression of Gn and Gc, human embryonic kidney (HEK) 293 cells were transfected with pDNA encoding these sequences and analysed using flow cytometry. To determine surface expression, transfected cells were stained with Gn and Gc monoclonal antibodies, followed by detection with phycoerythrin (PE)-conjugated secondary antibodies. Fluorescence intensity was performed using FlowJo software (version 10), with results reported as median fluorescence intensity (MFI). Statistical comparisons between constructs were done using the Kruskal–Wallis test with Dunn's correction for multiple comparisons. A p-value of <0.05 was considered significant.

All constructs except the Gn construct lacking the cytoplasmic tail and transmembrane domain expressed Gn on the cell surface (Figure 12A). Significant Gn expression compared to the negative control (Rabies G protein transfected cells) was observed for the Furin-T2A (MFI = 1457, SD = 187, $p = 0.004$) and K1050del (MFI = 1030, SD = 454, $p = 0.013$) constructs. These two constructs were also the only ones with a higher MFI than the WT consensus construct. For RVFV Gc, increased expression was observed for K1050del, K1064A, Gn-S-G, H727A, and H727A-S, although only the H727A construct exhibited significant expression compared to the untransfected negative control cells (MFI = 2147, SD = 127, $p = 0.04$). Surprisingly, Gc expression from the WT consensus and the Furin-T2A constructs was similar to that of the untransfected samples (Figure 12B).

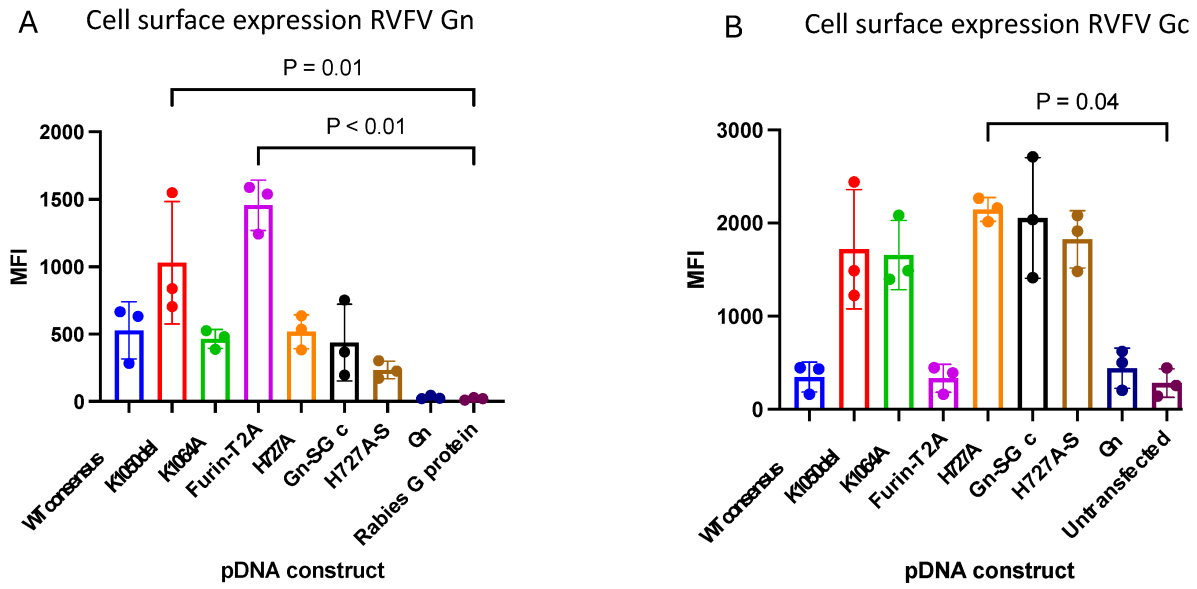

Figure 11: Cell surface expression of Gn and Gc by flow cytometry

Human embryonic kidney (HEK) 293 cells transfected with plasmid DNA (pDNA) vectors encoding various RVFV M segment sequences were assessed for cell surface expression of Gn and Gc by staining with anti-Gn or anti-Gc IgG monoclonal antibodies followed by phycoerythrin (PE)-conjugated IgG. Data acquisition was acquired using a BD LSR Fortessa flow cytometer, and expression was quantified as median fluorescence intensity (MFI) using FlowJo Software (version 10). (A) Cell surface expression of RVFV Gn. Significant RVFV Gn expression was observed for the Furin-T2A (MFI = 1457, SD = 187, p = 0.004) and K1050del (MFI = 1030, SD = 454, p = 0.013) constructs. (B) Cell surface expression of RVFV Gc. The H727A construct displayed significantly higher expression (MFI = 2147, SD = 127, p = 0.04). Other constructs, including K1050del, K1064A, Gn-S-G, and H727A-S, showed increased expression, but this did not reach statistical significance. Statistical analysis was performed using GraphPad Prism (version 10). The Kruskal–Wallis test corrected for multiple comparisons using Dunn's test was used to compare expressions between constructs. A p-value of <0.05 was considered statistically significant. Adapted from Figure 4 in Kitandwe, P. K., Rogers, P., Hu, K., Nayebare, O., Blakney, A. K., McKay, P. F., Kaleebu, P., & Shattock, R. J. (2024). A Lipid Nanoparticle-Formulated Self-Amplifying RNA Rift Valley Fever Vaccine Induces a Robust Humoral Immune Response in Mice. *Vaccines*, *12*(10), 1088. https://doi.org/10.3390/vaccines12101088, under the Creative Commons Attribution 4.0 International (CC BY 4.0) license.

Chapter Summary

This chapter focused on generating and optimising RVFV M segment constructs to enhance the plasma membrane expression of Gn and Gc. A consensus M segment sequence was

generated by aligning 151 complete RVFV sequences from GenBank and ViPR databases using the MUSCLE algorithm and truncated to start from the fourth methionine to ensure the expression of Gn and Gc only. Phylogenetic analysis demonstrated that the consensus sequence clustered with strains from recent outbreaks in East Africa, Sudan, Madagascar, and Saudi Arabia, offering broader cross-strain applicability than traditional vaccine strains such as Smithburn, MP-12, and Clone 13. This design improves the potential for inducing a more comprehensive immune response.

To optimise glycoprotein expression, site-directed mutations were introduced to the consensus RVFV M segment sequence, targeting the structural and functional properties of Gn and Gc. Eight constructs were individually cloned into the pcDNA3.1(+) mammalian expression vector and confirmed through restriction digestion and Sanger sequencing. Expression analysis revealed significant differences between the constructs. SDS-PAGE and western blot confirmed robust Gn expression under reducing conditions from all constructs, with bands consistent with predicted sizes. However, Gc was detected only under non-reducing conditions for a few constructs, highlighting challenges in antibody recognition or protein folding under reducing conditions.

Flow cytometry analysis demonstrated that constructs with cytoplasmic tail deletions showed significantly improved cell surface expression of Gn, with the construct that also included a Furin-T2A spacer between Gn and Gc having the highest expression. For Gc, the construct with a prefusion conformation stabilising mutation unexpectedly showed the highest surface expression. These results confirmed the ability of the inserted mutations to enhance glycoprotein surface localisation, albeit to varying degrees.

In conclusion, this chapter highlighted the potential of an RVFV M segment consensus sequence and a mutated RVFV M segment with enhanced Gn expression as promising saRNA vaccine antigens. These constructs provide a strong foundation for the further development of

immunogenic saRNA RVF vaccine candidates, addressing limitations in existing vaccine designs and offering a platform aligned with contemporary circulating RVFV strains.

CHAPTER FIVE RESULTS: SYNTHESIS AND CHARACTERISATION OF SaRNA ENCODING A CONSENSUS AND A MUTATED RVFV M SEGMENT SEQUENCE

5.1 Introduction

Self-amplifying RNA vaccines utilise viral replicase to amplify the RNA of the encoded antigen in host cells and therefore can express the same amount of antigen with a significantly lower dose compared to conventional mRNA vaccines [22]. Like conventional mRNA vaccines, saRNA vaccines can be rapidly produced and have a favourable safety profile, making them a desirable platform for developing vaccines against emerging infectious diseases like RVF.

Self-amplifying RNA vaccines have been used to develop vaccines for several infectious diseases, including a COVID-19 vaccine which has been approved for human use [24, 25]. However, until recently, no published studies had examined the development of a non-virally delivered saRNA vaccine against RVF, a gap this study aimed to address.

This chapter reports on the synthesis and characterisation of saRNA constructs encoding a consensus RVFV M segment sequence (WT consensus) and a mutated RVFV M segment sequence (Furin-T2A) which incorporates a furin cleavage site and T2A peptide between the two glycoproteins. In the previous chapter, the Furin-T2A sequence exhibited the highest plasma membrane expression of Gn among the eight RVFV M segment sequences that were evaluated. This construct was selected for further development into saRNA instead of the H727A construct, which had the highest cell surface expression of Gc by flow cytometry. This is because Gn-specific monoclonal antibodies have been demonstrated to have higher neutralising activity *in vitro* and protective efficacy than Gc-specific monoclonal antibodies [230]. In addition, Gc expression from the H727A construct was not demonstrated by SDS-PAGE and western blot, even though this could have been a limitation of the primary antibodies used.

Therefore, this chapter aims to synthesise and characterise saRNA constructs encoding a consensus and a mutated RVFV M segment sequence optimised for enhanced cell surface expression. It aims to evaluate the expression potential of these saRNA vaccines and lays the groundwork for their evaluation in animal models.

5.2 Cloning of the RVFV M segment sequences into the VEEV plasmid DNA vector

Double-stranded linear DNA fragments encoding the RVFV M segment consensus and Furin-T2A sequences were commercially synthesised using GeneArt Gene synthesis (Thermo Fisher Scientific, UK). They were then inserted into a Venezuelan equine encephalitis virus (VEEV) pDNA replicon by Gibson assembly using the chemical transformation protocol of the NEBuilder HiFi DNA assembly cloning kit (New England Biolabs, E5520S). The replicon was based on the Trinidad donkey VEEV alphavirus genome, whose structural genes, driven by the 26S subgenomic promoter, were replaced with the firefly luciferase (Fluc) gene. To confirm the successful cloning of the RVFV antigen sequences into the VEEV pDNA replicon, Sanger sequencing was performed by Eurofins Genomics (Ebersberg, Germany) on five *E. coli* clones transformed with the Gibson assembly product. The entire plasmid (backbone and insert) was sequenced using primers that were designed with the SnapGene software, version 4 (Dotmatics, Boston, MA, USA).

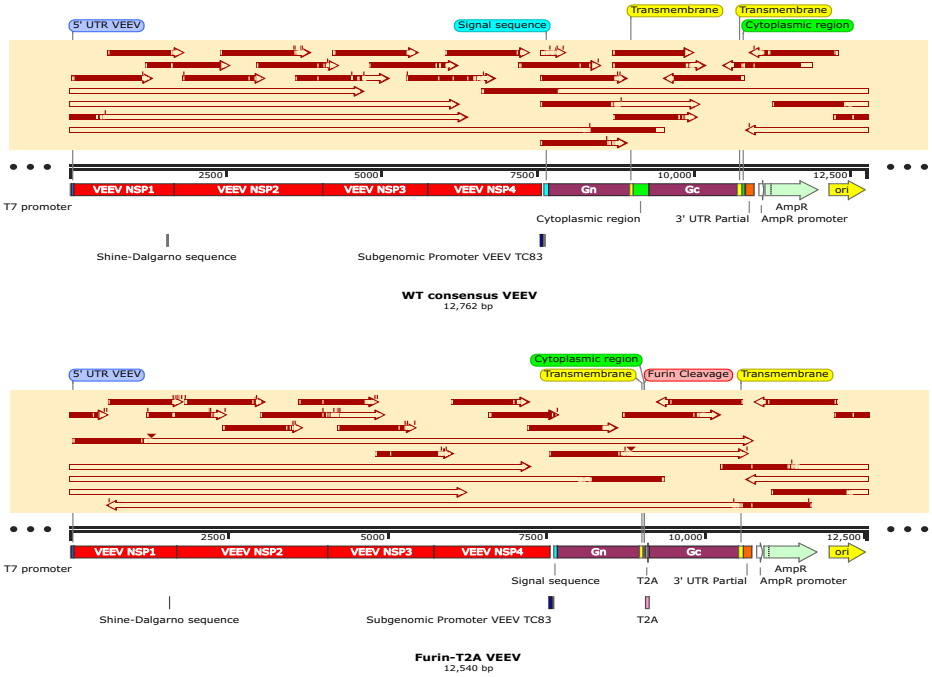

Figure 12: Sequencing of WT consensus and Furin-T2A plasmid DNA replicons

Sequencing of WT consensus and Furin-T2A plasmid DNA (pDNA) replicons. This figure illustrates the verification of the successful cloning of the wild-type (WT) consensus and Furin-T2A RVFV M segment sequences into the Venezuelan equine encephalitis (VEEV) plasmid DNA (pDNA) replicon using Sanger sequencing. Sequencing was performed by Eurofins Genomics and the results were verified by aligning each of the regions sequenced by the primers (red arrows) with the reference sequence using SnapGene software (version 4, Dotmatics, Boston, MA, USA). Breaks in the primer indicate nucleotide mismatches verified by comparing it with the sequence covered by the corresponding overlapping primer.

Sequencing chromatograms for the WT consensus and Furin-T2A constructs (Figure 13) demonstrated high-quality base calling and alignment with the reference sequence. The furin cleavage site and T2A modifications were correctly incorporated, with no off-target mutations or deletions observed. A comparison of the cloned sequences with the reference alignment revealed 100% identity with the reference sequence for both constructs. The successful cloning and sequence validation of the WT consensus and Furin-T2A RVFV M segment constructs established a strong foundation for their subsequent transcription into saRNA and further evaluation.

5.3 Self-amplifying RNA transcription and quality control

The quality of saRNA is critical for ensuring effective antigen expression and induction of immune responses. This section describes the transcription, capping, and quality assessment of saRNA constructs encoding the consensus RVFV M segment sequence (WT consensus) and its Furin-T2A mutant variant. These constructs were linearised, transcribed into saRNA, capped, purified, and analysed for structural integrity and purity.

In Vitro Transcription and Capping

The plasmid DNA (pDNA) constructs encoding the RVFV M segment sequences (consensus and Furin-T2A) were linearised using the MluI restriction enzyme, creating suitable templates for *in vitro* transcription. Restriction digestion was confirmed by agarose gel electrophoresis before proceeding to transcription (Figure 14A). The linearised templates were transcribed into saRNA using a T7 RNA polymerase-driven *in vitro* transcription (IVT) reaction, performed with the MEGAScript T7 RNA Polymerase Transcription Kit (Invitrogen, AM1334).

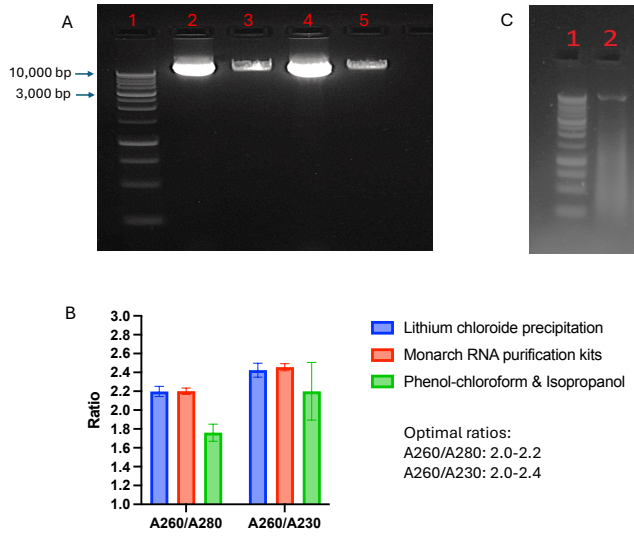

Figure 13: Verification of pDNA linearisation and saRNA quality

(A) Agarose gel electrophoresis showing pDNA linearisation. The VEEV pDNA replicon encoding WT consensus and Furin-T2A was linearised using the MluI restriction enzyme and evaluated on a 1% agarose gel in TBE buffer. Lanes 2&3-uncut and linearised WT consensus, respectively; Lanes 3 and 4 show uncut and linearised Furin-T2A, respectively. (B) Estimation of saRNA purity using spectrophotometry (NanoDrop). The bar graph shows mean ± SD A260/A280 and A260/A230 ratios for saRNA purified using different methods (LiCl precipitation, phenol-chloroform/isopropanol extraction and Monarch RNA purification kits). (C) Agarose gel electrophoresis showing the integrity of saRNA purified using phenol-chloroform/isopropanol extraction (Lanes 2-3) and LiCl precipitation (Lanes 4-5). Smears in lanes 2 and 3 show degraded saRNA, while distinct bands in lanes 4 and 5 show intact saRNA. The gel was prepared using the protocol adapted from Aranda et al. [225] and consisted of 1% agarose in TAE buffer with 0.07% sodium hypochlorite (2% household bleach) and 1X Gel Red (Biotium 41003).

Following transcription, a Cap 1 structure was enzymatically added to the 5′ end of the saRNA using the ScriptCap Cap 1 Capping System Kit (Cellscript Inc, CSCCS1710). The Cap 1 structure mimics the natural eukaryotic mRNA cap, enhancing RNA stability and ensuring efficient translation in mammalian cells.

After transcription and capping, the saRNA was purified to remove unincorporated nucleotides, enzymes, and other reaction by-products. Three purification methods were evaluated: (1) lithium chloride (LiCl) precipitation, (2) phenol-chloroform extraction followed by isopropanol precipitation, and (3) silica membrane-based purification using the Monarch RNA Cleanup Kit (New England Biolabs, T2050S). The purified saRNA was resuspended in either RNA storage buffer (10 mm HEPES, 0.1 mm EDTA, and 100 mg/mL trehalose) or nuclease-free water when intended for formulation with lipid nanoparticles or *in vivo*-jetRNA, respectively.

RNA Quality assessment

The purity of the saRNA purified by each of the three purification methods (LiCl precipitation, Phenol-chloroform/isopropanol and Monarch silica membranes) was estimated spectrophotometrically by measuring the A260/A280 and A260/A230 ratios on a NanoDrop

(Thermo Fisher Scientific). To ensure reproducibility, three batches of saRNA were synthesised and purified using each of the three purification methods over two days. The optimal A260/A280 and A260/A230 ratios were considered to be 2.0-2.2 and 2.0-2.4 respectively. The A260/A280 and A260/A230 ratios of saRNA purified using LiCl or Monarch RNA purification kits fell within the optimal range, while that purified using phenol-chloroform and isopropanol had a low A260/A230 ratio (Figure 14B).

To further assess the quality of the saRNA, its structural integrity was estimated using denaturing agarose bleach gel electrophoresis using a protocol adapted from Aranda et al. [225]. Self-amplifying RNA purified using phenol-chloroform and isopropanol was more degraded than that purified using LiCl precipitation (Figure 14C).

5.4 *In vitro* expression of RVFV Gn from saRNA

Following transfection of HEK293 cells with the WT Conesus and Furin-T2A saRNA, an SDS-PAGE and western blot were performed on the whole-cell lysates under reducing conditions to assess *in vitro* antigen expression. There was strong Gn detection with the wild-type consensus, and very weak Gn detection for the Furin-T2A construct (Figure 14A). Additionally, the cell surface expression of Gn from HEK293 cells transfected with the two saRNA constructs was assessed using flow cytometry 24 h after transfection. The cells were stained with Gn-specific IgG monoclonal antibodies and IgG PE primary and secondary antibodies, respectively. In contrast to SDS-PAGE and western blot, cells transfected with the Furin-T2A saRNA had significantly higher Gn expression compared to those that were transfected with the wild-type consensus saRNA (Figure 15B)

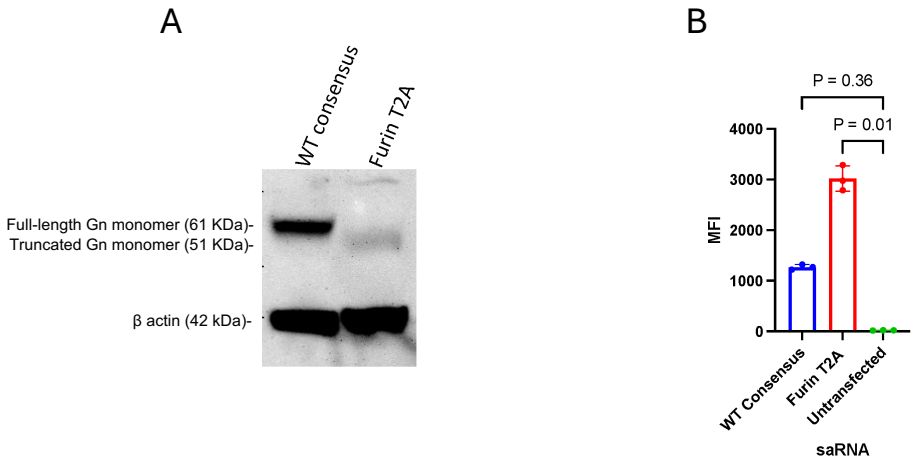

Figure 14: *In vitro* expression of Gn from saRNA-transfected HEK293 cells

Human embryonic kidney (HEK) 293 cells were transfected with wild-type (WT) consensus and Furin-T2A saRNA and assessed for Gn expression. (A) Detection of Gn using SDS-PAGE and western blot of reduced whole-cell lysates. The blots were probed with the Gn-specific IgG monoclonal antibody (RV Gn-1) followed by an HRP-conjugated secondary antibody. (B) Cell surface expression of RVFV Gn by flow cytometry. Cells were stained with RV Gn-1 and IgG PE and acquired on a BD LSR Fortessa flow cytometer. Flow data was analysed using FlowJo™ v10.10.0 software for Mac (BD Life Sciences), and expression measured as median fluorescence intensity (MFI). Statistical analysis was performed using GraphPad Prism (version 10). The Kruskal–Wallis test with Dunn's correction for multiple comparisons was used to compare expressions between constructs. A p-value of <0.05 was considered statistically significant. Adapted from Figure 5 in Kitandwe, P. K., Rogers, P., Hu, K., Nayebare, O., Blakney, A. K., McKay, P. F., Kaleebu, P., & Shattock, R. J. (2024). A Lipid Nanoparticle-Formulated Self-Amplifying RNA Rift Valley Fever Vaccine Induces a Robust Humoral Immune Response in Mice. *Vaccines*, *12*(10), 1088. https://doi.org/10.3390/vaccines12101088, under the Creative Commons Attribution 4.0 International (CC BY 4.0) license

5.5 Measurement of encapsulation efficiency

The efficient delivery of saRNA to target cells is critical for effective antigen expression. Encapsulation of saRNA protects it from degradation, ensures its efficient cellular uptake and endosomal escape, and enhances its stability. In this subsection, we show how the formulation efficiency of saRNA encapsulated using *in vivo*-jetRNA and *in vivo*-jetRNA+ was assessed using the Quant-iT RiboGreen RNA Reagent and Kit (Invitrogen) a fluorescence-based assay

for the detection of RNA in solution. Formulation efficiency was evaluated using a representative batch of saRNA as a proof-of-concept to validate the efficacy of the encapsulation method.

A standard curve was generated using various dilutions of a ribosomal RNA standard, and the fluorescence plotted against RNA concentrations. The curve demonstrated excellent linearity ($R^2 > 0.99$), ensuring the accuracy and reliability of the assay across the range of saRNA concentrations tested (Figure 16A).

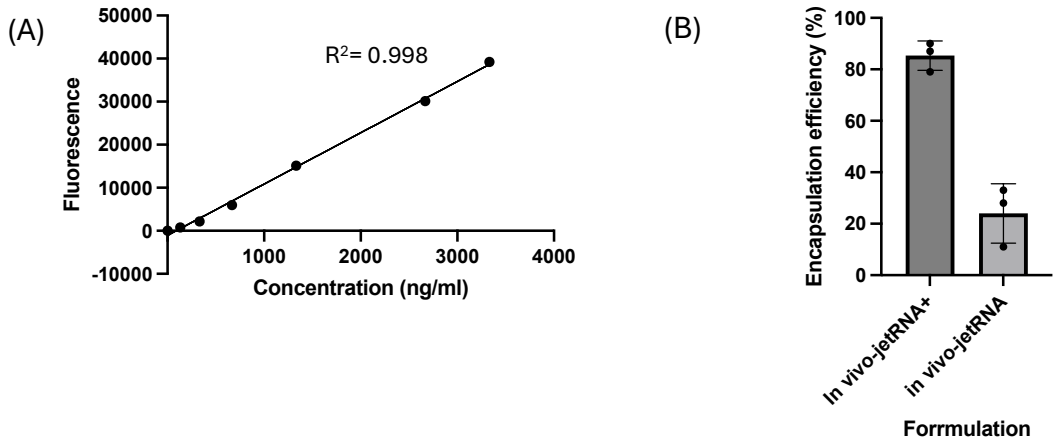

Figure 15: Encapsulation efficiency of saRNA measured by the RiboGreen assay

The encapsulation efficiency of saRNA *in vivo*-jetRNA+ was compared with *in vivo*-jetRNA using the RiboGreen assay. (a) Standard curve of the ribosomal RNA standard used to quantify the saRNA (b). Comparison of the encapsulation efficiency between *in vivo*-jetRNA+ and *in vivo*-jetRNA. Bars represent the mean ± SD from three independent experiments.

A comparison between the cationic lipid formulations revealed that *in vivo*-jetRNA+ had a significantly higher encapsulation efficiency of 84 ± 10% compared with 32 ± 5% for *in vivo*-jetRNA ($p<0.01$). According to the manufacturer Polyplus, *in vivo*-jetRNA+ can achieve an mRNA encapsulation efficiency of up to 100%; however, this could not be verified in independent peer-reviewed publications. The encapsulation efficiency of *in vivo*-jetRNA is not publicly available.

Chapter Summary

In this chapter, we report on the synthesis and characterisation of saRNA encoding a consensus and a mutated RVFV M segment sequence optimised for enhanced cell surface expression. Double-stranded DNA fragments encoding the WT consensus and Furin-T2A sequences were successfully cloned into the VEEV pDNA replicon using Gibson assembly. Using Sanger sequencing, we verified the integrity of the cloned sequences, showing 100% alignment with the reference sequences for both constructs. This step thus provided the foundation for the subsequent transcription and evaluation of the constructs. We proceeded to synthesise the saRNA using *in vitro* transcription followed by capping using a T7 polymerase reaction and Cap 1 enzymatic post-transcription reaction, respectively. Importantly, we estimated the purity and integrity of the saRNA transcripts using spectrophotometry and denaturing agarose gel electrophoresis, respectively. Self-amplifying RNA purified using LiCl or Monarch RNA clean-up kits (New England Biolabs) had optimal A260/A280 and A260/A230 ratios (2.0–2.2 and 2.0–2.4, respectively), indicating high purity and minimal contamination. In comparison, phenol-chloroform extraction produced lower-quality saRNA with lower A260/A280 ratios and evidence of degradation on agarose gel electrophoresis.

After completing the quality assessment of the saRNA, we then verified the *in vitro* expression of Gn from both WT consensus and Furin-T2A saRNA constructs using SDS-PAGE and western blot on reduced samples. Gn was readily detected from the WT consensus but weakly detected from the Furin-T2A, suggesting differential antigen processing. Interestingly, the Furin-T2A construct showed higher cell surface expression of Gn compared to the WT consensus construct as measured by MFI. We also evaluated the encapsulation efficiency of two cationic lipid formulations: the original, now discontinued *in vivo*-jetRNA and its

reportedly improved version in-vivo-jetRNA+. The saRNA encapsulation efficiency for *in vivo*-jetRNA+ was significantly higher than that of *in vivo*-jetRNA (84% vs 32%).

Overall, this chapter demonstrated the successful transcription of both WT consensus and Furin-T2A constructs, confirmed the production of high-quality saRNA, highlighted the superior encapsulation efficiency of *in vivo*-jetRNA+ over its predecessor *in vivo*-jetRNA, and established key quality control aspects ensuring the integrity and purity of *in vitro* transcribed saRNA.

These findings validate the Wild-Type (WT) consensus and the Furin-T2A constructs as suitable saRNA candidates. The Furin-T2A, a construct optimised for enhanced cell surface expression, was confirmed to enhance plasma membrane expression *in vitro* when delivered as saRNA, further validating the results of the previous chapter. Together, these results achieve the desired outcome of synthesising and characterising our WT consensus and Furin-T2A saRNA constructs.

CHAPTER SIX RESULTS: IMMUNE RESPONSES IN MICE IMMUNISED WITH CANDIDATE saRNA RVF VACCINES

6.1 Introduction

The ability of a vaccine to induce robust humoral and cellular immune responses is a critical determinant of its efficacy. For RVFV, neutralising antibodies targeting Gn and Gc, encoded by the viral medium (M) segment, are associated with protection [31]. By contrast, the role of T cells in RVFV immunity remains less well defined. However, immune responses such as the production of interferon-gamma (IFN-γ), TNF-α, IL-2, and the expression of CD107a, which are associated with viral immunity, have been reported to be induced in mice vaccinated with LNP-formulated RVFV vaccines [28].

This chapter reports on the immunogenicity of candidate saRNA RVFV vaccines in BALB/c mice, formulated using either LNPs or the cationic lipids *in vivo*-jetRNA and its improved version, *in vivo*-jetRNA+. The saRNA vaccines evaluated encoded either a WT consensus or Furin-T2A. We assessed the production of RVFV-specific IgG antibodies, RVFV-pseudovirus neutralisation activity, and T-helper cytokine expression.

6.2 Induction of anti-Gn IgG by RVFV pDNA vaccines

In preparation for immunogenicity experiments, 10 mice were immunised intramuscularly with 10 μg of the pDNA vectors expressing the WT consensus and Furin-T2A antigens (5 mice per group). Both groups of mice were boosted using the same antigens four weeks later. After eight weeks from the first immunisation, anti-Gn IgG ELISA was performed on the mouse serum. In both groups of mice, anti-Gn IgG was induced, with the Furin-T2A construct producing significantly higher amounts of IgG compared with the WT consensus (Figure 16). This result confirmed the immunogenicity of our antigens and the effectiveness of the Furin-T2A mutations. We therefore proceeded to evaluate these antigens as saRNA. This pilot study,

including mice immunisation, sample collection and ELISA was conducted by Imperial College London staff.

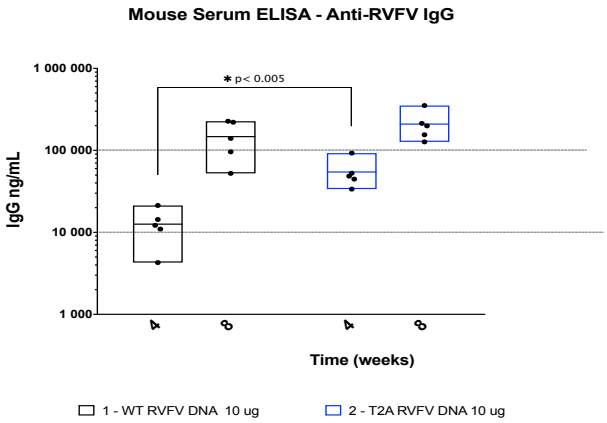

Figure 16: Anti-Gn IgG responses in BALB/c mice vaccinated with RVFV pDNA

Mice were immunised with pDNA vectors expressing RVFV surface glycoproteins. Five mice were immunised with the WT consensus pDNA construct and another 5 with the Furin-T2A pDNA construct. After 8 weeks, blood was collected, an RVFV Gn-specific ELISA was done to measure serum IgG levels. Data was analysed using a multiple t test and statistical significance was determined using the Holm-Sidak method, with $\alpha = 0.05$.

6.3 Anti-Gn IgG responses in mice immunised with LNP-saRNA RVF vaccines

Six-week-old BALB/c mice were immunised intramuscularly on day 0 and day 28 with either 0.1 µg, 1.0 µg, or 10 µg of the WT consensus or the Furin-T2A saRNA RVF candidate vaccine. Blood samples were collected on days 14, 28, and 42. Anti-Gn IgG was detected at all the sampling time points in all mice immunised with the candidate saRNA RVF vaccines (Figure 17). Antibody production was dose-dependent, increasing with higher vaccine doses. Both vaccines induced similar levels of RVFV Gn IgG antibodies, which increased substantially following the booster dose. Mice immunised with 10 µg doses of WT consensus and Furin-T2A LNP-formulated saRNA vaccines produced high levels of RVFV Gn-specific IgG by day

42. Mean antibody titres were significantly higher in the 10 µg group for both WT consensus (mean = 522,000; SD = 424,736; p < 0.01) and Furin-T2A (mean = 522,848; SD = 366,604; p < 0.01) compared to the lower doses (0.1 µg and 1 µg), where responses were negligible. Anti-Gn IgG responses were induced after the first dose but reached statistical significance only after the booster dose, indicating the importance of a prime-boost strategy. This study was done at Imperial College London with mice immunisation and sample collection performed by Robin Shattock's laboratory team.

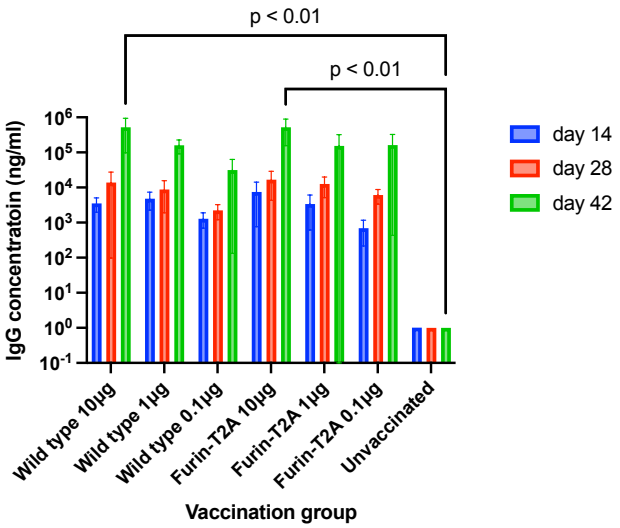

Figure 17: Anti-Gn IgG in mice immunised with candidate LNP-saRNA RVF vaccines

BALB/c mice (n = 35, five per group) were immunised intramuscularly on days 0 and 28 with 0.1 µg, 1.0 µg, or 10 µg of the WT consensus or the Furin-T2A candidate saRNA RVF vaccines and the RVFV Gn binding antibodies in serum were measured on days 14, 28 and 42 using an indirect ELISA. Statistically significant RVFV Gn antibody levels were observed only on day 42 in the mice that received 10 µg of the WT consensus vaccines (Mean = 522,000, SD = 424,736, $p < 0.01$) and Furin-T2A vaccines (Mean = 522,848, SD = 366,604, $p < 0.01$). Statistical analysis was performed using GraphPad Prism (version 10), applying two-way ANOVA with Dunnett's multiple comparison test and a single pooled variance. Bars represent the mean ± SD of measurements of five mice per group. Adapted with modifications from Figure 6 in Kitandwe, P. K., Rogers, P., Hu, K., Nayebare, O., Blakney, A. K., McKay, P. F., Kaleebu, P., & Shattock, R. J. (2024). A Lipid Nanoparticle-Formulated Self-Amplifying RNA Rift Valley Fever Vaccine Induces a Robust Humoral Immune Response in Mice. *Vaccines*, *12*(10), 1088. https://doi.org/10.3390/vaccines12101088, under the Creative Commons Attribution 4.0 International (CC BY 4.0) license.

6.4 Pseudovirus neutralising activity in LNP-saRNA RVF vaccine immunised mice

To assess the ability of our candidate vaccines to induce RVFV-neutralising antibodies, we conducted an RVFV pseudovirus-neutralising assay on day 42, two weeks after the booster dose. Neutralising activity was expressed as half-maximal inhibitory concentration (IC50), determined by measuring the luciferase signal in HEK 293T/17 cells cultured for 48 hours at 37 °C, 5% CO_2. Cells were exposed to serially diluted heat-inactivated serum pre-incubated for one hour at 37°C, 5% CO_2 with 100 $TCID_{50}$ of RVFV pseudoviruses. The $TCID_{50}$ was calculated using the Reed–Muench method, and IC50 values were determined by non-linear regression in GraphPad Prism (version 10) as recommended by Ferrera and Temperton [229].

The highest RVFV neutralising activity was observed in mice immunised with 10 μg of the WT consensus (median = 4495, IQR = 14,904, $p < 0.01$), followed by mice that received 1 μg of the same vaccine (median IC50 = 5089, IQR = 5500, $p < 0.01$). No RVFV pseudovirus-neutralising activity was detected in the mice that were immunised with 0.1 μg of the Furin-T2A vaccine and all but one of the mice that received 1.0 μg of the same vaccine. In contrast, low-level RVFV pseudovirus-neutralising activity was observed in mice vaccinated with 0.1 μg of the WT consensus and 10 μg of the Furin-T2A vaccine; however, this was not statistically significant compared with the unimmunised group ($p > 0.05$).

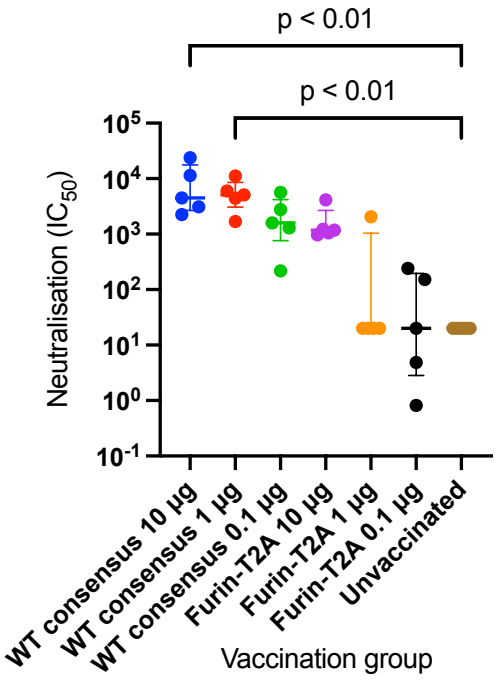

Figure 18: Pseudovirus neutralising activity in the serum of mice immunised with candidate LNP-saRNA RVFV vaccines

BALB/c mice (n = 35; five mice per group) were immunised intramuscularly on days 0 (baseline) and 28 with 0.1 µg, 1.0 µg, or 10 µg of the WT consensus or Furin-T2A candidate saRNA RVF vaccines and the RVFV pseudovirus neutralisation activity in serum was measured on day 42 as half-maximal inhibitory concentration (IC50). Statistically significant neutralising activity was observed in the mice that received either 1 µg or 10 µg of the WT consensus vaccines (median IC50 = 5089, IQR = 5500, $p < 0.01$) and (median = 4495, IQR= 14,904, $p < 0.01$) respectively. Statistical analysis was performed in GraphPad Prism (version 10) using the Kruskal–Wallis test with Dunn's correction for multiple comparisons. Only statistically significant p values ($p<0.05$) are shown. The plot shows the median with IQR of five mice per group. Adapted with slight modification from Figure 6 in Kitandwe, P. K., Rogers, P., Hu, K., Nayebare, O., Blakney, A. K., McKay, P. F., Kaleebu, P., & Shattock, R. J. (2024). A Lipid Nanoparticle-Formulated Self-Amplifying RNA Rift Valley Fever Vaccine Induces a Robust Humoral Immune Response in Mice. *Vaccines*, *12*(10), 1088. https://doi.org/10.3390/vaccines12101088, under the Creative Commons Attribution 4.0 International (CC BY 4.0) license.

6.5 Anti-Gn IgG responses in mice immunised with *in vivo*-jetRNA formulated vaccines

Following the assessment of our candidate vaccines formulated with LNPs, the same vaccines (WT consensus and Furin-T2A) were evaluated in the cationic lipid *in vivo*-jetRNA (Polyplus). This mouse immunogenicity study was conducted in Uganda with vaccinations and sample collection being done by staff at Makerere University School of Veterinary Medicine and Animal Resources (SVAR) at the College of Veterinary Medicine, Animal Resources and Biosecurity (CoVAB). The vaccines were synthesised at UVRI from pDNA glycerol stocks that were shipped to Uganda from Imperial College London. Formulation with *in vivo*-jetRNA

was chosen because it does not require any specialised equipment to use, unlike LNPs, for which formulation equipment was unavailable in Uganda.

Anti-Gn IgG responses in mice immunised with 1 µg, 5 µg, or 10 µg of the WT consensus or Furin-T2A candidate saRNA RVFV vaccines were assessed at baseline (day 0), day 21, day 42, and day 56. Unimmunised mice served as controls.

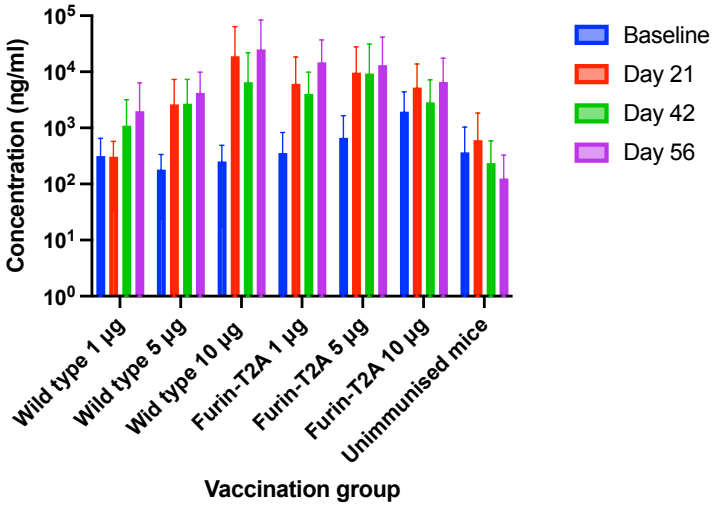

Figure 19: Anti-Gn IgG in mice immunised with *in vivo*-jetRNA saRNA RVFV vaccines

BALB/c mice (n = 42, six per group) were immunised intramuscularly on days 0, 21, and 42 with 1 µg, 5 µg, or 10 µg of the WT consensus or Furin-T2A candidate saRNA RVFV vaccines and the RVFV Gn-binding antibodies in serum were measured on days 14, 28, and 42 using an indirect ELISA for anti-Gn IgG. No significant differences in anti-Gn IgG were observed between vaccination groups or across the different time points. Statistical analysis was performed in GraphPad Prism (version 10) using two-way ANOVA with Geisser-Greenhouse correction.

Compared with the BALB/c mice used in the immunogenicity study conducted at Imperial College London, mice from CoVAB had high anti-Gn IgG background levels at baseline and in the unimmunised mice (Figure 19). On day 21, three weeks after the first vaccination, there was a noticeable increase in serum anti-Gn IgG in mice immunised with 5 µg and 10 µg of the WT consensus saRNA vaccine and those that received 1 µg and 5 µg of the Furin-T2A vaccine. These differences were, however, not statistically significant when compared with the baseline levels. Boosting at day 21 did not increase antibody levels three weeks later on day 42 in all vaccination groups except for a slight increase in the group that received 1 µg of the WT

consensus vaccine. Similarly, there was a slight increase in anti-Gn IgG values in all groups two weeks after the third and final boost.

In conclusion, these results indicate that the WT consensus and Furin-T2A saRNA RVF vaccine candidates were not immunogenic when formulated using *in vivo*-jetRNA cationic lipids, as they failed to induce significant anti-Gn IgG even after multiple doses.

6.6 Anti-Gn IgG levels in mice immunised with *in vivo*-jetRNA+ saRNA RVF vaccines

Given the poor immunogenicity of our candidate saRNA vaccines when formulated with *in vivo*-jetRNA, we evaluated an improved version of this cationic lipid–*in vivo*-jetRNA+. A similar study design was followed, except that the final booster was administered on day 63 instead of day 42 due to technical challenges with vaccine preparation.

Before proceeding, we first assessed the background anti-Gn IgG responses using BALB/c mice obtained from CoVAB and Mbarara University of Science and Technology (MUST). We investigated the effects of haemolysis, complement inactivation, and mouse source on the background anti-Gn IgG levels. Our results showed that haemolysis had no significant effect on the background anti-Gn IgG levels. Similarly, complement inactivation by heating serum at 56 ˚C for 30 minutes did not lower the background anti-Gn IgG levels but instead increased them. However, when we compared anti-Gn IgG levels according to the source, we observed significantly higher levels in mice from CoVAB compared to those from MUST (Figure 20).

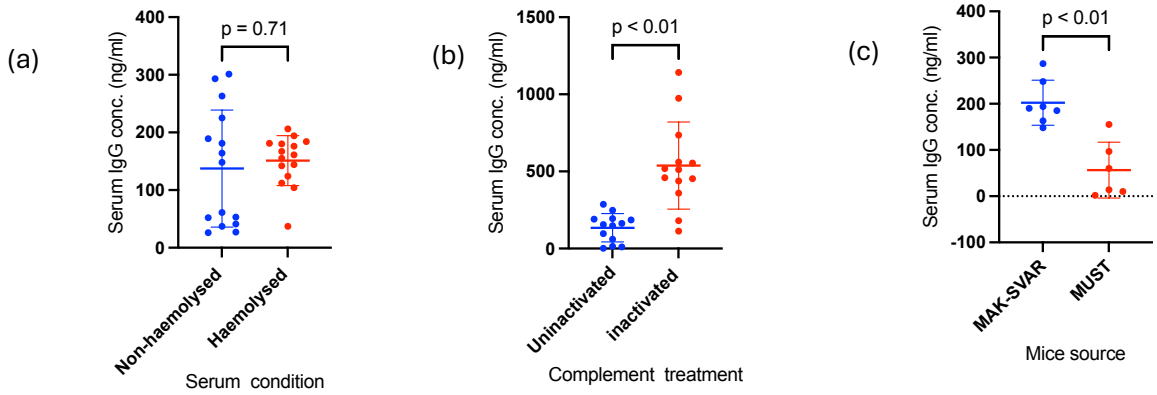

Figure 20: Baseline RVFV glycoprotein n (Gn) IgG ELISA responses in study mice

(a) Effect of haemolysis on RVFV Gn IgG levels. Haemolysed (red-coloured) mouse serum was tested in parallel (same ELISA plate) with non-haemolysed (clear) serum, n = 15. There was no statistically significant difference in the RVFV Gn IgG levels between the haemolysed serum (mean =151 ng/mL) and non-haemolysed serum (mean = 137 ng/mL), $p > 0.05$. (b) Effect of complement inactivation on RVFV Gn IgG levels. Serum from BALB/c mice sourced from Makerere University School of Veterinary Medicine and Animal Resources (MAK-SVAR) was complement-inactivated by heating at 56 ˚C for 30 minutes and tested alongside a non-inactivated aliquot of the same serum (n = 13). Complement-inactivated serum had significantly higher RVFV Gn IgG levels (mean = 539 ng/mL) compared to complement non-inactivated serum (mean = 135 ng/mL), $p < 0.01$. (c) Impact of mice source on the mean RVFV Gn IgG levels. Serum isolated from mice from MAK-SVAR was tested in parallel with serum isolated from mice from Mbarara University of Science and Technology (MUST). MAK-SVAR serum had significantly higher RVFV Gn IgG levels (mean = 202 ng/mL) than that from MUST (mean = 56 ng/mL), $p < 0.01$. Data analysis was performed in GraphPad Prism (version 10) using the Mann-Whitney test. A p-value of <0.05 was considered statistically significant. Error bars represent 95% CI.

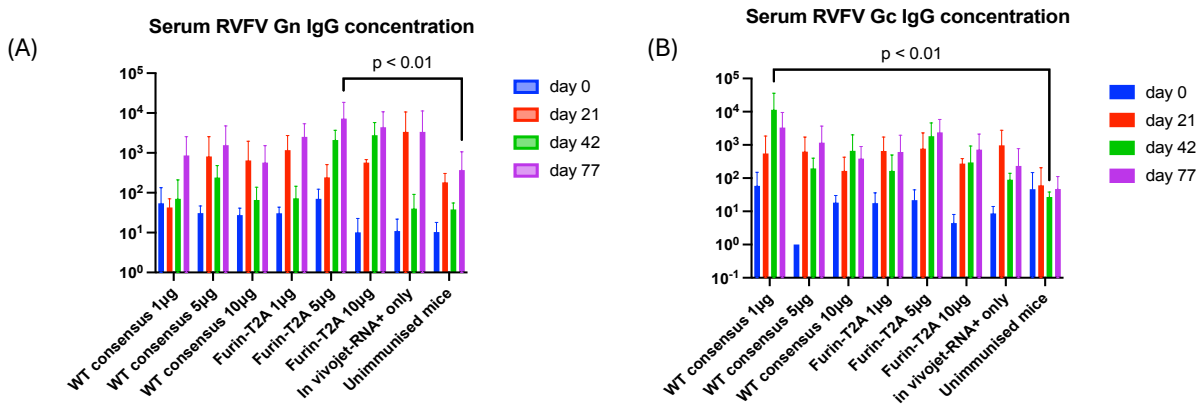

Figure 21: Anti-Gn and anti-Gc IgG in mice immunised with *in vivo*-jetRNA+ saRNA RVFV candidate vaccines

BALB/c mice (n = 48, six mice per group) were immunised intramuscularly on days 0 (baseline), 21, 42, and 63 with 1 µg, 5.0 µg, or 10 µg of the WT consensus or the Furin-T2A candidate saRNA RVFV vaccines. The concentrations of RVFV Gn and RVFV Gc binding antibodies in the serum were measured using indirect ELISA. (**a**) Serum RVFV Gn IgG concentration. Statistically significant RVFV Gn IgG levels were observed only on day 77 in the group that received 5 µg of the Furin-T2A vaccine (mean = 7254 ng/mL, SD = 11,271, $p < 0.01$). (**b**) Serum RVFV Gc IgG concentration. Statistically significant RVFV Gc IgG antibodies were observed only on day 42 in the group that received 1 µg of the WT consensus vaccine (Mean = 11438, SD = 24832, $p < 0.01$). Statistical analysis was performed using GraphPad Prism (version 10), applying two-way ANOVA with Dunnett's multiple comparison test assuming a single pooled variance. Bars represent the mean ± SD of six mice per group. Only statistically significant p-values ($p < 0.05$) are displayed.

We proceeded with the mouse study using mice from CoVAB as we could not obtain more BALB/c mice from MUST. Results showed that while IgG responses were dose-dependent, they were generally lower compared to the LNP-formulated vaccines. A statistically significant increase in RVFV Gn IgG levels compared to baseline was observed only on day 77 in the mice that received 5 µg of Furin-T2A saRNA RVF vaccine (mean = 7254; SD = 11,271; $p < 0.01$). For anti-Gc IgG, a statistically significant increase from baseline was observed only on day 42, in the group that received 1µg of the WT consensus vaccine (Mean = 11,438, SD = 24,832, $p < 0.01$).

These results showed a slight improvement in vaccine-induced immune responses in mice immunised with *in vivo*-jetRNA+ compared to those immunised with the *in vivo*-jetRNA formulation. However, this should be interpreted with caution as different mouse sources were used and animals were not randomised within a single experiment.

6.7 Pseudovirus neutralising activity in serum of mice immunised with *in vivo*-jetRNA+ candidate saRNA RVF vaccines

Following the assessment of the RVFV binding antibodies, we measured the neutralising activity of the serum in mice immunised with our candidate RVF saRNA vaccines. Neutralising activity–quantified as the half-maximal inhibitory concentration (IC50) –was determined by measuring the luciferase signal in HEK 293T/17 cells cultured for 48 hours at 37 °C and 5% CO_2. The cells were exposed to cell culture media containing serially diluted heat-inactivated serum. The serum was pre-incubated for one hour at 37 °C and 5% CO_2 with 100 tissue culture infectious doses ($TCID_{50}$) of RVFV pseudoviruses. The $TCID_{50}$ of the virus was determined using the Reed-Muench method, and the IC50 was calculated by non-linear regression in GraphPad Prism (version 10) as recommended by Ferrera and Temperton [229]. Neutralising activity was only detectable in mice immunised with 5 µg WT consensus saRNA RVF candidate vaccine (median IC50 = 4777, IQR = 5701, $p < 0.01$). Mice immunised with Furin-T2A saRNA RVF vaccines did not exhibit significant neutralisation activity at any dose (Figure 22).

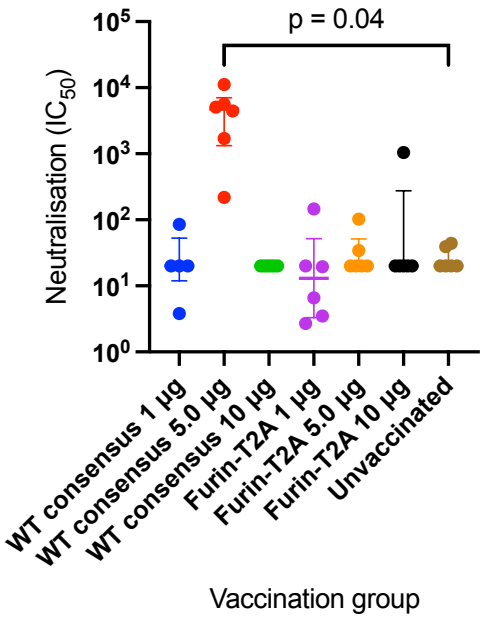

Figure 22: RVFV pseudovirus neutralising activity in serum from mice immunised with *in vivo*-jetRNA+ candidate saRNA RVFV vaccines

BALB/c mice (n = 48, six per group) were immunised intramuscularly on days 0 (baseline), 21, and 63 with 1 µg, 5 µg, or 10 µg of the wild-type (WT) consensus or Furin-T2A candidate saRNA RVF vaccines. On day 77, RVFV pseudovirus neutralising activity in serum was assessed in both saRNA vaccine-immunised and unimmunised mouse groups (n = 42, six mice per group) and expressed as the half-maximal inhibitory concentration (IC50). The graph shows the median IC50 value with the interquartile range. Statistically significant RVFV pseudovirus-neutralising activity was observed in mice that received 5 µg of the WT consensus vaccine (median IC50 = 4777, IQR = 5701, $p < 0.01$). Statistical analysis was performed in GraphPad Prism (version 10) using the Kruskal–Wallis test, followed by Dunn's post hoc test with correction for multiple comparisons. Only statistically significant p-values ($p < 0.05$) are displayed.

6.8 Assessment of IFN-γ production by ELISpot

To assess cellular immune responses, splenocytes from mice immunised with our *in vivo*-jetRNA+-formulated candidate vaccines were harvested on day 77. They were stimulated with 5 µg/mL (final concentration) of RVFV Gn peptide SYAHHRTLL and Gc peptides SYKPMIDQL and GGPLKTILL. IFN-γ production was then measured by ELISpot after an 18-hour stimulation, quantified as spot-forming units (SFU) per million splenocytes. Responses were normalised by subtracting the mock (no peptide) response. Statistically significant IFN-γ production was only observed in splenocytes from mice that received 5 µg

of the Furin-T2A vaccine following stimulation with the Gc peptide GGPLKTILL. IFN-γ production was also observed in other vaccination groups, but this was low and not statistically significant (Figure 23).

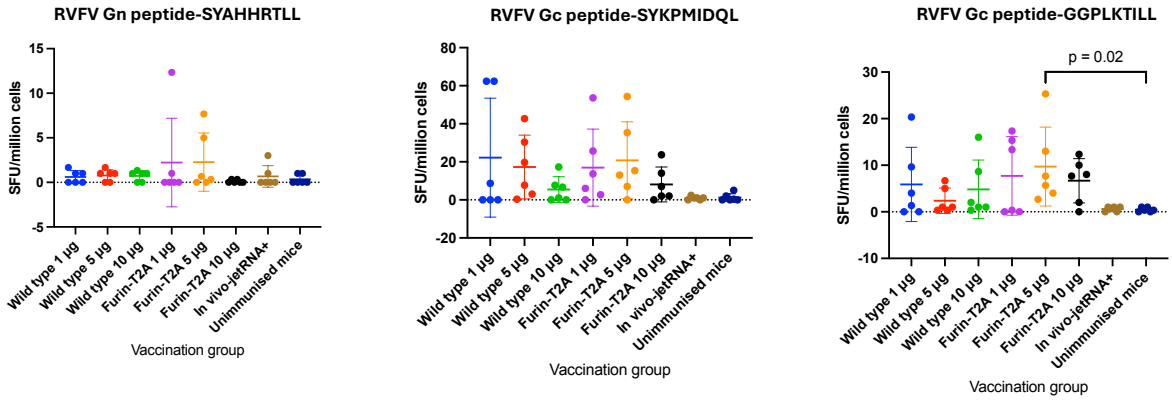

Figure 23: IFN-γ production by ELISpot in splenocytes from mice vaccinated with candidate saRNA RVFV vaccines

BALB/c mice (n = 48, six mice per group) were immunised intramuscularly on days 0 (baseline), 21, and 63 with 1 µg, 5 µg, or 10 µg of the wild-type (WT) consensus or Furin-T2A candidate saRNA RVFV vaccines. On day 77, their splenocytes were seeded in triplicate at 3.5 x10^5 cells/well in 96-well plates and stimulated for 18 hours at 37 °C and 5% CO_2 with 5 µg/mL (final concentration) of the RVFV Gn peptide SYAHHRTLL or Gc peptides SYKPMIDQL and GGPLKTILL. Interferon (IFN)-γ production was quantified as spot-forming units (SFU) per million splenocytes, and responses were normalised by subtracting the mock (no peptide) response. Statistical analysis was performed in GraphPad Prism (version 10) using the Kruskal–Wallis test, followed by Dunn's post hoc test with correction for multiple comparisons. Bars represent the mean ± SD of six mice per group. Only statistically significant p-values ($p < 0.05$) are displayed.

6.9. Multiple cytokine analysis

Cytokine production was analysed using the LEGENDplex multiplex assays to profile T-helper cell responses in the cell culture supernatant of splenocytes stimulated with RVFV-specific peptides. The splenocytes harvested on day 77, two weeks after the third and final booster vaccination, were stimulated with 5 µg/mL of the same peptides used for ELISpot. After 48 hours of incubation at 37 °C with 5% CO_2, the cytokines interleukin (IL)-2, IL-4, IL-5, IL-6, IL-9, IL-10, IL-13, IL-17A, IL-17F, IL-22, interferon (IFN)-γ, and tumour necrosis factor

(TNF)-α in the cell supernatant were quantified using the 12-plex LEGENDplex Mouse T-helper Cytokine Panel (BioLegend, 741043) on a Beckman Coulter CytoFLEX flow cytometer. Of the 12 cytokines that were measured, only mice that were immunised with 1 µg and 10 µg of the WT consensus showed significant cytokine levels of IL-2 (1 µg), IL-4 (1 µg), and IL-6 (10 µg).

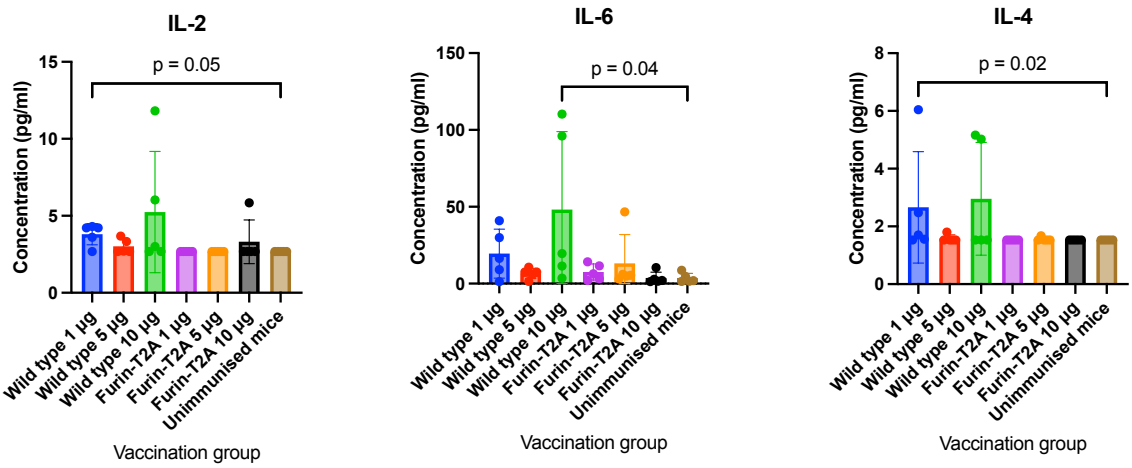

Figure 24: T-helper cytokine production in mice immunised with *in vivo*-jetRNA+ saRNA RVFV vaccines

BALB/c mice (n = 48, six mice per group) were immunised intramuscularly on days 0 (baseline), 21, and 63 with 1 µg, 5 µg, or 10 µg of the wild-type (WT) consensus or Furin-T2A candidate saRNA RVFV vaccines. On day 77, splenocytes from saRNA vaccine-immunised and unimmunised mice groups (n = 35, five mice per group) were stimulated with 5 µg/mL (final concentration) of the RVFV Gn peptide SYAHHRTLL and Gc peptides SYKPMIDQL and GGPLKTILL. After 48 hours of incubation at 37 °C with 5% CO_2, the cytokines interleukin (IL)-2, IL-4, IL-5, IL-6, IL-9, IL-10, IL-13, IL-17A, IL-17F, IL-22, interferon (IFN)-γ, and tumour necrosis factor (TNF)-α in the cell supernatant were quantified using the 12-plex LEGENDplex Mouse T-helper Cytokine Panel (BioLegend, 741043) on a Beckman Coulter CytoFLEX flow cytometer. Cytokine levels were calculated from a standard curve using Qognit software (BioLegend), and statistical analysis was conducted in GraphPad Prism (version 10) using the Kruskal-Wallis test with Dunn's correction for multiple comparisons between immunised and unimmunised groups. Bars represent the mean ± SD of five mice per group. Only statistically significant cytokines ($p < 0.05$) are shown.

Chapter Summary

The immunogenicity results in this chapter demonstrate that LNP-formulated saRNA RVF vaccines elicit superior humoral immune responses compared to the cationic lipid formulations *in vivo*-jetRNA and *in vivo*-jetRNA+. The LNP-formulated WT consensus and Furin-T2A vaccines both induced high levels of RVFV-specific IgG binding antibodies and neutralising activity particularly at the highest dose (10 μg). In contrast, the cationic lipid formulations *in vivo*-jetRNA and *in vivo*-jetRNA+ induced inconsistent and weak immune responses. Furthermore, in most cases, the Furin-T2A construct, designed to enhance antigen expression on the plasma membrane, did not exhibit superior immunogenicity over the WT consensus vaccine. These findings underscore the potential of the LNP-formulated WT consensus saRNA as a promising RVFV vaccine candidate and provide a strong foundation for further preclinical development.

CHAPTER SEVEN: DISCUSSION

7.1 Introduction

The discussion section synthesises the results presented in earlier chapters and contextualises them within the broader framework of vaccine research. It addresses key themes, including the role of molecular modifications in enhancing glycoprotein expression and functionality, the immunogenic potential of saRNA vaccines, and the challenges associated with, and feasibility of using cationic lipid formulations for delivery. The significance of unexpected findings is critically analysed to explore their implications for vaccine development. By comparing our findings with existing literature, the discussion identifies how this research contributes to addressing knowledge gaps and advancing the field of saRNA vaccine development. Furthermore, the broader relevance of this work is highlighted, particularly in the context of global efforts to develop scalable, effective, and accessible vaccines for emerging and re-emerging infectious diseases. In conclusion, this discussion not only evaluates the contributions of this thesis to the field of RVFV vaccine research but also underscores its potential impact on future vaccine strategies.

7.2 RVFV M segment consensus sequence characteristics

In the first objective, we generated a consensus RVFV M segment sequence by aligning all the complete and near-complete RVFV M segment sequences deposited in GenBank and ViPR databases by the end of 2018. This consensus sequence clustered with sequences from recent RVF outbreaks in East Africa, Madagascar, and Saudi Arabia. This clustering is likely due to the predominance of sequences from the 2006–2007 Kenya outbreak in the databases used to generate our consensus. The greater number of RVFV sequences from these outbreaks is likely due to the increased sequencing efforts and data submission to these databases. It also

highlights the re-emergence and spread of RVF in these countries at the dawn of the 21st century.

This approach addresses the challenge of genetic variability within RVFV, ensuring that the vaccine antigens used can elicit immune responses against antigens representative of recent and epidemiologically relevant viral strains. By creating candidates that address genetic diversity within RVFV, this approach may facilitate scalability and global preparedness against disease outbreaks. This is relevant for RVFV because the current licensed livestock and candidate RVFV vaccines were developed using RVFV strains isolated several decades ago and may not be as effective against more recent epidemiologically diverse strains [20].

A potential limitation of using a consensus RVFV M segment sequence to design an RVFV vaccine antigen is that such an antigen can be biased by differences in the viral sequencing capacities of countries experiencing RVFV outbreaks. In our case, the two databases we used to obtain the sequences from which the consensus was made (GenBank and ViPR) were dominated by sequences from one RVF outbreak, namely, the 2006–2007 Kenya outbreak. Therefore, our consensus sequence was inevitably biased towards these sequences. This limitation illustrates the critical role of using representative genomic data to inform vaccine design because the dominance of sequences from a few areas can introduce biases. It highlights the need for balanced sequencing efforts in all countries affected by RVF and other viral outbreaks to avoid underrepresenting potentially significant viral strains. A possible solution to this problem is to mitigate this bias by choosing a model that selects sequences using preset criteria rather than including the entire data set. This could mean limiting the percentage of sequences from any given country so that the consensus is not biased towards any particular geographical region.

7.3 *In vitro* expression of Gn and Gc by SDS-PAGE and western blot

Detection of Gc expression by protein denaturing SDS-PAGE and western blot was much less than that for Gn. Under reducing conditions, Gc was not detected from the cell lysates of HEK 293 cells transfected with any RVFV M segment constructs. However, when the samples were analysed under non-reducing conditions, Gc expression was observed for some of the constructs namely, WT consensus, K1064A, and K1050del. The failure to detect Gc by western blot under reducing conditions could have resulted from poor antibody recognition under such conditions. The antibodies we used may be conformation-specific, rendering them unable to detect linear epitopes. Forsström et al. showed that many of the antibodies directed towards conformational epitopes failed to bind to their target proteins in western blot assays [231]. In our study, the antibodies used (anti-RVFV Gc clone 9C10 and anti-RVFV Gc clone 1G4, BEI Resources) are not reported to be reactive in western blot assays, further supporting the possibility that they are ineffective at detecting linear epitopes under denaturing conditions.

In the non-reducing western blot, there was very weak detection of Gn from the RVFV M segment encoding pDNA constructs with cysteine mutations intended to induce disulfide bonds between Gn and Gc. We suspect these bonds may have disrupted the folding or stability of the Gn-Gc heterodimer, leading to aggregation or degradation that prevented efficient transfer during western blotting. This misfolding could also have obscured the epitopes recognised, thereby reducing antibody accessibility during detection.

7.4 Cell surface expression of Gn and Gc by flow cytometry

A significant increase in Gn cell surface expression was observed only in constructs with cytoplasmic tail deletions (Furin-T2A and K1050del). The highest expression was observed in the Furin-T2A construct that combined cytoplasmic tail deletions in both Gn and Gc, with a furin cleavage site and a T2A self-cleaving peptide spacer between the two glycoproteins. In

the Furin-T2A construct, these mutations removed the Golgi localisation signal in Gn and the ER retention signal in Gc, while in K1050del, only the Gc tail was deleted. Therefore, these deletions disrupted Gn's Golgi localisation signal, reducing its intracellular retention and enabling more efficient export to the plasma membrane.

Overby et al. [34] showed that the Gc cytoplasmic tail of the Uukuniemi Virus contains a lysine residue at position −3 from the C-terminus, which is highly conserved across other Phleboviruses. Altering this single amino acid causes mislocalisation of both Gc and Gn to the plasma membrane. Consistent with this finding, mutant RVFV strain MP-12, which lacks the five terminal amino acids of the Gc C-terminus, is predominantly localised to the Golgi with some translocation to the plasma membrane [33]. Our findings are therefore consistent with these previous reports.

The addition of a furin cleavage site and a T2A self-cleaving peptide enhanced the cleavage between Gn and Gc, enabling Gn to be more effectively transported to the plasma membrane. Furin cleavage promotes efficient processing and functionality of cleaved polyproteins [220, 232]. The use of a T2A self-cleaving peptide in combination with furin enhanced this process. This peptide is a commonly used self-cleaving sequence that enhances polyprotein cleavage efficiency [233]. Thus, our strategy of enhancing membrane expression by optimising cleavage and removing intracellular retention signals resulted in the highest level of cell surface expression of Gn among all RVFV M segment pDNA constructs.

Another important observation from our study was that introducing glycoprotein stabilising mutations increased the cell surface expression of Gc. This occurs because Gc depends on its interaction with Gn to mask its ER retention signals in its short C-terminal domain [85]. Complex formation between the two glycoproteins leads to masking this retention signal,

enabling Gc trafficking to the Golgi apparatus. In addition, unlike Gn, Gc lacks Golgi apparatus localisation signals, which are critical for the proper trafficking of both glycoproteins. Gc thus relies on its interaction with Gn for proper localisation. This dependency means that Gc relies on Gn to reach the Golgi and, subsequently, the cell surface. Therefore, mutations stabilising the interaction between the two glycoproteins may enhance the trafficking of Gc to the cell surface. Our findings suggest that the increased Gc expression observed in constructs with stabilising mutations may be due to improved interaction between the RVFV glycoproteins, facilitating Gc trafficking to the cell surface.

Unexpectedly, the H727A construct designed to stabilise the Gn and Gc heterodimer in its pre-fusion conformation exhibited significantly elevated levels of Gc expression at the cell surface. Stabilising the prefusion state is expected to affect protein structure rather than expression levels, which are influenced by folding, trafficking, interaction with Gn, signal sequences, and cleavage efficiency. Therefore, a deeper investigation is warranted to understand why prefusion stabilisation of the Gn and Gc heterodimer could significantly enhance Gc cell surface expression.

7.5 Encapsulation efficiency of *in vivo*-jetRNA and *in vivo*-jetRNA+

Encapsulation efficiency (EE) is a critical parameter in mRNA and saRNA vaccine delivery, as it determines the proportion of mRNA and saRNA that is effectively protected and available for cellular uptake. A high EE ensures that a substantial amount of mRNA or saRNA is shielded from degradation, contributing to efficient transfection and robust antigen expression–both of which are essential for eliciting a strong immune response [180].

In formulating our candidate saRNA RVF vaccines, we used a standard LNP formulation consisting of an ionizable cationic lipid, phosphatidylcholine, cholesterol, and polyethylene

glycol lipid. We also evaluated novel delivery systems–*in vivo*-jetRNA and its improved version, *in vivo*-jetRNA+. These cationic lipids were chosen for their straightforward preparation, as they do not require specialised equipment potentially making them suitable for resource-limited settings where LNP formulations may be less accessible due to cost or equipment requirements.

Our results showed that *in vivo*-jetRNA had a very low encapsulation efficiency (EE) of 32%. In contrast, its improved version, *in vivo*-jetRNA+, had a much higher encapsulation efficiency of 84%. While the encapsulation efficiency of *in vivo*-jetRNA is not publicly available, the manufacturer reports that *in vivo*-jetRNA+ can achieve up to 100% efficiency [234]. It is important to note that the manufacturer's claims are based on conventional mRNA formulation, not saRNA. Self-amplifying RNA molecules are up to ten times larger than non-amplifying mRNA and possess more complex secondary structures making them more difficult to encapsulate efficiently [235]. Therefore, the lower encapsulation efficiency seen with these cationic lipids relative to the manufacturer's claims may be attributed to differences in RNA type. This result highlights the need for independent validation when adapting technologies designed for mRNA to saRNA applications.

7.6 Immunogenicity of LNP-Formulated saRNA RVFV Candidate Vaccines

Our results showed that LNP-formulated candidate saRNA RVF vaccines elicited dose- and time-dependent anti-Gn IgG responses. Both the WT consensus and Furin-T2A vaccines induced similar antibody levels, indicating that increased plasma membrane expression by Furin-T2A did not enhance antibody production. Additionally, although anti-Gn IgG were induced after the first vaccination and boosted after the second, a statistically significant increase in these antibodies was observed only after the third dose and only in mice that received the highest dose (10) µg of either vaccine.

The lack of increase in anti-Gn IgG levels induced by the Furin-T2A construct despite the increased cell membrane expression of Gn could be attributed to several factors. It is possible that mutations that were introduced to the Furin-T2A construct altered the conformation and epitope presentation of Gn, yet this is critical for effective recognition by B cells, which require properly folded antigens to generate strong humoral responses [236]. Another reason could be suboptimal MHC class II peptide loading. The antigenic peptides generated from the Furin-T2A construct may not have been efficiently presented by MHC class II molecules on antigen-presenting cells (APCs). This would limit T-helper cell activation, which is crucial for B-cell-mediated IgG production [237]. It is also plausible that the threshold of immune response saturation was reached in which the WT consensus construct may have already induced near-maximal IgG production, and further increases in antigen expression from the Furin-T2A construct may not translate into significantly higher IgG titres [238].

The observation that significant IgG responses occurred only at the highest dose highlights the dose dependency of the vaccine-induced humoral immunity and is consistent with the well-documented relationship between mRNA vaccine dose and immune response magnitude [182]. The IgG levels we observed were also comparable to those reported for other saRNA vaccines targeting viral pathogens, such as SARS-CoV-2 and Zika virus [21, 239].

To identify the most likely cause(s) of the lack of increased anti-Gn-IgG induction, several investigations could be done, including 1) epitope mapping to determine whether the Furin-T2A mutations altered epitope availability or dominance, 2) T-cell activation assays to assess whether antigen processing and MHC presentation differ between WT consensus and Furin-T2A constructs, and 3) Neutralisation assays to evaluate the functionality of IgG antibodies generated by both constructs.

We also observed moderate but significant RVFV pseudovirus-neutralising activity in the mice that received the higher doses of the wild-type consensus saRNA candidate vaccines. However, the high variability in neutralising activity among the mice in these groups suggests challenges in consistently eliciting robust neutralising responses.

The failure of the Furin-T2A construct to induce significant RVFV pseudovirus-neutralising antibodies may be attributed to conformational changes that we postulate were induced by the mutations introduced in this construct. These conformational changes may have impaired the proper presentation of key epitopes necessary for generating effective RVFV pseudovirus-neutralising antibodies.

In conclusion, our LNP-formulated candidate saRNA RVF vaccines were immunogenic in mice as they induced robust levels of anti-Gn IgG. These findings highlight the importance of not only increasing antigen expression but also ensuring proper antigen conformation, processing, and presentation to achieve optimal immunogenicity.

7.7 Immunogenicity of cationic lipid-formulated candidate saRNA RVFV vaccines

This study also assessed the ability of our candidate vaccines to stimulate humoral and T-cell immune responses after formulation with the cationic lipids *in vivo*-jetRNA and *in vivo*-jetRNA+. The results showed weak and inconsistent immune activation, as evidenced by minimal interferon-gamma (IFN-γ) production, low cytokine levels, and poor humoral immune responses. In mice vaccinated with saRNA formulated using *in vivo*-jetRNA, no significant differences in anti-Gn IgG levels were observed. In contrast, mice that received saRNA formulated using *in vivo*-jetRNA+, statistically significant anti-Gn IgG were induced, but only after the second or third dose, and only at a single dose level for each vaccine. The absence of a clear dose-response relationship or significant differences between vaccines suggests

potential limitations in antigen presentation or vaccine formulation. Although modest increases in antibody levels were observed after vaccination, they lacked a clear dose-dependent pattern. These results indicate that these formulations failed to achieve consistent intracellular delivery or sustained antigen expression. Although cationic lipid-based reagents such as lipofectamine while highly efficient for mRNA transfection *in vitro* including in primary cells, their *in vivo* efficacy has been reported to be limited [182].

To overcome the challenges observed with *in vivo*-jetRNA and *in vivo*-jetRNA+, further optimisation of these formulations is required. The poor immunogenicity observed with in vivo-jetRNA likely resulted from its low encapsulation efficiency. Whereas the manufacturer tried to address this problem by discontinuing *in vivo*-jetRNA and introducing *in vivo*-jetRNA+, our results indicate that although encapsulation efficiency improved significantly with *in vivo*-jetRNA+, the corresponding enhancement in immunogenicity was minimal. Therefore, factors beyond encapsulation efficiency such as intracellular trafficking, endosomal escape, or RNA stability should be investigated to improve the immunogenicity of saRNA formulated with *in vivo*-jetRNA+.

This study highlights the importance of optimising delivery platforms for RNA-based vaccines. The limitations of cationic lipids observed in our study are similar to the challenges faced in early mRNA vaccine development namely, mRNA instability, high innate immunogenicity and inefficient *in vivo* delivery [182]. While saRNA offers advantages such as self-adjuvanticity and dose-sparing, its effectiveness depends heavily on efficient delivery platforms, which is particularly critical for saRNA due to its larger molecular size compared to conventional mRNA [21]. Optimising saRNA delivery platforms is thus critical for the successful adoption of this platform.

CHAPTER EIGHT: CONCLUSION

This PhD research aimed to develop and evaluate a self-amplifying RNA (saRNA) vaccine for Rift Valley Fever Virus (RVFV) while addressing three specific objectives and the hypothesis: "**Directing Gn-Gc expression to the plasma membrane enhances the immunogenicity of RVFV envelope glycoproteins**". The research findings provide critical insights into saRNA vaccine development, antigen design, and delivery systems.

Objective 1: To design and evaluate the *in Vitro* expression of Gn and Gc from consensus and mutated RVFV M segment sequences

This objective was addressed by generating a consensus M segment sequence and introducing mutations to enhance the cell surface expression of Gn and Gc. These constructs were tested using western blotting and flow cytometry, with significant increases in plasma membrane expression of Gn observed for two constructs. However, despite these improvements in *in vitro* expression, the hypothesis that enhanced expression would improve immunogenicity was not supported, as this increase did not translate into stronger immune responses *in vivo* under the tested conditions. This finding highlights the complexity of vaccine antigen design, where *in vitro* expression does not always predict immune responses *in vivo*.

Objective 2: To synthesise and characterise saRNA constructs encoding consensus and mutated RVFV M segment sequences

The saRNA constructs encoding the consensus and mutated M segment sequences were synthesised using a Venezuelan equine encephalitis virus (VEEV) replicon-based system. Their quality and integrity were confirmed through *in vitro* characterisation, including sequence validation and functional testing.

For delivery, this study directly assessed the encapsulation efficiency of saRNA using cationic lipid formulations (*in vivo*-jetRNA and *in vivo*-jetRNA+). *In vivo*-jetRNA+ achieved a significantly higher encapsulation efficiency (84%) than *in vivo*-jetRNA (32%). Additionally, Dr, Anna K Blakney assessed the encapsulation efficiency of LNPs, reporting high encapsulation efficiency consistent with published data.

Objective 3: To assess the humoral and cellular immune responses in mice immunised with candidate saRNA RVF vaccines

The immunogenicity of saRNA vaccines formulated with LNPs and cationic lipids was evaluated in BALB/c mice. LNP-formulated vaccines elicited robust anti-Gn IgG responses and pseudovirus-neutralising antibodies, indicating strong humoral immunogenicity and the potential for protective efficacy. In contrast, the cationic lipid formulations yielded weak and inconsistent immune responses, highlighting their limitations in effectively delivering saRNA. Cellular immune responses, only assessed for the cationic lipid formulations, were suboptimal highlighting the need for more efficient antigen delivery and presentation.

Addressing the Hypothesis

The hypothesis that plasma membrane localization of Gn and Gc enhances immunogenicity was not supported. The Furin-T2A mutation increased Gn expression at the plasma membrane but did not lead to stronger humoral or cellular immune responses in mice. This discrepancy suggests that plasma membrane expression alone is insufficient to enhance immunogenicity, highlighting the need to investigate other factors in vaccine antigen design.

Summary of Key Findings

Design and Optimization of Antigens:

A consensus RVFV M segment sequence was developed by aligning sequences from Genbank and ViPR ensuring broad applicability for vaccine antigens.

Stabilisation and cell membrane expression-enhancing mutations were introduced to the M segment as a strategy to improve vaccine immunogenicity. While these mutations increased expression *in vitro*, they did not translate into improved immunogenicity *in vivo*. This discrepancy highlights the complexity of translating *in vitro* antigen expression to effective immune responses, highlighting the need for further optimisation in antigen design.

Delivery System Performance:

Lipid nanoparticle (LNP) and cationic lipid formulations were evaluated for saRNA vaccine delivery. The encapsulation efficiency of saRNA vaccines varied significantly between delivery platforms. *In vivo*-jetRNA+ showed higher encapsulation efficiency (84%) than *in vivo*-jetRNA (32%), but both elicited weak and inconsistent immune responses in mice.

In contrast, lipid nanoparticles (LNPs) demonstrated superior performance, eliciting significant levels of anti-Gn IgG and RVFV pseudovirus-neutralising activity. This finding emphasises the critical role of optimising the delivery platform for saRNA vaccines.

Immune Responses:

The LNP-formulated saRNA vaccines induced strong humoral responses characterised by robust anti-Gn IgG titres and neutralising antibodies. However, the cationic lipid-based formulations elicited weak and inconsistent humoral and cellular responses, irrespective of dose or antigen construct. Cellular immunity, including IFN-γ production and cytokine release, remained weak across all formulations, highlighting the need for improved antigen presentation and T-cell priming

Study Limitations

Suboptimal Delivery Systems:

The cationic lipids *in vivo*-jetRNA and *in vivo*-jetRNA+ offered simplicity and cost-effectiveness, but elicited weak immune responses compared to LNPs. Despite *in vivo*-jetRNA+ achieving much higher encapsulation efficiency (84%) than *in vivo*-jetRNA (32%), neither formulation induced a robust immune response in mice, underscoring the critical role of delivery system efficiency in saRNA vaccine performance

Antigen Design Challenges:

Introduction of furin cleavage site and T2A mutation increased Gn and Gc cell surface expression *in vitro* but did not enhance humoral or cellular immune responses *in vivo*, including RVFV pseudovirus-neutralising activity. This discrepancy indicates that mutation-induced enhanced cell membrane expression alone was insufficient to improve immunogenicity, limiting the effectiveness of this antigen design.

Preclinical Model Constraints:

While valuable for initial immunogenicity assessments, the murine model does not fully replicate the immunological environment of large animals or humans. Future studies should include additional animal models such as sheep and goats to validate these findings.

Lack of efficacy data

Another major limitation of this work is that evaluations such as plaque reduction neutralisation tests and virus challenge (efficacy) studies were not performed due to a lack of appropriate biosafety containment facilities to conduct these tests at Imperial College London and at UVRI.

This limitation restricted a comprehensive evaluation of the vaccine's potential to confer protection against RVFV.

Future Directions

Delivery System Advancements

The transition from cationic lipids to LNPs, which provide superior saRNA protection, efficient endosomal escape, and enhanced immunogenicity, should be prioritised. Hybrid delivery systems combining the simplicity of cationic lipids with the efficiency of LNPs could also be explored.

Antigen Engineering

Further refinements to antigen design should focus on preserving the native conformation of Gn and Gc to optimise epitope exposure. Prefusion stabilisation strategies, similar to those used in SARS-CoV-2 vaccines, may improve immunogenicity. The H727A prefusion conformation-stabilising mutation, which exhibited enhanced Gc plasma membrane expression, should be explored further.

To enhance antigen processing and immune recognition, the co-expression of Gn and Gc, mimicking their natural heterodimeric structure, should be investigated.

Optimising Immunisation Strategies

Alternative dosing regimens should be evaluated to maximise immune priming and memory responses, including intermediate doses and extended intervals between boosters.

Exploring the use of needle-free delivery systems, such as electroporation or intranasal administration, could improve the efficiency and practicality of vaccine deployment.

Preclinical and Translational Studies

Expanding preclinical studies to include larger animal models, such as sheep or non-human primates, will provide insights into the translational potential of the saRNA platform for RVFV and other zoonotic diseases. Measure the durability of immune responses and identify potential correlates of protection to support the progression of vaccine candidates to clinical trials.

Broader Implications of this work

Advancing saRNA vaccine Platforms

This study underscores the potential of saRNA vaccines for addressing zoonotic pathogens like Rift Valley Fever Virus (RVFV). While saRNA offers advantages such as dose-sparing and rapid manufacturing, this study has further highlighted the importance of optimised delivery systems and antigen design. These findings contribute to the growing body of evidence that saRNA can be adapted for the development of vaccines against emerging pathogens.

Insights for RVFV Vaccine Development

The limited immunogenicity observed with cationic lipids reinforces the need for robust delivery systems tailored specifically for large, complex RNA molecules like saRNA. This finding informs the design of scalable RVFV vaccines, offering promise for protecting populations in endemic regions where the disease poses significant health and economic threats.

Transfer of capacity for preclinical development of saRNA vaccines to a Low- and middle-income country

This work has successfully established the capacity for preclinical development of saRNA vaccines against infectious diseases in Uganda, a previously non-existent capability. Through this effort, we built valuable collaborations with Imperial College London under the guidance of Prof. Robin Shattock, and locally with Makerere College of Veterinary Medicine, Animal Resources and Biosecurity, where the mice immunisations were conducted. At UVRI, we have now developed the capacity to design, synthesise, and perform *in vitro* evaluations of saRNA vaccines targeting infectious diseases, marking a significant milestone in advancing Uganda's contribution to saRNA vaccine research and development.

Relevance to Global Health Preparedness

This study demonstrates the feasibility of technological transfer of saRNA vaccine research capacity to low and middle-income countries. Lessons learned from this work establish a model for equipping such regions with the tools to respond to emerging infectious diseases thereby strengthening global health security.

Conclusion

This PhD research has advanced the understanding of saRNA vaccine development for RVFV by re-enforcing critical factors that influence immunogenicity, including antigen design and delivery system performance. The success of LNP-formulated vaccines and the establishment of preclinical vaccine development capacity in Uganda mark significant steps toward scalable, effective solutions for RVFV and other emerging infectious diseases. These contributions strengthen the global effort to develop adaptable vaccine platforms, fostering resilience against future pandemics

References

1. Wright, D., et al., *Rift Valley fever: biology and epidemiology.* J Gen Virol, 2019. **100**(8): p. 1187-1199.
2. Daubney, R., J. Hudson, and P. Garnham, *Enzootic hepatitis or Rift Valley fever. An undescribed virus disease of sheep cattle and man from East Africa.* The Journal of pathology and bacteriology, 1931. **34**(4): p. 545-579.
3. Ikegami, T. and S. Makino, *The pathogenesis of Rift Valley fever.* Viruses, 2011. **3**(5): p. 493-519.
4. Hartman, A., *Rift Valley Fever.* Clin Lab Med, 2017. **37**(2): p. 285-301.
5. Javelle, E., et al., *The challenging management of Rift Valley Fever in humans: literature review of the clinical disease and algorithm proposal.* Ann Clin Microbiol Antimicrob, 2020. **19**(1): p. 4.
6. Paweska, J.T. and P.J. van Vuren, *Rift Valley fever virus: a virus with potential for global emergence*, in *The role of animals in emerging viral diseases*. 2014, Elsevier. p. 169-200.
7. Mandell, R. and R. Flick, *Rift Valley fever virus: a real bioterror threat.* Journal of Bioterrorism & Biodefense, 2011. **2**(2).
8. World Organisation for Animal Health, *OIE-Listed diseases, infections and infestations in force in 2019.* 2019.
9. Centers for Disease Control and Prevention and United States Department of Agriculture, *Select Agents and Toxins List.* 2017.
10. Mehand, M.S., et al., *The WHO R&D Blueprint: 2018 review of emerging infectious diseases requiring urgent research and development efforts.* Antiviral research, 2018. **159**: p. 63-67.
11. Mohamed, A.M., et al., *Seroepidemiological survey on Rift Valley fever among small ruminants and their close human contacts in Makkah, Saudi Arabia, in 2011.* Rev Sci Tech, 2014. **33**(3): p. 903-15.
12. Soumaré, B., et al., *Effects of Livestock Import Bans Imposed by Saudi Arabia on Somaliland for Sanitary Reasons Related to Rift Valley Fever.* Outlook on Agriculture, 2006. **35**(1): p. 19-24.
13. Ng'ang'a, C.M., S.A. Bukachi, and B.K. Bett, *Lay perceptions of risk factors for Rift Valley fever in a pastoral community in northeastern Kenya.* BMC Public Health, 2016. **16**(1): p. 32.
14. *RIft Valley Fever*. 2024 [cited 2024 30 July 2024]; Available from: https://www.woah.org/en/disease/rift-valley-fever/.
15. Nielsen, S.S., et al., *Rift Valley Fever - assessment of effectiveness of surveillance and control measures in the EU.* Efsa j, 2020. **18**(11): p. e06292.
16. Himeidan, Y.E., *Rift Valley fever: current challenges and future prospects.* Res Rep Trop Med, 2016. **7**: p. 1-9.
17. *Rift Valley Fever*. 2018 [cited 2024 6 August 2024]; Available from: https://www.who.int/news-room/fact-sheets/detail/rift-valley-fever.
18. Ikegami, T., *Candidate vaccines for human Rift Valley fever.* Expert Opin Biol Ther, 2019. **19**(12): p. 1333-1342.
19. Alhaj, M., *Safety and Efficacy Profile of Commercial Veterinary Vaccines against Rift Valley Fever: A Review Study.* J Immunol Res, 2016. **2016**: p. 7346294.

20. Kitandwe, P.K., et al., *An Overview of Rift Valley Fever Vaccine Development Strategies.* Vaccines (Basel), 2022. **10**(11).
21. Blakney, A.K., S. Ip, and A.J. Geall, *An Update on Self-Amplifying mRNA Vaccine Development.* Vaccines (Basel), 2021. **9**(2).
22. Vogel, A.B., et al., *Self-Amplifying RNA Vaccines Give Equivalent Protection against Influenza to mRNA Vaccines but at Much Lower Doses.* Mol Ther, 2018. **26**(2): p. 446-455.
23. Sandbrink, J.B. and R.J. Shattock, *RNA Vaccines: A Suitable Platform for Tackling Emerging Pandemics?* Front Immunol, 2020. **11**: p. 608460.
24. Bloom, K., F. van den Berg, and P. Arbuthnot, *Self-amplifying RNA vaccines for infectious diseases.* Gene Ther, 2021. **28**(3-4): p. 117-129.
25. Dolgin, E., *Self-copying RNA vaccine wins first full approval: what's next?* Nature, 2023. **624**(7991): p. 236-237.
26. Heise, M.T., et al., *An alphavirus replicon-derived candidate vaccine against Rift Valley fever virus.* Epidemiol Infect, 2009. **137**(9): p. 1309-18.
27. Gorchakov, R., et al., *Comparative analysis of the alphavirus-based vectors expressing Rift Valley fever virus glycoproteins.* Virology, 2007. **366**(1): p. 212-25.
28. Bian, T., et al., *A Rift Valley fever mRNA vaccine elicits strong immune responses in mice and rhesus macaques.* npj Vaccines, 2023. **8**(1): p. 164.
29. McMillen, C.M., et al., *A highly potent human neutralizing antibody prevents vertical transmission of Rift Valley fever virus in a rat model.* Nat Commun, 2023. **14**(1): p. 4507.
30. Chapman, N.S., et al., *Potent neutralization of Rift Valley fever virus by human monoclonal antibodies through fusion inhibition.* Proc Natl Acad Sci U S A, 2021. **118**(14).
31. Doyle, J.D., et al., *Immune correlates of protection following Rift Valley fever virus vaccination.* npj Vaccines, 2022. **7**(1): p. 129.
32. Gerrard, S.R. and S.T. Nichol, *Characterization of the Golgi retention motif of Rift Valley fever virus GN glycoprotein.* Journal of virology, 2002. **76**(23): p. 12200-12210.
33. Murakami, S., et al., *Development of a novel, single-cycle replicable rift valley Fever vaccine.* PLoS Negl Trop Dis, 2014. **8**(3): p. e2746.
34. Overby, A.K., et al., *The cytoplasmic tails of Uukuniemi Virus (Bunyaviridae) G(N) and G(C) glycoproteins are important for intracellular targeting and the budding of virus-like particles.* J Virol, 2007. **81**(20): p. 11381-91.
35. Samy, A.M., A.T. Peterson, and M. Hall, *Phylogeography of Rift Valley fever virus in Africa and the Arabian Peninsula.* PLoS neglected tropical diseases, 2017. **11**(1): p. e0005226.
36. Madani, T.A., et al., *Rift Valley fever epidemic in Saudi Arabia: epidemiological, clinical, and laboratory characteristics.* Clinical Infectious Diseases, 2003. **37**(8): p. 1084-1092.
37. Laughlin, L.W., et al., *Epidemic Rift Valley fever in Egypt: observations of the spectrum of human illness.* Transactions of the Royal Society of Tropical Medicine and Hygiene, 1979. **73**(6): p. 630-633.
38. Ikegami, T., *Molecular biology and genetic diversity of Rift Valley fever virus.* Antiviral research, 2012. **95**(3): p. 293-310.
39. Murithi, R.M., et al., *Rift Valley fever in Kenya: history of epizootics and identification of vulnerable districts.* Epidemiology and Infection, 2011. **139**(3): p. 372-380.

40. van Velden, D.J., et al., *Rift Valley fever affecting humans in South Africa: a clinicopathological study.* S Afr Med J, 1977. **51**(24): p. 867-71.
41. Laughlin, L.W., et al., *Epidemic Rift Valley fever in Egypt: observations of the spectrum of human illness.* Trans R Soc Trop Med Hyg, 1979. **73**(6): p. 630-3.
42. Samy, A.M., A.T. Peterson, and M. Hall, *Phylogeography of Rift Valley Fever Virus in Africa and the Arabian Peninsula.* PLoS Negl Trop Dis, 2017. **11**(1): p. e0005226.
43. Baiersdörfer, M., et al., *A Facile Method for the Removal of dsRNA Contaminant from In Vitro-Transcribed mRNA.* Mol Ther Nucleic Acids, 2019. **15**: p. 26-35.
44. Daubney, R. and J. Hudson, *Enzootic Hepatitis or Rift Valley Fever. An Un-described Virus Disease of Sheep, Cattle and Man from East Africa.* 1931.
45. Van Velden, D., * Meyer, JD,* Olivier, J.,* Gear, JHS** and B. McIntosh, *Rift valley fever affecting humans in South Africa-a clinicopathological study.* South African Medical Journal, 1977. **51**(24): p. 867-871.
46. Meegan, J.M., *The Rift Valley fever epizootic in Egypt 1977-78. 1. Description of the epizzotic and virological studies.* Trans R Soc Trop Med Hyg, 1979. **73**(6): p. 618-23.
47. Alkan, C., E. Jurado-Cobena, and T. Ikegami, *Advancements in Rift Valley fever vaccines: a historical overview and prospects for next generation candidates.* npj Vaccines, 2023. **8**(1): p. 171.
48. Madani, T.A., et al., *Rift Valley fever epidemic in Saudi Arabia: epidemiological, clinical, and laboratory characteristics.* Clin Infect Dis, 2003. **37**(8): p. 1084-92.
49. Hassan, O.A., et al., *The 2007 Rift Valley fever outbreak in Sudan.* PLoS Negl Trop Dis, 2011. **5**(9): p. e1229.
50. Clark, M.H.A., et al., *Systematic literature review of Rift Valley fever virus seroprevalence in livestock, wildlife and humans in Africa from 1968 to 2016.* PLoS Negl Trop Dis, 2018. **12**(7): p. e0006627.
51. *About Rift Valley Fever (RVF)*. May 2024 [cited 2024 15 November]; Available from: https://www.cdc.gov/rift-valley-fever/about/index.html.
52. Wright, D., et al., *Rift Valley fever: biology and epidemiology.* Journal of General Virology, 2019. **100**(8): p. 1187-1199.
53. Grossi-Soyster, E.N., et al., *The influence of raw milk exposures on Rift Valley fever virus transmission.* PLoS Negl Trop Dis, 2019. **13**(3): p. e0007258.
54. Adam, I. and M.S. Karsany, *Case report: Rift Valley fever with vertical transmission in a pregnant Sudanese woman.* Journal of medical virology, 2008. **80**(5): p. 929-929.
55. Wichgers Schreur, P.J., et al., *Co-housing of Rift Valley fever virus infected lambs with immunocompetent or immunosuppressed lambs does not result in virus transmission.* Frontiers in microbiology, 2016. **7**: p. 287.
56. Davies, F. and R. Highton, *Possible vectors of Rift Valley fever in Kenya.* Transactions of the Royal Society of Tropical Medicine and Hygiene, 1980. **74**(6): p. 815-816.
57. Linthicum, K.J., S.C. Britch, and A. Anyamba, *Rift Valley fever: an emerging mosquito-borne disease.* Annual review of entomology, 2016. **61**: p. 395-415.
58. Linthicum, K., et al., *Rift Valley fever virus (family Bunyaviridae, genus Phlebovirus). Isolations from Diptera collected during an inter-epizootic period in Kenya.* Epidemiology & Infection, 1985. **95**(1): p. 197-209.
59. Murithi, R., et al., *Rift Valley fever in Kenya: history of epizootics and identification of vulnerable districts.* Epidemiology & Infection, 2011. **139**(3): p. 372-380.

60. Rostal, M.K., et al., *Identification of potential vectors of and detection of antibodies against Rift Valley fever virus in livestock during interepizootic periods.* American journal of veterinary research, 2010. **71**(5): p. 522-526.
61. Matiko, M.K., et al., *Serological evidence of inter-epizootic/inter-epidemic circulation of Rift Valley fever virus in domestic cattle in Kyela and Morogoro, Tanzania.* PLOS Neglected Tropical Diseases, 2018. **12**(11): p. e0006931.
62. Gerken, K.N., et al., *Paving the way for human vaccination against Rift Valley fever virus: A systematic literature review of RVFV epidemiology from 1999 to 2021.* PLoS Negl Trop Dis, 2022. **16**(1): p. e0009852.
63. Evans, A., et al., *Prevalence of antibodies against Rift Valley fever virus in Kenyan wildlife.* Epidemiology & Infection, 2008. **136**(9): p. 1261-1269.
64. Paweska, J.T., *Rift Valley fever.* Rev Sci Tech, 2015. **34**(2): p. 375-89.
65. Paweska, J.T., *Rift valley fever*, in *Emerging Infectious Diseases*. 2014, Elsevier. p. 73-93.
66. Swanepoel, R., * Manning, B.** and J. Watt, *Fatal Rift Valley fever of man in Rhodesia.* Central African Journal of Medicine, 1979. **25**(1): p. 1-8.
67. Abdel-Wahab, K.S., et al., *Rift Valley Fever virus infections in Egypt: Pathological and virological findings in man.* Trans R Soc Trop Med Hyg, 1978. **72**(4): p. 392-6.
68. Sabin, A.B. and R.W. Blumberg, *Human infection with Rift Valley fever virus and immunity twelve years after single attack.* Proc Soc Exp Biol Med, 1947. **64**(4): p. 385-9.
69. Siam, A.L., J.M. Meegan, and K.F. Gharbawi, *Rift Valley fever ocular manifestations: observations during the 1977 epidemic in Egypt.* Br J Ophthalmol, 1980. **64**(5): p. 366-74.
70. Deutman, A.F. and H.J. Klomp, *Rift Valley fever retinitis.* Am J Ophthalmol, 1981. **92**(1): p. 38-42.
71. Newman-Gerhardt, S., et al., *Potential for autoimmune pathogenesis of Rift Valley Fever virus retinitis.* Am J Trop Med Hyg, 2013. **89**(3): p. 495-7.
72. Anywaine, Z., et al., *Clinical manifestations of Rift Valley fever in humans: Systematic review and meta-analysis.* PLoS Negl Trop Dis, 2022. **16**(3): p. e0010233.
73. Organization, W.H., *Rift Valley fever fact sheet:(Revised in September 2007).* Weekly Epidemiological Record= Relevé épidémiologique hebdomadaire, 2008. **83**(02): p. 17-22.
74. Lapa, D., et al., *Rift Valley Fever Virus: An Overview of the Current Status of Diagnostics.* Biomedicines, 2024. **12**(3): p. 540.
75. Thompson, P.N. *Rift Valley Fever in Animals*. 2022 2022/09 [cited 2022; Available from: https://www.merckvetmanual.com/generalized-conditions/rift-valley-fever/rift-valley-fever-in-animals.
76. *Manual of Diagnostic Tests and Vaccines for Terrestrial Animals*, in *Manual of Diagnostic Tests and Vaccines for Terrestrial Animals, thirteenth edition 2024*. 2024, World Organisation for Animal Health (WOAH). p. 613-632.
77. Lozach, P.-Y., et al., *DC-SIGN as a receptor for phleboviruses.* Cell host & microbe, 2011. **10**(1): p. 75-88.
78. Phoenix, I., et al., *N-glycans on the Rift Valley fever virus envelope glycoproteins Gn and Gc redundantly support viral infection via DC-SIGN.* viruses, 2016. **8**(5): p. 149.
79. Harmon, B., et al., *Rift Valley fever virus strain MP-12 enters mammalian host cells via caveola-mediated endocytosis.* Journal of virology, 2012. **86**(23): p. 12954-12970.

80. De Boer, S., et al., *Acid-activated structural reorganization of the Rift Valley fever virus Gc fusion protein.* Journal of virology, 2012. **86**(24): p. 13642-13652.
81. Ikegami, T., et al., *Rift Valley fever virus NSs mRNA is transcribed from an incoming anti-viral-sense S RNA segment.* Journal of virology, 2005. **79**(18): p. 12106-12111.
82. Spiegel, M., T. Plegge, and S. Pöhlmann, *The role of phlebovirus glycoproteins in viral entry, assembly and release.* Viruses, 2016. **8**(7): p. 202.
83. Gerrard, S.R. and S.T. Nichol, *Synthesis, proteolytic processing and complex formation of N-terminally nested precursor proteins of the Rift Valley fever virus glycoproteins.* Virology, 2007. **357**(2): p. 124-133.
84. Carnec, X., et al., *Role of the cytosolic tails of Rift Valley fever virus envelope glycoproteins in viral morphogenesis.* Virology, 2014. **448**: p. 1-14.
85. Överby, A.K., et al., *The cytoplasmic tails of Uukuniemi virus (Bunyaviridae) GN and GC glycoproteins are important for intracellular targeting and the budding of virus-like particles.* Journal of virology, 2007. **81**(20): p. 11381-11391.
86. Spiegel, M., T. Plegge, and S. Pöhlmann, *The Role of Phlebovirus Glycoproteins in Viral Entry, Assembly and Release. Viruses. 2016; 8 (7)*. Epub 2016/07/21. https://doi. org/10.3390/v8070202 PMID: 27455305.
87. Bouloy, M. and F. Weber, *Molecular biology of Rift Valley fever virus.* The open virology journal, 2010. **4**: p. 8.
88. Weingartl, H.M., et al., *Rift Valley fever virus incorporates the 78 kDa glycoprotein into virions matured in mosquito C6/36 cells.* PLoS One, 2014. **9**(1): p. e87385.
89. Won, S., et al., *NSm protein of Rift Valley fever virus suppresses virus-induced apoptosis.* Journal of virology, 2007. **81**(24): p. 13335-13345.
90. Ikegami, T., et al., *Rift Valley fever virus NSs protein promotes post-transcriptional downregulation of protein kinase PKR and inhibits eIF2alpha phosphorylation.* PLoS Pathog, 2009. **5**(2): p. e1000287.
91. Habjan, M., et al., *NSs protein of rift valley fever virus induces the specific degradation of the double-stranded RNA-dependent protein kinase.* J Virol, 2009. **83**(9): p. 4365-75.
92. Gerrard, S.R., et al., *The NSm proteins of Rift Valley fever virus are dispensable for maturation, replication and infection.* Virology, 2007. **359**(2): p. 459-465.
93. Bird, B.H., et al., *Rift valley fever virus lacking the NSs and NSm genes is highly attenuated, confers protective immunity from virulent virus challenge, and allows for differential identification of infected and vaccinated animals.* Journal of virology, 2008. **82**(6): p. 2681-2691.
94. Freiberg, A.N., et al., *Three-dimensional organization of Rift Valley fever virus revealed by cryoelectron tomography.* Journal of virology, 2008. **82**(21): p. 10341-10348.
95. Huiskonen, J.T., et al., *Electron cryo-microscopy and single-particle averaging of Rift Valley fever virus: evidence for GN-GC glycoprotein heterodimers.* Journal of virology, 2009. **83**(8): p. 3762-3769.
96. Sherman, M.B., et al., *Single-particle cryo-electron microscopy of Rift Valley fever virus.* Virology, 2009. **387**(1): p. 11-15.
97. Wang, X., et al., *Structure of Rift Valley Fever Virus RNA-Dependent RNA Polymerase.* Journal of Virology, 2022. **96**(3): p. e01713-21.
98. Le May, N., et al., *A SAP30 complex inhibits IFN-beta expression in Rift Valley fever virus infected cells.* PLoS Pathog, 2008. **4**(1): p. e13.

99. Baer, A., et al., *Induction of DNA damage signaling upon Rift Valley fever virus infection results in cell cycle arrest and increased viral replication.* J Biol Chem, 2012. **287**(10): p. 7399-410.
100. Austin, D., et al., *p53 Activation following Rift Valley fever virus infection contributes to cell death and viral production.* PLoS One, 2012. **7**(5): p. e36327.
101. Habjan, M., et al., *Processing of genome 5' termini as a strategy of negative-strand RNA viruses to avoid RIG-I-dependent interferon induction.* PLoS One, 2008. **3**(4): p. e2032.
102. Chaplin, D.D., *Overview of the immune response.* J Allergy Clin Immunol, 2010. **125**(2 Suppl 2): p. S3-23.
103. Akira, S., S. Uematsu, and O. Takeuchi, *Pathogen recognition and innate immunity.* Cell, 2006. **124**(4): p. 783-801.
104. Broz, P. and D.M. Monack, *Newly described pattern recognition receptors team up against intracellular pathogens.* Nat Rev Immunol, 2013. **13**(8): p. 551-65.
105. Jansen van Vuren, P., et al., *Serum levels of inflammatory cytokines in Rift Valley fever patients are indicative of severe disease.* Virol J, 2015. **12**: p. 159.
106. Nfon, C.K., et al., *Innate immune response to Rift Valley fever virus in goats.* PLoS Negl Trop Dis, 2012. **6**(4): p. e1623.
107. Klimstra, W.B., et al., *DC-SIGN and L-SIGN can act as attachment receptors for alphaviruses and distinguish between mosquito cell- and mammalian cell-derived viruses.* J Virol, 2003. **77**(22): p. 12022-32.
108. Shabman, R.S., et al., *Differential induction of type I interferon responses in myeloid dendritic cells by mosquito and mammalian-cell-derived alphaviruses.* J Virol, 2007. **81**(1): p. 237-47.
109. Pepin, M., et al., *Rift Valley fever virus (Bunyaviridae: Phlebovirus): an update on pathogenesis, molecular epidemiology, vectors, diagnostics and prevention.* Veterinary research, 2010. **41**(6): p. 61.
110. LaBeaud, D., *Towards a safe, effective vaccine for Rift Valley fever virus.* Future virology, 2010. **5**(6): p. 675-678.
111. Wang, Q., et al., *Neutralization mechanism of human monoclonal antibodies against Rift Valley fever virus.* Nature Microbiology, 2019. **4**(7): p. 1231-1241.
112. Allen, E.R., et al., *A protective monoclonal antibody targets a site of vulnerability on the surface of Rift Valley fever virus.* Cell reports, 2018. **25**(13): p. 3750-3758. e4.
113. Dodd, K.A., et al., *Rift Valley fever virus clearance and protection from neurologic disease are dependent on CD4+ T cell and virus-specific antibody responses.* Journal of virology, 2013. **87**(11): p. 6161-6171.
114. Wonderlich, E.R., et al., *Peripheral blood biomarkers of disease outcome in a monkey model of Rift Valley fever encephalitis.* Journal of virology, 2018. **92**(3).
115. McElroy, A.K. and S.T. Nichol, *Rift Valley fever virus inhibits a pro-inflammatory response in experimentally infected human monocyte derived macrophages and a pro-inflammatory cytokine response may be associated with patient survival during natural infection.* Virology, 2012. **422**(1): p. 6-12.
116. Smithburn, K., *Rift Valley fever: the neurotropic adaptation of the virus and the experimental use of this modified virus as a vaccine.* British journal of experimental pathology, 1949. **30**(1): p. 1.

117. Anthony, T., et al., *Vaccination with Rift Valley fever virus live attenuated vaccine strain Smithburn caused meningoencephalitis in alpacas.* J Vet Diagn Invest, 2021. **33**(4): p. 777-781.
118. Botros, B., et al., *Adverse response of non-indigenous cattle of European breeds to live attenuated Smithburn Rift Valley fever vaccine.* J Med Virol, 2006. **78**(6): p. 787-91.
119. Kamal, S.A., *Pathological studies on postvaccinal reactions of Rift Valley fever in goats.* Virol J, 2009. **6**: p. 94.
120. Swanepoel, R., J. Coetzer, and R. Tustin, *Infectious diseases of livestock with special reference to southern Africa.* 2004.
121. Dungu, B., B.A. Lubisi, and T. Ikegami, *Rift Valley fever vaccines: current and future needs.* Curr Opin Virol, 2018. **29**: p. 8-15.
122. Muller, R., et al., *Characterization of clone 13, a naturally attenuated avirulent isolate of Rift Valley fever virus, which is altered in the small segment.* The American journal of tropical medicine and hygiene, 1995. **53**(4): p. 405-411.
123. Makoschey, B., et al., *Rift Valley Fever Vaccine Virus Clone 13 Is Able to Cross the Ovine Placental Barrier Associated with Foetal Infections, Malformations, and Stillbirths.* PLoS Negl Trop Dis, 2016. **10**(3): p. e0004550.
124. Ahmed Kamal, S., *Observations on rift valley fever virus and vaccines in Egypt.* Virology journal, 2011. **8**(1): p. 532.
125. Barnard, B. and M. Botha, *An inactivated rift valley fever vaccine.* Journal of the South African Veterinary Association, 1977. **48**(1): p. 45-48.
126. Davies, F.G. and V. Martin, *Recognizing rift valley fever*. 2003: Food & Agriculture Org.
127. Jose, J., J.E. Snyder, and R.J. Kuhn, *A structural and functional perspective of alphavirus replication and assembly.* Future microbiology, 2009. **4**(7): p. 837-856.
128. Lundstrom, K., *Alphavirus-based vaccines.* Current opinion in molecular therapeutics, 2002. **4**(1): p. 28.
129. Vander Veen, R.L., D.H. Harris, and K.I. Kamrud, *Alphavirus replicon vaccines.* Animal health research reviews, 2012. **13**(1): p. 1-9.
130. Beissert, T., et al., *A trans-amplifying RNA vaccine strategy for induction of potent protective immunity.* Molecular therapy, 2020. **28**(1): p. 119-128.
131. Spuul, P., et al., *Assembly of alphavirus replication complexes from RNA and protein components in a novel trans-replication system in mammalian cells.* Journal of virology, 2011. **85**(10): p. 4739-4751.
132. Schmidt, C., et al., *A Bivalent trans-amplifying RNA vaccine candidate induces potent chikungunya and Ross River virus specific immune responses.* Vaccines, 2022. **10**(9): p. 1374.
133. Fuller, D.H. and P. Berglund, *Amplifying RNA vaccine development.* New England Journal of Medicine, 2020. **382**(25): p. 2469-2471.
134. Kwon, H., et al., *Emergence of synthetic mRNA: In vitro synthesis of mRNA and its applications in regenerative medicine.* Biomaterials, 2018. **156**: p. 172-193.
135. Devarkar, S.C., et al., *Structural basis for m7G recognition and 2'-O-methyl discrimination in capped RNAs by the innate immune receptor RIG-I.* Proceedings of the National Academy of Sciences, 2016. **113**(3): p. 596-601.
136. Sahin, U., K. Karikó, and Ö. Türeci, *mRNA-based therapeutics—developing a new class of drugs.* Nature reviews Drug discovery, 2014. **13**(10): p. 759-780.

137. Wadhwa, A., et al., *Opportunities and Challenges in the Delivery of mRNA-based Vaccines.* Pharmaceutics, 2020. **12**(2).
138. Brito, L.A., et al., *Self-amplifying mRNA vaccines*, in *Advances in genetics*. 2015, Elsevier. p. 179-233.
139. Roers, A., B. Hiller, and V. Hornung, *Recognition of endogenous nucleic acids by the innate immune system.* Immunity, 2016. **44**(4): p. 739-754.
140. Diebold, S.S., et al., *Innate antiviral responses by means of TLR7-mediated recognition of single-stranded RNA.* Science, 2004. **303**(5663): p. 1529-31.
141. Anderson, B.R., et al., *Incorporation of pseudouridine into mRNA enhances translation by diminishing PKR activation.* Nucleic Acids Res, 2010. **38**(17): p. 5884-92.
142. Xia, X., *Detailed Dissection and Critical Evaluation of the Pfizer/BioNTech and Moderna mRNA Vaccines.* Vaccines (Basel), 2021. **9**(7).
143. Mayr, C., *Regulation by 3'-untranslated regions.* Annual review of genetics, 2017. **51**: p. 171-194.
144. Orlandini von Niessen, A.G., et al., *Improving mRNA-Based Therapeutic Gene Delivery by Expression-Augmenting 3' UTRs Identified by Cellular Library Screening.* Mol Ther, 2019. **27**(4): p. 824-836.
145. Zarghampoor, F., et al., *Improved translation efficiency of therapeutic mRNA.* Gene, 2019. **707**: p. 231-238.
146. Mugridge, J.S., J. Coller, and J.D. Gross, *Structural and molecular mechanisms for the control of eukaryotic 5'–3' mRNA decay.* Nature structural & molecular biology, 2018. **25**(12): p. 1077-1085.
147. Kormann, M.S., et al., *Expression of therapeutic proteins after delivery of chemically modified mRNA in mice.* Nature biotechnology, 2011. **29**(2): p. 154-157.
148. Lima, S.A., et al., *Short poly (A) tails are a conserved feature of highly expressed genes.* Nature structural & molecular biology, 2017. **24**(12): p. 1057-1063.
149. Schlake, T., et al., *Developing mRNA-vaccine technologies.* RNA biology, 2012. **9**(11): p. 1319-1330.
150. Holtkamp, S., et al., *Modification of antigen-encoding RNA increases stability, translational efficacy, and T-cell stimulatory capacity of dendritic cells.* Blood, 2006. **108**(13): p. 4009-4017.
151. Gustafsson, C., S. Govindarajan, and J. Minshull, *Codon bias and heterologous protein expression.* Trends in biotechnology, 2004. **22**(7): p. 346-353.
152. Kudla, G., et al., *High guanine and cytosine content increases mRNA levels in mammalian cells.* PLoS Biol, 2006. **4**(6): p. e180.
153. Shabalina, S.A., A.Y. Ogurtsov, and N.A. Spiridonov, *A periodic pattern of mRNA secondary structure created by the genetic code.* Nucleic Acids Res, 2006. **34**(8): p. 2428-37.
154. Mauger, D.M., et al., *mRNA structure regulates protein expression through changes in functional half-life.* Proc Natl Acad Sci U S A, 2019. **116**(48): p. 24075-24083.
155. Linares-Fernández, S., et al., *Tailoring mRNA vaccine to balance innate/adaptive immune response.* Trends in molecular medicine, 2020. **26**(3): p. 311-323.
156. Zhang, J., et al., *Recent Advances and Innovations in the Preparation and Purification of In Vitro-Transcribed-mRNA-Based Molecules.* Pharmaceutics, 2023. **15**(9).

157. Barlow, J.J., et al., *A SIMPLE METHOD FOR THE QUANTITATIVE ISOLATION OF UNDEGRADED HIGH MOLECULAR WEIGHT RIBONUCLEIC ACID.* Biochem Biophys Res Commun, 1963. **13**: p. 61-6.
158. Toni, L.S., et al., *Optimization of phenol-chloroform RNA extraction.* MethodsX, 2018. **5**: p. 599-608.
159. Minnaert, A.K., et al., *Strategies for controlling the innate immune activity of conventional and self-amplifying mRNA therapeutics: Getting the message across.* Adv Drug Deliv Rev, 2021. **176**: p. 113900.
160. Karikó, K., et al., *Generating the optimal mRNA for therapy: HPLC purification eliminates immune activation and improves translation of nucleoside-modified, protein-encoding mRNA.* Nucleic acids research, 2011. **39**(21): p. e142-e142.
161. Lukavsky, P.J. and J.D. Puglisi, *Large-scale preparation and purification of polyacrylamide-free RNA oligonucleotides.* Rna, 2004. **10**(5): p. 889-893.
162. Easton, L.E., Y. Shibata, and P.J. Lukavsky, *Rapid, nondenaturing RNA purification using weak anion-exchange fast performance liquid chromatography.* Rna, 2010. **16**(3): p. 647-53.
163. Fukuda, R., Y. Iwakura, and A. Ishihama, *Heterogeneity of RNA polymerase in Escherichia coli: I. A new holoenzyme containing a new sigma factor.* Journal of Molecular Biology, 1974. **83**(3): p. 353-367.
164. Mencin, N., A. Krušic, and J. Ličen, *Increasing dynamic binding capacity of oligo (dT) for mRNA purification: experimental results using CIM 96-well plates.* Bioprocess Int, 2022.
165. Wadhwa, A., et al., *Opportunities and Challenges in the Delivery of mRNA-based Vaccines.* Pharmaceutics, 2020. **12**(2): p. 102.
166. Li, J., C. Zhang, and H. Shan, *Advances in mRNA vaccines for infectious diseases.* Frontiers in Immunology, 2019. **10**: p. 594.
167. Morse, M.A., et al., *An alphavirus vector overcomes the presence of neutralizing antibodies and elevated numbers of Tregs to induce immune responses in humans with advanced cancer.* The Journal of clinical investigation, 2010. **120**(9): p. 3234-3241.
168. Morrison, J. and S. Plotkin, *Viral Vaccines: Fighting Viruses with Vaccines*, in *Viral pathogenesis*. 2016, Elsevier. p. 253-269.
169. Pardi, N., et al., *mRNA vaccines—a new era in vaccinology.* Nature reviews Drug discovery, 2018. **17**(4): p. 261.
170. Anderluzzi, G., et al., *Investigating the Impact of Delivery System Design on the Efficacy of Self-Amplifying RNA Vaccines.* Vaccines, 2020. **8**(2): p. 212.
171. Han, X., et al., *An ionizable lipid toolbox for RNA delivery.* Nat Commun, 2021. **12**(1): p. 7233.
172. Hou, X., et al., *Lipid nanoparticles for mRNA delivery.* Nat Rev Mater, 2021. **6**(12): p. 1078-1094.
173. Cheng, X. and R.J. Lee, *The role of helper lipids in lipid nanoparticles (LNPs) designed for oligonucleotide delivery.* Adv Drug Deliv Rev, 2016. **99**(Pt A): p. 129-137.
174. Blakney, A.K., et al., *One size does not fit all: the effect of chain length and charge density of poly (ethylene imine) based copolymers on delivery of pDNA, mRNA, and RepRNA polyplexes.* Biomacromolecules, 2018. **19**(7): p. 2870-2879.

175. Blakney, A.K., et al., *Big is beautiful: enhanced saRNA delivery and immunogenicity by a higher molecular weight, bioreducible, cationic polymer.* ACS nano, 2020. **14**(5): p. 5711-5727.
176. Blakney, A.K., et al., *Polymeric and lipid nanoparticles for delivery of self-amplifying RNA vaccines.* J Control Release, 2021. **338**: p. 201-210.
177. Ott, G., et al., *A cationic sub-micron emulsion (MF59/DOTAP) is an effective delivery system for DNA vaccines.* J Control Release, 2002. **79**(1-3): p. 1-5.
178. Brito, L.A., et al., *A cationic nanoemulsion for the delivery of next-generation RNA vaccines.* Mol Ther, 2014. **22**(12): p. 2118-2129.
179. Liu, Y., Y. Li, and Q. Hu, *Advances in saRNA Vaccine Research against Emerging/Re-Emerging Viruses.* Vaccines (Basel), 2023. **11**(7).
180. Zeng, C., et al., *Formulation and Delivery Technologies for mRNA Vaccines.* Curr Top Microbiol Immunol, 2022. **440**: p. 71-110.
181. Liang, F., et al., *Efficient Targeting and Activation of Antigen-Presenting Cells In Vivo after Modified mRNA Vaccine Administration in Rhesus Macaques.* Mol Ther, 2017. **25**(12): p. 2635-2647.
182. Pardi, N., et al., *mRNA vaccines - a new era in vaccinology.* Nat Rev Drug Discov, 2018. **17**(4): p. 261-279.
183. Pepini, T., et al., *Induction of an IFN-mediated antiviral response by a self-amplifying RNA vaccine: implications for vaccine design.* The Journal of Immunology, 2017. **198**(10): p. 4012-4024.
184. De Beuckelaer, A., et al., *Type I interferons interfere with the capacity of mRNA lipoplex vaccines to elicit cytolytic T cell responses.* Molecular Therapy, 2016. **24**(11): p. 2012-2020.
185. Pollard, C., et al., *Type I IFN counteracts the induction of antigen-specific immune responses by lipid-based delivery of mRNA vaccines.* Molecular Therapy, 2013. **21**(1): p. 251-259.
186. Heil, F., et al., *Species-specific recognition of single-stranded RNA via toll-like receptor 7 and 8.* Science, 2004. **303**(5663): p. 1526-9.
187. Miyake, K., et al., *Nucleic acid sensing by toll-like receptors in the endosomal compartment.* Frontiers in Immunology, 2022. **13**: p. 941931.
188. Barral, P.M., et al., *Functions of the cytoplasmic RNA sensors RIG-I and MDA-5: key regulators of innate immunity.* Pharmacol Ther, 2009. **124**(2): p. 219-34.
189. Hornung, V., et al., *5'-Triphosphate RNA is the ligand for RIG-I.* Science, 2006. **314**(5801): p. 994-7.
190. Sabbah, A., et al., *Activation of innate immune antiviral responses by Nod2.* Nat Immunol, 2009. **10**(10): p. 1073-80.
191. Drappier, M. and T. Michiels, *Inhibition of the OAS/RNase L pathway by viruses.* Curr Opin Virol, 2015. **15**: p. 19-26.
192. Lamers, M.M., B.G. van den Hoogen, and B.L. Haagmans, *ADAR1: "Editor-in-Chief" of Cytoplasmic Innate Immunity.* Front Immunol, 2019. **10**: p. 1763.
193. Demongeot, J. and C. Fougère, *mRNA COVID-19 Vaccines-Facts and Hypotheses on Fragmentation and Encapsulation.* Vaccines (Basel), 2022. **11**(1).
194. Andries, O., et al., *N(1)-methylpseudouridine-incorporated mRNA outperforms pseudouridine-incorporated mRNA by providing enhanced protein expression and reduced immunogenicity in mammalian cell lines and mice.* J Control Release, 2015. **217**: p. 337-44.

195. Karikó, K., et al., *Suppression of RNA recognition by Toll-like receptors: the impact of nucleoside modification and the evolutionary origin of RNA.* Immunity, 2005. **23**(2): p. 165-75.
196. Maruggi, G., et al., *mRNA as a Transformative Technology for Vaccine Development to Control Infectious Diseases.* Mol Ther, 2019. **27**(4): p. 757-772.
197. Azizi, H., et al., *Self-amplifying RNAs generated with the modified nucleotides 5-methylcytidine and 5-methyluridine mediate strong expression and immunogenicity in vivo.* NAR Molecular Medicine, 2024. **1**(2).
198. Erasmus, J.H., et al., *Intramuscular Delivery of Replicon RNA Encoding ZIKV-117 Human Monoclonal Antibody Protects against Zika Virus Infection.* Mol Ther Methods Clin Dev, 2020. **18**: p. 402-414.
199. Zhong, Z., et al., *Corticosteroids and cellulose purification improve, respectively, the in vivo translation and vaccination efficacy of sa-mRNAs.* Mol Ther, 2021. **29**(4): p. 1370-1381.
200. Beissert, T., et al., *Improvement of In Vivo Expression of Genes Delivered by Self-Amplifying RNA Using Vaccinia Virus Immune Evasion Proteins.* Human Gene Therapy, 2017. **28**(12): p. 1138-1146.
201. Blakney, A.K., et al., *Innate Inhibiting Proteins Enhance Expression and Immunogenicity of Self-Amplifying RNA.* Mol Ther, 2021. **29**(3): p. 1174-1185.
202. Heesters, B.A., et al., *Antigen Presentation to B Cells.* Trends Immunol, 2016. **37**(12): p. 844-854.
203. Kim, J., et al., *Self-assembled mRNA vaccines.* Adv Drug Deliv Rev, 2021. **170**: p. 83-112.
204. Lizée, G., G. Basha, and W.A. Jefferies, *Tails of wonder: endocytic-sorting motifs key for exogenous antigen presentation.* Trends Immunol, 2005. **26**(3): p. 141-9.
205. Zhang, Y., et al., *Efficient signal sequence of mRNA vaccines enhances the antigen expression to expand the immune protection against viral infection.* Journal of Nanobiotechnology, 2024. **22**(1): p. 295.
206. Meyer, M., et al., *Modified mRNA-based vaccines elicit robust immune responses and protect guinea pigs from Ebola virus disease.* The Journal of infectious diseases, 2018. **217**(3): p. 451-455.
207. Schudel, A., D.M. Francis, and S.N. Thomas, *Material design for lymph node drug delivery.* Nat Rev Mater, 2019. **4**(6): p. 415-428.
208. Vashishtha, V.M. and P. Kumar, *The durability of vaccine-induced protection: an overview.* Expert Rev Vaccines, 2024. **23**(1): p. 389-408.
209. Rocha, B. and C. Tanchot, *Towards a cellular definition of CD8+ T-cell memory: the role of CD4+ T-cell help in CD8+ T-cell responses.* Curr Opin Immunol, 2004. **16**(3): p. 259-63.
210. López-Gil, E., et al., *MVA Vectored Vaccines Encoding Rift Valley Fever Virus Glycoproteins Protect Mice against Lethal Challenge in the Absence of Neutralizing Antibody Responses.* Vaccines (Basel), 2020. **8**(1).
211. Gans, H.A., et al., *Humoral and cell-mediated immune responses to an early 2-dose measles vaccination regimen in the United States.* J Infect Dis, 2004. **190**(1): p. 83-90.
212. Pickett, B.E., et al., *ViPR: an open bioinformatics database and analysis resource for virology research.* Nucleic acids research, 2012. **40**(D1): p. D593-D598.
213. Kumar, S., et al., *MEGA X: molecular evolutionary genetics analysis across computing platforms.* Molecular biology and evolution, 2018. **35**(6): p. 1547-1549.

214. Overby, A.K., R.F. Pettersson, and E.P. Neve, *The glycoprotein cytoplasmic tail of Uukuniemi virus (Bunyaviridae) interacts with ribonucleoproteins and is critical for genome packaging.* Journal of virology, 2007. **81**(7): p. 3198-3205.
215. Murakami, S., et al., *Development of a novel, single-cycle replicable Rift Valley fever vaccine.* PLoS neglected tropical diseases, 2014. **8**(3).
216. Gerrard, S.R. and S.T. Nichol, *Characterization of the Golgi retention motif of Rift Valley fever virus G(N) glycoprotein.* J Virol, 2002. **76**(23): p. 12200-10.
217. Daniels, R.W., et al., *Expression of multiple transgenes from a single construct using viral 2A peptides in Drosophila.* PLoS One, 2014. **9**(6): p. e100637.
218. Donnelly, M.L.L., et al., *Analysis of the aphthovirus 2A/2B polyprotein 'cleavage' mechanism indicates not a proteolytic reaction, but a novel translational effect: a putative ribosomal 'skip'.* J Gen Virol, 2001. **82**(Pt 5): p. 1013-1025.
219. Szymczak, A.L., et al., *Correction of multi-gene deficiency in vivo using a single'self-cleaving'2A peptide–based retroviral vector.* Nature biotechnology, 2004. **22**(5): p. 589-594.
220. Thomas, G., *Furin at the cutting edge: from protein traffic to embryogenesis and disease.* Nat Rev Mol Cell Biol, 2002. **3**(10): p. 753-66.
221. Hosaka, M., et al., *Arg-X-Lys/Arg-Arg motif as a signal for precursor cleavage catalyzed by furin within the constitutive secretory pathway.* J Biol Chem, 1991. **266**(19): p. 12127-30.
222. Kampmann, T., et al., *The role of histidine residues in low-pH-mediated viral membrane fusion.* Structure, 2006. **14**(10): p. 1481-1487.
223. Bulleid, N.J., *Disulfide bond formation in the mammalian endoplasmic reticulum.* Cold Spring Harbor perspectives in biology, 2012. **4**(11): p. a013219.
224. Halldorsson, S., et al., *Shielding and activation of a viral membrane fusion protein.* Nature communications, 2018. **9**(1): p. 1-9.
225. Aranda, P.S., D.M. LaJoie, and C.L. Jorcyk, *Bleach gel: a simple agarose gel for analyzing RNA quality.* Electrophoresis, 2012. **33**(2): p. 366-9.
226. Polyplus. *in vivo-jetRNA+*. 2024; Available from: https://www.polyplus-sartorius.com/products/in-vivo-jetrna-plus.
227. McKay, P.F., et al., *Self-amplifying RNA SARS-CoV-2 lipid nanoparticle vaccine candidate induces high neutralizing antibody titers in mice.* Nat Commun, 2020. **11**(1): p. 3523.
228. Lei, C., et al., *On the Calculation of TCID50 for Quantitation of Virus Infectivity.* Virologica Sinica, 2021. **36**(1): p. 141-144.
229. Ferrara, F. and N. Temperton, *Pseudotype Neutralization Assays: From Laboratory Bench to Data Analysis.* Methods Protoc, 2018. **1**(1).
230. Wang, Q., et al., *Neutralization mechanism of human monoclonal antibodies against Rift Valley fever virus.* Nature Microbiology, 2019. **4**(7): p. 1231-1241.
231. Forsström, B., et al., *Dissecting antibodies with regards to linear and conformational epitopes.* PLoS One, 2015. **10**(3): p. e0121673.
232. Nakayama, K., *Furin: a mammalian subtilisin/Kex2p-like endoprotease involved in processing of a wide variety of precursor proteins.* Biochem J, 1997. **327 (Pt 3)**(Pt 3): p. 625-35.
233. Liu, Z., et al., *Systematic comparison of 2A peptides for cloning multi-genes in a polycistronic vector.* Scientific Reports, 2017. **7**(1): p. 2193.

234. *in vivo-jetRNA+*. 2023 [cited 2023 19 September]; Available from: https://www.polyplus-sartorius.com/products/in-vivo-jetrna-plus.
235. Ly, H.H., et al., *Optimization of Lipid Nanoparticles for saRNA Expression and Cellular Activation Using a Design-of-Experiment Approach.* Mol Pharm, 2022. **19**(6): p. 1892-1905.
236. Scheiblhofer, S., et al., *Influence of protein fold stability on immunogenicity and its implications for vaccine design.* Expert Rev Vaccines, 2017. **16**(5): p. 479-489.
237. Blum, J.S., P.A. Wearsch, and P. Cresswell, *Pathways of antigen processing.* Annu Rev Immunol, 2013. **31**: p. 443-73.
238. Budroni, S., et al., *Antibody avidity, persistence, and response to antigen recall: comparison of vaccine adjuvants.* npj Vaccines, 2021. **6**(1): p. 78.
239. McKay, P.F., et al., *Self-amplifying RNA SARS-CoV-2 lipid nanoparticle vaccine candidate induces high neutralizing antibody titers in mice.* Nature Communications, 2020. **11**(1): p. 3523.